

Acknowledgement

At the very onset, I surrender myself before the Almighty Lord for blessing me with the best of what I could have had. Be it this thesis, the personnel associated with it or the outcome of this research pursuit, all of it is his Grace, Mercy, and Blessings. He has made this possible, and I thank the Almighty Lord with all humility and surrender.

My journey during the last three years of undertaking this Ph.D. study has been a truly life-changing experience and it would not have been possible to do without the support and guidance that I received from many people.

*I would like to express my sincere gratitude to my supervisor **Prof. R.K Thapa** for the continuous support of my Ph.D. study and related research, for his patience, motivation, and immense knowledge. His guidance helped me in all the time of research and writing of this thesis. I could not have imagined having a better supervisor and mentor for my Ph.D. study.*

*I take this opportunity to thank **Prof. Zaithanzauva Pachuau**, Dean, SPS, and **Prof. Suman Rai**, Head, Physics Department, for extending all the necessary help during the course of my Ph.D. works. Thanks are also to **Prof. R.C. Tiwari**, **Dr. Hranghmingthanga**, **Dr. Lalthakimi Zadeng** and **Dr. B. Lalremruata** for all the useful discussions and help.*

*This Ph.D. study would not have been possible without the co-operation and support extended by my research colleagues **Rebecca Lalngaihawmi**, **Leishangthem Nirmala Devi**, **Himanshu Joshi**, **K. Neupane** and to the **Benjamin Vanlalruata (L)**, a*

Acknowledgement

*brilliant mind, who unfortunately had an untimely demise. A special thank you to **Mr. V. Malsawma**, Technical Assistant for his kind assistance in technical problems. My deep appreciation goes out to **Mrs. Kamala Thapa** for the warm hospitality and atmosphere and the support she has provided for me.*

*I owe my sincere thanks and gratitude to dear **Vanlalfakawmi Hauhnar** who has been a constant source of support and encouragement during the work.*

*I also convey my sincere thanks to my sisters' **Lalnunmawii Hnamte**, **Khawlrinawii** and **Lalhmuntiani Hnamte** who shared their words of advice and encouragement to finish this research.*

*Thanks to my precious daughter **Unique Vanlalpekhlui Hnamte**, without her presence, I'll not have the courage and passion to make this through.*

*Last but not the least, I would like to thank my parents **Lallura Hnamte** and **Vanramengi** for bearing me through the thick and thin of my Ph. D tenure. If it were not for their support, co-operation, and encouragement, this endeavor would not have been possible. My words of thanks cannot compensate their contribution, yet with all humility, I thank them for their noble gesture and splendid support.*

Dated: 19th Nov. 2018

(LALHRIATPUIA HNAMTE)

Department of Physics

Mizoram University, Aizawl

CURRICULUM VITAE

Name : Lalhriatpuia Hnamte
Father's Name : Lallura Hnamte
Mother's Name : Vanramengi
Date of Birth : 03-03-1990
Nationality : Indian
Marital Status : Single
Permanent Address : House No. A-36/1, Saron Veng, Aizawl
Contact No. : 8794400190
E-Mail : lahriatpuiaht@gmail.com
Work Experience : (i) One year teaching at Providence Higher Secondary School, Aizawl
(ii) Three years teaching at Victory Path, Career Point and Career Coaching Centre

Academic Qualification:

Sl. No.	Examination	Division /Grade	Year	Board / University
1	HSLC	II	2005	MBSE
2	HSSLC	II	2009	MBSE
3	B.Sc (Physics)	I	2013	MZU
4	M.Sc (Physics)	I	2015	MZU

Research Experiences : 3 yrs.

Doing research work in Theoretical Condensed Matter Physics with effect from August, 2015 for Ph. D degree under Prof. R. K. Thapa, Physics Department, Mizoram University.

मिज़ोरम विश्वविद्यालय
भौतिक विज्ञान विभाग
आइजोल ७९६००४ मिज़ोरम
फोन : ०३८९-३३०५२२, ९४३६९४०५२३ (मो०)
फैक्स : ०३८९-२३३०५२२

प्रोफेसर राम कुमार थापा



MIZORAM UNIVERSITY
PHYSICS DEPARTMENT
AIZAWL 796 004 MIZORAM
Phones : 0389 - 2330522, 9436140523(M)
FAX : 0389 - 2330522
E-mail : r.k.thapa@gmail.com
Prof. Ram Kumar Thapa

No. MZU/PHYS/RKT/PHD/2018/021

Dt. 19th Nov. 2018

Certificate

This is to certify that Lalhriatpuia Hnamte has carried out research works under my personal supervision and guidance in the Department of Physics, Mizoram University. The results of research works done by Lalhriatpuia Hnamte have been presented in this thesis entitled “**Theoretical Investigation of Electronic and Optical Properties of Double Perovskites $AA'BB'O_6$ ($A, A' =$ Alkaline Earth, Transition, Rare Earth and $B, B' =$ Transition Metals)**” and the same has been submitted to the Mizoram University, Aizawl, Mizoram, for the degree of Doctor of Philosophy.

Lalhriatpuia Hnamte has fulfilled all the requirements under the Ph. D. regulations of the Mizoram University. To the best of my knowledge, this thesis as a whole or any part thereof has not been submitted to this University or any other institution for any degree or diploma.

(Prof. R. K. THAPA)
Supervisor

1

Introduction

The understanding of physical properties of different materials for their potential applications in the day today life has always been prime field of interest of the human civilization. The tremendous increase in the number of materials available and their varying physical properties, coupled with demands from new applications and more service requirements, have brought about many changes in attitudes and viewpoints. Advances in fundamental science have led to the development of a new technical area which might be called as unified science and technology of materials or generally “Materials Science”.

Recent developments in materials science lead towards a new understanding of the nature of materials and suggest a more basic approach to their application. Techniques are available for describing the properties of existing materials and are becoming available for predicting properties of new materials, in terms of their atomic and molecular structures. With rapid evolution of theoretical methodologies based on quantum mechanics and the support of computational resources, the scientific research have been able to design, predict and extract valuable information across a wide range of materials. The matter is usually regarded to exist in a solid or a fluid state. The fluid state is further subdivided into gaseous and liquid states.

All the materials are composed of atoms and molecules. Modern tools and the available experimental techniques have reached the ability to control size, composition and functionality of matter which provides complete and more accurate characterization of materials. Similarly, the rapid evolution of theoretical methodologies based on the quantum mechanics with the support of computational resources, the scientific research has been able to design, predict and extract valuable information of finite and extended systems. The rapid advancement in experimental side increases the importance of having theoretical and computational tools due to its capacity to interpret, complement and guide the experimental methodology.

Exact solutions for electrons in materials are important to understand the significant properties of given materials. The calculation of total electronic energy values of the matter with high accuracy is the major requirements of the computational methods. With the increase in computational power, ab-initio calculations and methods have become a powerful tool in understanding the electronic band structure, magnetic and optical properties of materials.

In this thesis, the study will be mainly focused on the structural, electronic and optical properties of perovskite. There are several combinations of elements to form the perovskites including double perovskites. In our case here, the study will be focused on the double perovskites like $AA'BB'O_6$ types, where AA' will be alkaline earth elements, transition and rare earth elements, B or B' will be transition elements. Named after the Russian mineralogist Lev Perovski, 'Perovskites' refers to the class of compounds with a general formula ABX_3 , where A and B are two differently sized cations and X is an anion that bonds with both A and B . In our case, we restrict ourselves to systems with Oxygen as the anion and therefore generally refer to the oxide perovskites of the form ABO_3 . Due to the versatile capability of incorporating a large portion of elements of the periodic table into its structure, perovskites are arguably one of the largest studied

classes of materials across the branches of chemistry, physics and materials science (Goodenough *et al.*, 1971; Rao *et al.*, 1998).

Double Perovskites, its unique quality lies in the ability to tune their electronic structure to a large extent by choosing various combinations of A and B-site cations. It is due to this versatility that a wide range of functionalities can be deterministically engineered in perovskites. For instance, depending upon the distribution of the electronic bands, one can have either insulating, semiconducting or metallic perovskites; based on electron-electron correlations, some perovskites may be ferromagnetic, antiferromagnetic or diamagnetic; based on optical absorption characteristics, perovskites may also be rendered optically transparent or opaque; atomic displacements can also yield ferroelectricity; and sometimes, perovskites can be multifunctional by the co-existence of two or more of the above qualities. Thus a wide range of properties could be engineered into perovskites depending upon the desired functionality.

In addition to compositional variations of A and B cations in the simple ABO_3 perovskites, another effective approach to functional engineering that has been widely explored is the partial substitution of A or B cations. Particularly interesting are compounds, where exactly half of the A or B sites are substituted by a second cation giving rise to compounds of the form $A_{0.5}A'_{0.5}BO_3$ and $AB_{0.5}B'_{0.5}O_3$. In some compounds, the substituted cations have been found occupy the cationic sites in an ordered manner within the crystal structure. For such compounds, it has been common practice to denote with a doubled chemical formula as $AA'B_2O_6$ and $A_2BB'O_6$. These ordered half-substituted multi-cation perovskites are commonly referred to as double perovskites and constitute a significantly large field of research by themselves. This study is focused on the B-site ordered double perovskite and hence we restrict this introductory section also to the $A_2BB'O_6$ type of compounds. For a more detailed introduction, the reader is directed to Ref. (Chakraborty *et al.*,

2017; Murthy *et al.*, 2015) which provide extensive reviews on the structure and properties of $A_2BB'O_6$ double perovskites. Some aspects from these review articles have been adapted into this introduction due to their relevance to this study.

However, it should be noted both these reviews cover mainly the bulk studies on double perovskites. Thin film approach to double perovskites is comparatively younger and smaller field of study at the moment, but has been gaining growing amount of relevance in recent years.

Some of the earliest reports on this class of compounds date back to the 1960's where possibilities of room temperature magnetism in Rhenium based double perovskites were explored by Longo and Ward (Longo *et al.*, 1961). A more recent revival of the field was marked by the publication of Kobayashi *et al.*, in 1998 who reported on half-metallicity or the fully spin polarized electronic conduction in Sr_2FeMoO_6 double perovskites (Kobayashi *et al.*, 1998). The possible application of such a material in spin-electronic devices garnered huge amount of interest in this compound and paved way for several exploratory efforts on the double perovskite compound in the following years. The versatility of the double perovskite compounds lie in their ability to accommodate a vast number of elemental combinations which can be a boon to materials engineers aiming to tailor functionalities by design. In their review article, Vasala *et al.* (2015) estimate that - within structural limitations, there are nearly 2×10^4 possible double perovskite compositions, among which only about 1000 compounds have been so far experimentally reported in the literature. This stands as evidence for the large untapped potential of double perovskites as functional oxides.

Pb-based double perovskites with magnetic cations in the B-sites are potentially good candidates for both magnetic and ferroelectric orderings. Pb_2FeNbO_6 and Pb_2FeTaO_6 have been extensively studied since both exhibit ferroelectric order close to RT with polarization (\mathbf{P}_s) || $\langle 111 \rangle$

and antiferromagnetic (AFM) order below a Néel Temperature (T_N) ~ 150 K. These materials frequently exhibit superparamagnetic clusters even above RT, and due to the biquadratic magnetoelectric coupling ($\sim M^2P^2$) the magnetic susceptibility exhibits anomalies at the ferroelectric phase transition temperature (Jeong *et al.*, 2011; Martinez *et al.*, 2010). Pb_2ScTaO_6 and Pb_2ScNbO_6 compounds is in paraelectric state at 400K and differs to ferroelectric phase at 4.2K and 200K by cooperative ion shift (Kishi, 2001). Pb_2ScTaO_6 showed ferroelectric in the ordered structure and relaxor ferroelectric in the disordered phase (Setter, 1980). Studies of $Pb(Mg_{1/3}Ta_{2/3})O_3:PbZrO_3$ had shown contradictory results different to the commonly accepted relationship between the order/disorder state and the behaviour of normal/relaxor ferroelectrics (Akbas, 1997). Pb_2ScNbO_6 (PSN) ceramics, a promising relaxor ferroelectric material, its powder mechanically activated at various pressures occur in different metastable structural states (Ubushaev, 2011). Pb_2YbNbO_6 at room temperature show antiferroelectric and upon when heating, it undergoes an antiferroelectric to paraelectric phase transition at 578 K (Isupov, 1965). The observation of diffuse character from paraelectric to ferroelectric phase transition and observed Curie temperature at $(18 \pm 1) ^\circ C$ for Pb_2ScTaO_6 (PST) and $(87 \pm 1) ^\circ C$ for $Pb(Sc_{0.5}Nb_{0.5})O_3$ (PSN) (Caranoni, 1993).

Extensive research has been pursued on these ordered double perovskites by large number of researchers in ideal, double and complex structures. Lufaso *et al.*, (2006) by using synchrotron X-ray powder diffraction and studied the structural phase transition of double perovskite Ba_2YTaO_6 . It is observed that this compound undergoes a phase transition from cubic structure (Fm-3m) to tetragonal (I4/m) structure under pressure. Magnetic properties of pentavalent Osmium-containing oxides have been aroused a great deal of interest, because the Os^{5+} ion has the largest possible spin ($S = 3/2$) (Lam, 2002). The structure and magnetic properties of the double

perovskites Ba_2CaMO_6 ($M = \text{W}, \text{Re}, \text{Os}$) were investigated by Yamamura *et al.*, (2006) and found that $\text{Ba}_2\text{CaReO}_6$ undergo a second order transition from cubic $Fm-3m$ to tetragonal $I4/m$ near 120K, whereas Ba_2CaWO_6 make a transition from $I4/m$ to monoclinic $I2/m$ at 295K. Magnetic susceptibility measurements show that $\text{Ba}_2\text{CaReO}_6$ and $\text{Ba}_2\text{CaOsO}_6$ transform to an antiferromagnetic state below 15.4 and 51K, respectively. Single crystals of the tungstates Ba_2MgWO_6 and Ba_2ZnWO_6 have been grown by Bugaris *et al.*, (2011) and studied their structural parameters by single crystal X-ray diffraction. They found that both the compounds exhibit luminescence property at room temperature with green and yellow emissions respectively. Day *et al.*, (2012) reported the crystal structures of tungsten and molybdenum containing perovskite oxides using neutron and X-ray powder diffraction. The structural stability in these compounds is mainly controlled by the tolerance factor.

Enormous amount of work has been done theoretically and experimentally on these semiconducting oxides with perovskite structure in ideal, double and complex structures. Lufaso *et al.*, (2008) synthesized and characterized new Osmate $\text{Sr}_2\text{CuOsO}_6$ using synchrotron X-ray powder diffraction. Their studies reveal that applications of hydrostatic pressure upto 6 Gpa significantly decrease the lattice parameter demonstrating the primary compression mechanism in $\text{Sr}_2\text{CuOsO}_6$. First principle investigation on $\text{Sr}_2\text{BB}'\text{O}_6$ ($B, B' = 3d$ transition metal) was carried out by Liu *et al.*, (2012) with both generalized gradient approximation (GGA) and GGA+U approaches in these compounds indicates that the five compounds $\text{Sr}_2\text{ScCrO}_6$, $\text{Sr}_2\text{TiCrO}_6$, $\text{Sr}_2\text{MnCrO}_6$, $\text{Sr}_2\text{ZnMnO}_6$ and $\text{Sr}_2\text{ZnFeO}_6$ found to be a promising candidates for half-metallic (HM) materials. Yan Qian *et al.*, (2012) studied the structural, electronic, and magnetic properties of Sr_2FeMO_6 under the external hydrostatic high- pressure using density-functional calculations. The results show that no structural symmetry change in Sr_2FeMO_6 is found in the whole applied pressure.

However, at the pressure of about 33-36 GPa, there is a spin crossover of Fe ion from high-spin to low-spin state. Raman spectroscopy studies on high temperature induced phase transitions in Sr_2ZnWO_6 and Sr_2CoWO_6 investigated by Manoun *et al.*, (2012) showed that Sr_2ZnWO_6 undergoes a phase transition from monoclinic ($P21/n$) to tetragonal ($I4/m$) at 80°C , whereas Sr_2CoWO_6 compound exhibits a phase transition from tetragonal ($I4/m$) to cubic ($\text{Fm-}3\text{m}$) around 420°C . Recently by using first principles calculations, Li *et al.* (2014) reported that $\text{Sr}_2\text{AlTaO}_6$ exhibit induced ferromagnetism due to vacancy in Al and Ta. The induced magnetism is different for Al and Ta vacancy. Their study reveals that $\text{Sr}_2\text{AlTaO}_6$ with O vacancy is nonmagnetic but energetically more favorable than the other vacancies created by either Al or Nb.

Among the $\text{R}_2\text{BB}'\text{O}_6$ series compounds, the magnetic properties in R_2NiMnO_6 have been reported recently (Chakraborty *et al.*, 2017, Yadav *et al.*, 2015, Chanda *et al.*, 2015, Guo *et al.*, 2013). Double perovskites R_2NiMnO_6 and R_2CoMnO_6 , with Ni and Mn 1:1 ordered along (1 1 1) plane, are ferromagnetic oxides with $P21/n$ symmetry (Booth *et al.*, 2009, Bull *et al.*, 2004). Here, Ni^{2+} , Co^{2+} and Mn^{4+} ions present $t^2_{2g}e^2_g$, $t^5_{2g}e^2_g$ and $t^3_{2g}e^0_g$ configuration respectively. The virtual hopping of electrons from half-filled e.g. orbital of $\text{Ni}^{2+}/\text{Co}^{2+}$ to vacant e.g. orbital of Mn^{4+} leads to ferromagnetic exchange interaction according to Goodenough–Kanamori rule (Kumar *et al.*, 2014). Also, Kumar *et al.* (2014) have confirmed the impact of r_R on the spin-phonon coupling in ordered bulk R_2CoMnO_6 ($R = \text{La, Pr, Nd}$) by analyzing the softening of the Raman modes at $\sim 610 \text{ cm}^{-1}$ (symmetry stretching) and $\sim 490 \text{ cm}^{-1}$ (antisymmetry stretching) positions near the magnetic transition temperature. Recently, Chakraborty *et al.* (2017) have studied the magnetic and MCE properties in R_2NiMnO_6 ($R = \text{Pr, Nd, Tb, Ho, and Y}$) by magnetization measurements, the R_2NiMnO_6 compounds undergo PM to FM transitions around 215, 191, 113, 86, and 81 K for $R = \text{Pr, Nd, Tb, Ho, and Y}$, respectively, and the corresponding values of maximum magnetic entropy

change (under the magnetic field change of 0-5 T) are 4.9, 2.3, 5.2, 6.4, and 5.4 J kg⁻¹ K⁻¹ (Sharma *et al.*, 2014). Very recently, Murthy *et al.* (2015) have investigated the MCE in Gd₂NiMnO₆ and Gd₂CoMnO₆ by magnetic and heat capacity measurements. Both compounds exhibit giant MCE at low temperature, the maximum values of magnetic entropy change reach -35.5 and -24 J kg⁻¹ K⁻¹ (under the magnetic field change of 0-7 T) for Gd₂NiMnO₆ and Gd₂CoMnO₆, respectively. La₂NiMnO₆ (LNMO) is also the most studied compound both as bulk and thin film. Bulk LNMO shows a near room temperature ferromagnetic transition, accompanied by large magneto-capacitance and magnetoresistance effects (Choudhury *et al.*, 2012).

1.1 APPLICATIONS OF PEROVSKITES

The perovskite structure class encompasses a huge variety of compounds. Most of the metallic ions in the periodic table can be incorporated into the perovskite structure. Oxides and fluorides comprise the vast majority of perovskite compounds (Goodenough *et al.*, 1970) but the perovskite structure is found for many combinations of cations and anions. Chlorides (Brynestad *et al.*, 1966), Bromides (Knochenmuss *et al.*, 1986), Hydrides (Messer *et al.*, 1964), Oxynitrides (Bacher *et al.*, 1988) and Sulfides (Clearfield *et al.*, 1963; Rodier *et al.*, 1970) are all known with the perovskite structure.

Perovskite structured compounds are used as Electrostrictive actuators (components which modify an electrical signal depending upon its frequency, such as a band pass filter) are based on a class of materials known as “relaxor ferroelectrics”. These materials are similar to normal ferroelectric materials in that the application of an electric field can cause some of the atoms to shift their positions in the unit cell. This causes a net polarization of the material which remains even after the external field has been removed. Relaxor ferroelectric materials differ from normal ferroelectric materials in several ways (Randall *et al.*, 1990).

In normal ferroelectrics, the dielectric constant changes dramatically near the Curie temperature as they undergo sharp 1st and 2nd order transitions. However, in relaxor ferroelectrics the broad-diffuse phase transition removes the sharp temperature dependent changes of the dielectric constant. This property is of great importance in applications where the temperature may approach the Curie temperature of normal ferroelectric materials (Galasso *et al.*, 1970). Another important difference is that the dielectric constant is weakly frequency dependent in normal ferroelectrics, but is strongly frequency dependent in relaxor ferroelectrics. This is the basis for an electrostrictive actuator. Another difference is that normal ferroelectrics have a strong remnant polarization while relaxor ferroelectrics do not. Another application of perovskite compounds is the giant magnetoresistance (GMR). In such compounds the resistance is very sensitive to the presence of magnetic fields. The primary application for such materials is the realm of magnetic data storage and retrieval (Hwang *et al.*, 1995b).

Interestingly, the magnetoresistive effect is very sensitive to the exact structure of the compound. In particular, octahedral tilting distortions have been shown to play a critical role in determining the size of the magnetoresistive effect and the Curie temperature (Hwang *et al.*, 1995a; Fontcuberta *et al.*, 1996). Large number of perovskite structured compounds with general formula ABO_3 has been widely investigated in the past few decades due to their nature of exhibiting variety of physical properties.

Recent interest on double perovskite type oxides is because of their application as an electrode material for solid state fuel cells and a promising material as host for phosphorus (Dong *et al.*, 2013). Series of double perovskite system with general formula $A_2BB'O_6$ have attracted considerable attention due to their correlation of dielectric and the magnetic properties (Kobayashi *et al.*, 1999). In recent years, these double perovskites are studied extensively owing to their

technological applications like memory devices, charge storage devices, phase shifters, second harmonic generators, solid oxide fuel cells, sensors and radio frequency (rf) filters (Hoffman *et al.*, 2011; Grimaud *et al.*, 2013). The above discussion only focuses on some of the important properties and applications of perovskites. However, properties like, optical, magnetic, conducting, vibrational and thermoelectric properties in these materials are in need of through investigation.

1.2 Review of Literature

Double perovskite $AA'BB'O_6$ have been investigated by several workers. For example, Ba_2LnSbO_6 ($Ln =$ lanthanides) compounds with double perovskite $AA'BB'O_6$ structure have been extensively studied in the past (Blasse 1965, Garcia Cascado *et al.*, 1984, Alonso *et al.*, 1997, Karunadasa *et al.*, 2003). Among these materials, Ba_2GdSbO_6 compound was of special interest because of its applications (Kurian *et al.*, 1995) as substrate for high temperature superconducting $YBa_2Cu_3O_{7-\delta}$ films. The crystal structure of Ba_2GdSbO_6 material was reported as double cubic perovskite (Kurian *et al.*, 1995).

Karunadasa *et al.*, (2003) studied f.c.c. lanthanide double perovskite of Ba_2LnSbO_6 and Sr_2LnSbO_6 ($Ln = Dy, Ho, Gd$) described that double perovskite with Ln^{3+} , Sb^{5+} ordering on the B sites and found out that the anti-ferromagnetic near-neighbor coupling found for the Ho- and Dy-based double perovskite is different from the spin-ice pyrochlores based on those elements where the nearest neighbor coupling is ferromagnetic. Observation of the spin-ice behavior in the Dy and Ho pyrochlores is the presence of significant magnet crystalline anisotropy.

Vijayakumar *et al.*, (2008) studied synthesis, characterization, sintering and dielectric properties of nanostructured perovskite Ba_2GdSbO_6 , described that Ba_2GdSbO_6 has been synthesized as single phase nanocrystals (30–60 nm) via an exothermic chemical process for the

first time. The solid combustion product obtained was characterized by X-ray diffraction (XRD), electron diffraction, differential thermal analysis (DTA), thermo gravimetric analysis (TGA), infrared spectroscopy (FT-IR) and transmission electron microscope (TEM). X-ray diffraction and electron diffraction have shown that the as prepared powder is phase pure $\text{Ba}_2\text{GdSbO}_6$ and has a complex cubic perovskite $\text{AA}'\text{BB}'\text{O}_6$ structure with lattice constant, $a = 8.449 \text{ \AA}$. DTA and TGA studies have shown that there is no phase transition taking place in the as prepared powder. The transmission electron microscopy image of the as prepared powder reveals that the particle size is in the range 30–60 nm. The nano powder could be sintered to a density of 96% of the theoretical density at 1560°C for 3h. The scanning electron microscope (SEM) image of the sintered material indicates high densification of the material with average grain size of 500 nm. The room temperature dielectric constant (ϵ_r) and loss factor ($\tan\delta$) of the sintered pellet at 3 MHz was 20 and 0.03, respectively which indicates that the material is suitable for microwave applications. The combustion synthesis has an advantage that the phase pure $\text{Ba}_2\text{GdSbO}_6$ could be obtained by a single step process without the need of any calcination step.

Jing Wang *et al.*, (2012) studied theoretical investigation on the magnetic and electronic properties of $\text{La}_2\text{NiIrO}_6$ and find out that the possible crystal structures (cubic Fm-3m, tetragonal I4/m and monoclinic P21/n) and magnetic interactions (ferromagnetic and A-type antiferromagnetic couplings), it has been found that monoclinic P21/n with A-type antiferromagnetic coupling is the most stable.

Saad (2012) has done the first-principles linear muffin-tin orbital investigations to understand the electronic and magnetic structures of double perovskites Ba_2TMO_6 ($\text{T} = \text{V}, \text{Cr}, \text{Mn}, \text{Fe}$ and Co). He found that the local spin density approximation with coulomb interaction (LSDA+U) calculations depicted well the proper half metallic ferromagnetic ground states for

$\text{Ba}_2\text{CrMoO}_6$, $\text{Ba}_2\text{FeMoO}_6$ and $\text{Ba}_2\text{CoMoO}_6$. Half-metallic ferromagnetic nature is observed in Ba_2VMoO_6 , whereas insulating antiferromagnetic behaviour is observed in $\text{Ba}_2\text{MnMoO}_6$, consistent with the theoretical and experimental results. He clearly observed that the Mo ($4d$)– t_{2g} states are responsible for the conductivity feature in all compounds, except for Ba_2VMoO_6 and for the insulator $\text{Ba}_2\text{Mn-MoO}_6$. On the other hand, T($3d$) elements have great contribution on the magnetic properties of double perovskites Ba_2TMoO_6 , due to the orbits hybridization and polarization among the T($3d$), O($2p$) and Mo($4d$) ions. Mo ($4d$) ion has a little contribution in the total magnetic moment in all materials. Due to the strong hybridization, the conduction charges can be redistributed as T^{3+} ($3d^n$)– O^{2-} ($2p$)– Mo^{5+} ($4d^1$), where n is more than zero in the non-filling $3d$ orbits.

Saad (2012) has also studied the half-metallic ferromagnetism in double perovskites Ba_2VTO_6 (T= Nb and Mo) and find out that LSDA+U calculations depicted well the proper half-metallic ferromagnetic (HM-FM) ground states with total spin magnetic moments of $2.1021 \mu_B$ and $3.0633 \mu_B$ per formula unit cell for Ba_2VNbO_6 and Ba_2VMoO_6 , respectively. V($3d$) ions have great effect on the magnetic properties of double perovskites Ba_2VTO_6 , due to the orbits hybridization and polarization between V($3d$),O($2p$) and T($4d$) ions. Whereas, Nb^{5+} ($4d^0$) and Mo^{5+} ($4d^1$) ions have small contribution in the total magnetic moment in their material. Due to the strong hybridization, the conduction charges can be redistributed as the bridge-interaction form; V^{3+} ($3d^2$)– O^{2-} ($2p$)– T^{5+} ($4d^n$), where $n = 0$ or 1 , in the non-filling $4d$ orbits. HM-FM nature in Ba_2VNbO_6 and Ba_2VMoO_6 compounds organizes from the ddp_π -superexchange interactions $3d-t_{2g}^2 \uparrow - 2p-3d-t_{2g}^n \uparrow$ ($n = 0$ or 1), conformity with Zener–Goodenough Kanamori (ZGK) rules.

Thapa and others (2015) studied the electronic, magnetic and optical properties of double perovskites A_2FeReO_6 ($A = Sr, Ba$). They have found semiconducting behavior of majority electrons with a finite gap at its E_F and the presence of metallic band predicts that A_2FeReO_6 to be a half metallic ferrimagnets.

Ghimire *et al.*, (2015) also studied the electronic and magnetic properties of double perovskites Nd_2MgIrO_6 , found that by using first-principles density functional calculations, Nd_2MgIrO_6 to be an antiferromagnetic Mott-Hubbard insulator. The study suggests that the enhanced magnetic moment is a result of it in exchange rather than the exchange interaction involving individual ions of Nd and Ir atoms.

In this thesis, we will present the results of density of states (DOS), band structures, magnetic moments and optical properties of double perovskites $AA'BB'O_6$ by using full potential linearized augmented plane wave (FP-LAPW). The FP-LAPW technique is based on DFT to solve the Kohn-Sham of a many electron systems by presenting a basis set for the given system. This is achieved by partitioning the cell into non-overlapping atomic circles and an interstitial region. The detailed technique is discussed in chapter 2. We also make use of the modified Becke-Johnson potential (mBJ) to have a better description of the band gap deficiency offered by GGA and LDA exchange-correlation potentials. First principle calculations are done for the systems A_2MgWO_6 ($A = Ba, Sr$), $Pb_2ScB'O_6$ ($B' = Sb, Ta$), $Ba_2VB'O_6$ ($B' = Nb, Mo$), and $La_2CrB'O_6$ ($B' = Co, Ni$) using this approach.

The thesis is organized in the following manner.

In chapter 2, we describe the theory and methodology used in our calculation. We will present an outline of the density functional theory (DFT), FP-LAPW model using GGA as well as mBJ methods.

In chapter 3, we describe the electronic and optical properties of double perovskites A_2MgWO_6 with alkaline earth element AA' as Ba and Sr; and transition metals B as Mg and B' as W.

In Chapter 4, we describe the electronic and optical properties of double perovskites $Pb_2ScB'O_6$ with alkaline earth element AA' as Pb; and transition metals B as Sc and B' as Sb, Ta.

In Chapter 5, we discuss the electronic and optical properties of double perovskites $Ba_2VB'O_6$ with alkaline earth element $A=A' = Ba$; and transition metals B as V and B' as Nb, Mo.

In Chapter 6, we discuss the electronic and optical properties of double perovskites $La_2CrB'O_6$ with alkaline earth element AA' as La; and transition metals B as Cr and B' as Co, Ni.

Chapter 7 contains the concluding part of the thesis where we summarize the results obtained in the case of double perovskites $AA'BB'O_6$. This is followed by references.

2

Theoretical Formalism and Methodology

In this chapter, we will discuss the theory, methods, and approximations used in the calculations of DOS, band structures magnetic moments and optical properties of double perovskites compound.

Density-functional theory is one of the most popular and successful quantum mechanical approaches to matter. It is nowadays routinely applied for calculating, e.g., the binding energy of molecules in chemistry and the band structure of solids in physics. First applications relevant for fields traditionally considered more distant from quantum mechanics, such as biology and mineralogy are beginning to appear. Superconductivity, atoms in the focus of strong laser pulses, relativistic effects in heavy elements and in atomic nuclei, classical liquids, and magnetic properties of alloys have all been studied with DFT.

DFT owes this versatility to the generality of its fundamental concepts and the flexibility one has in implementing them. In spite of this flexibility and generality, DFT is based on quite a rigid conceptual framework. This section introduces some aspects of this framework in general terms. The next section, 2.2 is about the *Born-Oppenheimer approximation* followed by the two core elements of DFT, the Hohenberg-Kohn theorem and the Kohn-Sham equations in section 2.3.1 and 2.3.2 respectively.

2.1 Theory

To get a first idea of what density-functional theory is about, it is useful to take a step back and recall some elementary quantum mechanics. A solid is made up of heavy, positively charged particles (nuclei) and lighter, negatively charged particles (electrons). So for N nuclei, we are dealing with a problem of $N+ZN$ electromagnetically interacting particles. Thus we have a many-body problem where quantum mechanics is needed: a quantum many body problem. The Hamiltonian for many-particle system is:

$$\hat{H} = -\frac{\hbar^2}{2} \sum_i \frac{\nabla_{\mathbf{R}_i}^2}{M_i} - \frac{\hbar^2}{2} \sum_i \frac{\nabla_{\mathbf{r}_i}^2}{m_e} - \frac{1}{4\pi\epsilon_0} \sum_{i,j} \frac{e^2 Z_i Z_j}{|\mathbf{R}_i - \mathbf{R}_j|} + \frac{1}{8\pi\epsilon_0} \sum_{i \neq j} \frac{e^2}{|\mathbf{r}_i - \mathbf{r}_j|} + \frac{1}{8\pi\epsilon_0} \sum_{i \neq j} \frac{e^2 Z_i Z_j}{|\mathbf{R}_i - \mathbf{R}_j|} \quad (2.1)$$

The mass of the nucleus at \mathbf{R}_i is M_i , the electrons have mass m_e and are at \mathbf{r}_i . The first term is the kinetic energy operator for the nuclei, the second for the electrons. The last three terms describe the Coulomb interaction between electrons and nuclei, between electrons and other electrons, and between nuclei and other nuclei. Solving for this Eqn. provides the all the possible information of the system.

2.2 Born-Oppenheimer approximation

The nuclei are much heavier and therefore much slower than the electrons. They can be 'frozen' at fixed positions and assume the electrons to be in instantaneous equilibrium with them. In other words: only the electrons are kept as players in our many body problem. The nuclei are deprived from this status, and reduced to a given source of positive charge, they become 'external' to the electron cloud. After having applied this approximation, we are left with a collection of NZ

interacting negative particles, moving in the (now external or given) potential of the nuclei.

Now we consider the importance of the Born-Oppenheimer approximation on the Hamiltonian in Eqn. 2.1. The nuclei do not move any more, their kinetic energy is zero and the first term disappears. The last term reduces to a constant. We are left with the kinetic energy of the electron gas, the potential energy due to electron-electron interactions and the potential energy of the electrons in the (now external) potential of the nuclei which is written as:

$$\hat{H} = \hat{T} + \hat{V} + \hat{V}_{ext} \quad (2.2)$$

The kinetic and electron-electron terms of Eqn. 2.2 depend only on the fact that we are dealing with a many-electron system.

2.3 DFT General Formulation

The quantum many body problem obtained after the Born-Oppenheimer approximation is much simpler than the original one, but still far too difficult to solve. Several methods exist to reduce Eqn. 2.2 to an approximate but tractable form. The Hartree-Fock method (HF), performs very well for atoms and molecules, and is therefore used a lot in quantum chemistry. However for solids it is less accurate. But the most successful mean-field approaches is the density functional theory (DFT) formulated in the 1960's by Hohenberg, Kohn and Sham (Hohenberg and Kohn, 1964; Kohn and Sham, 1965), which has become the standard method in the calculation of the electronic structure of solids.

2.3.1 Hohenberg and Kohn's Theorem

The formulation of the two theorems of Hohenberg and Kohn is as follows:

First theorem: *There is a one-to-one correspondence between the ground-state density $\rho(r)$ of a many-electron system (atom, molecule, solid) and the external potential V_{ext} . An immediate consequence is that the ground-state expectation value of any observable \hat{O} is a unique functional of the exact ground-state electron density:*

$$\langle \Psi | \hat{O} | \Psi \rangle = O[\rho] \quad (2.3)$$

Second theorem: *For \hat{O} being the Hamiltonian \hat{H} , the ground-state total energy functional $H[\rho] = E_{V_{ext}}[\rho]$ is of the form*

$$E_{V_{ext}}[\rho] = \langle \Psi | \hat{T} + \hat{V} | \Psi \rangle + \langle \Psi | \hat{V}_{ext} | \Psi \rangle \quad (2.4)$$

$$= F_{HK}[\rho] + \int \rho(\mathbf{r}) V_{ext}(\mathbf{r}) d\mathbf{r} \quad (2.5)$$

where the Hohenberg-Kohn density functional $F_{HK}[\rho]$ is universal for any many-electron system. $E_{V_{ext}}[\rho]$ reaches its minimal value (equal to the ground-state total energy) for the ground-state density corresponding to V_{ext} .

From the one-to-one correspondence between ground-state density and external potential we see that a given many-electron system has a unique external potential, which by the Hamiltonian of Eqn. 2.2 and the Schrödinger Eqn. yields a unique ground-state many particle wave function. From this wave function, the corresponding electron density is easily found. An external potential hence leads in a well-defined way to a unique ground-state density corresponding to it. But

intuitively it looks like the density contains less information than the wave function. If this would be true, it would not be possible to find a unique external potential if only a ground-state density is given. The first theorem of Hohenberg and Kohn tells exactly that this is possible! The density contains as much information as the wave function does (i.e. everything you could possibly know about an atom, molecule or solid). All observable quantities can be retrieved therefore in a unique way from the density only, i.e. they can be written as functionals of the density.

The universality of $F_{HK}[\rho]$ in Eqn. 2.5 is written down by using the density Operator. The density operator $\hat{\rho}(\mathbf{r})$ for an N-particle system is defined

$$\hat{\rho}(\mathbf{r}) = \sum_{i=1}^N \delta(\mathbf{r}_i - \mathbf{r}) \quad (2.6)$$

as such that its evaluation for a many body wave function Ψ yields the density:

$$\hat{\rho}(\mathbf{r}) = \langle \Psi(\mathbf{r}_1, \mathbf{r}_2, \dots, \mathbf{r}_N) | \hat{\rho}(\mathbf{r}) | \Psi(\mathbf{r}_1, \mathbf{r}_2, \dots, \mathbf{r}_N) \rangle \quad (2.7)$$

$$= \langle \Psi(\mathbf{r}_1, \mathbf{r}_2, \dots, \mathbf{r}_N) \left| \sum_{i=1}^N \delta(\mathbf{r}_i - \mathbf{r}) \right| \Psi(\mathbf{r}_1, \mathbf{r}_2, \dots, \mathbf{r}_N) \rangle \quad (2.8)$$

$$= \sum_{i=1}^N \int \Psi^*(\mathbf{r}_1, \mathbf{r}_2, \dots, \mathbf{r}_i \equiv \mathbf{r}, \dots, \mathbf{r}_N) \Psi(\mathbf{r}_1, \mathbf{r}_2, \dots, \mathbf{r}_i \equiv \mathbf{r}, \dots, \mathbf{r}_N) d\mathbf{r}_1 d\mathbf{r}_2 \dots d\mathbf{r}_N \quad (2.9)$$

Supposing the ground-state density is known, the contribution to the total energy from the external potential can be exactly calculated. An explicit expression for the Hohenberg-Kohn functional F_{HK} is not known. F_{HK} is a universal functional for any many-electron system as it does not contain information on the nuclei and

their position. This means that in principle an expression for $F_{HK}[\rho]$ exists which can be used for every atom, molecule or solid which can be imagined.

The second theorem makes it possible to use the variational principle of Rayleigh-Ritz in order to find the ground-state density. Out of the infinite number of possible densities, the one which minimizes $E_{V_{ext}}[\rho]$ is the ground-state density corresponding to the external potential $V_{ext}(\mathbf{r})$. Of course, this can be done only if an approximation to $F_{HK}[\rho]$ is known. But having found ρ , all knowledge about the system is within reach. It is useful to stress the meaning of the energy functional $E_{V_{ext}}[\rho]$ when it is evaluated for the density ρ corresponding to the particular V_{ext} for this solid, it gives the ground state energy. When it is evaluated for any other density however, the results has no physical meaning.

2.3.2 Kohn Sham Equations

The equations of Kohn and Sham, turn DFT into a practical procedure to obtain the ground state density. Rewriting the Hohenberg-Kohn functional, the correlation energy is defined as this part of the total energy which is present in the exact solution, but absent in the Hartree-Fock solution. The total energy functionals $E_e[\rho]$ and $E_{HF}[\rho]$ corresponding to the exact and Hartree-Fock Hamiltonians respectively, are:

$$E_e = T + V \tag{2.10}$$

$$E_{HF} = T_0 + (V_H + V_x) \tag{2.11}$$

Here T and V are the exact kinetic and electron-electron potential energy functionals, T_0 is the functional for the kinetic energy of a non-interacting electron gas, V_H stands for the Hartree contribution and V_x for the exchange contribution. By subtracting 2.11 from 2.10, the functional for the correlation contribution is

$$V_c = T_0 - T \quad (2.12)$$

The exchange contribution to the total energy is defined as the part which is present in the Hartree-Fock solution, but absent in the Hartree solution. Obviously, with the Hartree functional given by

$$E_H = T_0 + V_H \quad (2.13)$$

Which is defined as

$$V_x = V - V_H \quad (2.14)$$

Rewriting the Hohenberg-Kohn functional in the following way:

$$\begin{aligned} F_{HK} &= T + V + T_0 - T_0 \\ &= T_0 + V + \underbrace{(T - T_0)}_{V_c} \\ &= T_0 + V + V_c + V_H - V_H \\ &= T_0 + V_H + V_c + \underbrace{(V - V_H)}_{V_x} \\ &= T_0 + V_H + \underbrace{V_x + V_c}_{V_{xc}} \end{aligned}$$

Here V_{xc} is the exchange-correlation energy functional. Again we can write explicitly the energy functional:

$$E_{V_{ext}}[\rho] = T_0[\rho] + V_H[\rho] + V_{xc}[\rho] + V_{ext}[\rho] \quad (2.15)$$

By taking the above expression as the energy functional of a non-interacting classical electron gas, subject to two external potentials: one due to the nuclei, and one due to exchange and correlation effects. The corresponding Hamiltonian - called the Kohn-Sham Hamiltonian is

$$\hat{H}_{KS} = \hat{T}_0 + \hat{V}_H + \hat{V}_{xc} + \hat{V}_{ext} \quad (2.16)$$

$$= -\frac{\hbar^2}{2m_e} \vec{\nabla}_i^2 + \frac{e^2}{4\pi\epsilon_0} \int \frac{\rho(\mathbf{r}')}{|\mathbf{r} - \mathbf{r}'|} d\mathbf{r}' + V_{xc} + V_{ext} \quad (2.17)$$

where the exchange-correlation potential is given by the functional derivative

$$\hat{V}_{xc} = \frac{\delta V_{xc}[\rho]}{\delta \rho} \quad (2.18)$$

The theorem of Kohn and Sham can now be formulated as follows:

The exact ground-state density $\rho(\mathbf{r})$ of an N-electron system is

$$\rho(\mathbf{r}) = \sum_{i=1}^N \varphi_i(\mathbf{r})^* \varphi_i(\mathbf{r}) \quad (2.19)$$

where the single-particle wave functions $\varphi_i(\mathbf{r})$ are the N lowest-energy solutions of the Kohn-Sham Eqn.

$$\hat{H}_{KS} \varphi_i = \varepsilon_i \varphi_i \quad (2.20)$$

The single-particle wave functions φ_i are not the wave functions of electrons. They describe mathematical quasi-particles, without a direct physical meaning. Only the overall density of these quasi-particles is guaranteed to be equal

to the true electron density. Also the single-particle energies ε_i are not single-electron energies.

2.4 Local Density Approximation (LDA)

The LDA has been the most widely used approximation to the exchange-correlation energy in the density functional theory (DFT), for a long time. It has been proposed by Kohn and Sham (1965). The main idea is to consider general inhomogeneous electronic systems as locally homogeneous and then to use exchange-correlation hole corresponding to the homogeneous electron gas. LDA has been widely applied to portray a variety of close-ranged exchange-correlation interactions for instance, covalent bonding systems. However, LDA has serious limitation that this approximation cannot provide estimation to the long-ranged exchange-correlation interaction as typified by the Van der Waals (VdW) interaction. The VdW interaction is one of the long-ranged electronic interactions which mainly add to the first stage of the material reactions such as the chemical reaction, crystal growth and physical absorption. To assess the VdW interaction, many efforts have been devoted to develop useful calculating recipes for the non-local exchange-correlation term. The Hohenberg-Kohn theorem states that the energy of the ground state of a system of electrons is a functional of the electronic density especially, the exchange and correlation (XC) energy is also a functional of the density (this energy can be seen as the quantum part of the electron-electron interaction). This XC functional is not identified accurately and must be approximated. LDA is the simplest approximation for this functional, it is local in the sense that the electron exchange and correlation energy at any point in space is a

function of the electron density at that point only. The XC functional is the total of a correlation functional and an exchange functional:

$$E_{XC} = E_X + E_C \quad (2.21)$$

LDA uses the exchange for the uniform electron gas of a density equal to the density at the point where the exchange is to be assessed

$$E_{XC} = \int d^3r n(\mathbf{r}) \left(\frac{-3e^2}{4\pi} \right) \left(3\pi^2 n(\mathbf{r})^{1/3} \right) \quad (2.22)$$

It is found that all quantities are represented as functional of the electronic charge density. The significant point that makes this system easier to solve is that the efficient possibility is local. Therefore there is no more complication added in solving Schrodinger Eqn.. Of course, this is only true if the exchange-correlation energy can be portrayed as a function of the local charge density. A technique of doing this is known as the local density approximation (LDA). As mentioned above in LDA, the exchange-correlation energy of an electronic system is built by taking for granted that the exchange-correlation energy for each electron at a point r in the electron gas is equal to the exchange-correlation energy for each electron in a identical electron gas that has the same electron density at the point r . It follows therefore

$$E_{XC} [n(r)] = \int \varepsilon_{XC} (n(r)) n(r) dr \quad (2.23)$$

with

$$\varepsilon_{xc} (n(r)) = \varepsilon_{xc}^{\text{hom}} (n(r)) \quad (2.24)$$

where $\varepsilon_{xc}^{\text{hom}} (n(r))$ is exchange-correlation energy in identical electron gas.

Eqn. (2.24) is the supposition that the exchange-correlation energy is purely local.

Several parameterizations for $\varepsilon_{xc}^{\text{hom}}(n(r))$ exists, such as parameterization of Perdew and Zunger (1981).

2.5 Generalized Gradient Approximation

The first logical step to go beyond LDA is the use of not only the information about the density $\rho(\mathbf{r})$ at a particular point \mathbf{r} , but to supplement the density with information about the gradient of the charge density, $\nabla\rho(\mathbf{r})$ in order to account for the non-homogeneity of the true electron density. In other words, the gradient of the density will play a role. This approximation is therefore called the Generalized Gradient Approximation (GGA). Although GGA performs in general slightly better than LDA, there are a few drawbacks. There is only one LDA exchange-correlation functional, because there is a unique definition for ε_{xc} . But there is some freedom to incorporate the density gradient, and therefore several versions of GGA exist. Moreover, in practice one often fits a candidate GGA-functional with free parameters to a large set of experimental data on atoms and molecules. The best values for these parameters are fixed then, and the functional is ready to be used routinely in solids. Therefore such a GGA-calculation is strictly spoken not an ab initio calculation, as some experimental information is used. Thus, we write the exchange correlation energy in the following form termed Generalized Gradient Approximation (GGA)

$$E_{XC}^{GGA}[\rho_{\downarrow}, \rho_{\uparrow}] = \int \rho(\mathbf{r}) \varepsilon_{XC}^{\text{hom}}(\rho(\mathbf{r})) F_{XC}(\rho_{\downarrow}, \rho_{\uparrow}, |\nabla\rho_{\uparrow}(\mathbf{r})|, |\nabla\rho_{\downarrow}(\mathbf{r})|, \dots) d\mathbf{r} \quad (2.25)$$

Where F_{XC} is a dimensionless quantity and $\varepsilon_{XC}^{\text{hom}}$ is the exchange energy of the unpolarized gas. The largest error of this approximation actually arises from the gradient contribution to the correlation term. The early work of Gross and Dreizler, (1981) provided a derivation of second order expansion of the exchange density

matrix, which was later re-analysed and extended by Perdew, (1985). GGAs are typically based either on theoretical developments that reproduce a number of exact results in some known limits, for example 0 and ∞ density or the correlation potential in the He atom, or are generated by fitting a number of parameters to a molecular database. Normally, these improve over some of the drawbacks of the LDA, although this not always the case. What is needed for the functional is a form that mimics a re-summation to infinite order, and this is the main idea of the GGA, for which there is not a unique recipe. Naturally, not all the formal properties can be enforced at the same time, and differentiates one functional from another. A thorough comparison of different GGAs are done by Filippi *et al.* (1994). The generalized gradient approximation (GGA) has attracted much attention for its abstract simplicity and moderate computational workloads. At present, two GGA functional, one suggested by Becke and Perdew (BP) and one suggested more recently by Perdew and Wang (PW), are the most popular ones in the literature (Perdew *et al.*, 1996). Many calculations assessing the accuracy of the GGA have been reported and commonly demonstrate that the GGA substantially corrects the LDA error in the cohesive energies of molecules and solids. Generalized gradient approximations (GGA's) to the exchange-correlation (XC) energy in density-functional theory are at present receiving increasing attention as a straightforward substitute to improve over the local-density approximation (LDA) in *ab initio* total-energy calculations (Kresse and Furthmuller, 1996). The lattice parameters always rise in comparison with the LDA, a closer agreement with experimental data is reported for alkali metals, 3d metals, and some 4d metals.

2.6 Local Spin density approximation (LSDA)

In magnetic systems or, in other words we can say that the systems where open electronic shells are involved, better approximations to the exchange-correlation functional can be obtained by introducing the two spin densities such as $n \uparrow(\rho(r))$ and $n \downarrow(\rho(r))$ in LDA to obtain LSDA. The $E_{xc}[n^\sigma(r)]$ energy is a functional of both the spin-up and down spin densities. With such distinction, the Kohn-Sham Eqn. can be written as:

$$\left[-\frac{1}{2}\nabla^2 + V_{KS}^\sigma \right] \phi_i^\sigma(r) = \varepsilon_i^\sigma \phi_i^\sigma(r) \quad (2.26)$$

where V_{KS}^σ and $n^\sigma(r)$ are the spin extension of the previous quantities.

$$V_{KS}^\sigma(r) = v(r) + e^2 \int \frac{\rho(r')}{|r-r'|} dr' + \frac{\delta E_{xc}[n \uparrow, n \downarrow]}{\delta \rho^\sigma(r)}$$

$$v_{xc}^\sigma(r) = \frac{\delta E_{xc}[n \uparrow, n \downarrow]}{\delta \rho^\sigma(r)}, \rho^\sigma(r) = \sum |\phi_i^\sigma|^2, \rho(r) = \sum_\sigma \rho^\sigma(r) \quad (2.27)$$

The imbalance between $n \uparrow$ and $n \downarrow$ producing the magnetization $M = n \uparrow - n \downarrow$, is given by the exchange-correlation potential $U_{\sigma xc}(r)$ which accounts for the different populations $n \uparrow$ and $n \downarrow$ by the derivative. In the local spin density approximation (LSDA), the exchange and correlation contributions are separated as:

$$E_x^{LSDA}[\rho(r)] = \sum_\sigma \int \varepsilon_{xc}^{\text{hom}}(\rho^\sigma(r)) \rho^\sigma(r) dr \quad (2.28)$$

$$E_c^{LSDA}[\rho(r), \xi(r)] = \int \left[\varepsilon_c^U(\rho(r)) + f(\xi(r))(\varepsilon_c^P(\rho(r)) - \varepsilon_c^U(\rho(r))) \right] \rho(r) dr$$

where $\xi(r) = \left| \frac{n \uparrow(\rho(r)) - n \downarrow(\rho(r))}{n \uparrow(\rho(r)) + n \downarrow(\rho(r))} \right|$ is the normalized magnetization, $f(\xi(r))$ is a smoothing function, and ε_c^P and ε_c^U are proper functional representing the correlation energies for the spin-polarized and unpolarized systems, respectively.

2.7 The full-potential linearized augmented-plane wave (FP-LAPW) method

The full-potential linearized augmented-plane wave (FP-LAPW) technique is well known to allow most precise calculation of the electronic structure and magnetic qualities of crystals and surfaces. The application of atomic forces has greatly maximized its applicability, but it is still commonly supposed that FP-LAPW computations need considerable higher computational effort in comparison with the pseudopotential plane wave (PPW) based techniques. FP-LAPW has recently showed important progress. For example, researchers habitually work out magnetism and nuclear quantities (for example, isomer shifts, hyperfine fields, electric field gradients, and core level shifts). Also, forces and molecular dynamics have been applied, and recent optimizations have decreased the CPU time of FP-LAPW calculations significantly. Nevertheless, because the computational expense and memory requirements are still fairly high, FP-LAPW implementations are suitable only to fairly complicated systems. One successful implementation of the FP-LAPW technique is the program package WIEN2K, a code enhanced by Blaha, Schwarz and coworkers (Blaha *et al.*, 2008). It has been successfully implemented to a various scope of difficulties such as electric field gradients and systems such as high-temperature superconductors, minerals, surfaces of transition metals, or anti-ferromagnetic oxides and even molecules (Ernst *et al.*, 2005). So far the main disadvantage of the FP-LAPW-technique in comparison with the pseudopotential plane-wave (PPW) method has been its higher computational expense. This may be largely because of an inconsistency in optimization efforts spent on both techniques, and so we have investigated the FP-LAPW technique from a computational arithmetical viewpoint. Lately, the development of the Augmented Plane Wave

(APW) techniques from Slater's APW, to LAPW and the new APW+lo was portrayed by Schwarz *et al.* (2003).

One of the most precise techniques for performing electronic structure calculations for crystals is the FP-LAPW technique. It is based on DFT for the handling of exchange and correlation and uses (for example, the LSDA). Effects, for valence states relativistic, can be incorporated either in a scalar relativistic handling or with the second dissimilarity technique including spin-orbit coupling. Core states are treated fully relativistically. The FP-LAPW technique, which is like most energy-band techniques is a process for solving the Kohn-Sham Eqns. for the ground state density, total energy, and (Kohn-Sham) eigen values (energy bands) of a many-electron system by presenting a basis set which is particularly modified to the problem. This alteration is achieved by partitioning the unit cell (Fig. 2.) into (I) non-overlapping atomic circles (centered at the atomic sites) and (II) an interstitial region, that's to say, a region between two spaces. In the two sorts of regions diverse basis sets are used:

(i) Inside atomic sphere t of radius R_t a linear combination of radial functions times spherical harmonics $Y_{lm}(r)$ is used:

$$\phi_{k_n} = \sum_{lm} [A_{lm}u_l(\mathbf{r}, E_l) + B_{lm}u_l(\mathbf{r}, E_l)] Y_{lm}(\mathbf{r}) \quad (2.29)$$

where $u_l(r, E_l)$ is the (at the origin) normal way out of the radial Schrodinger Eqn. for energy E_l and the spherical part of the potential inside sphere, $u_l(r, E_l)$ is the energy derived of u_l taken at the similar energy. A linear mixture of these two functions comprise the linearization of the radial function; the coefficients A_{lm} and B_{lm} are functions of k_n decided by requiring that this root function u_l goes with the

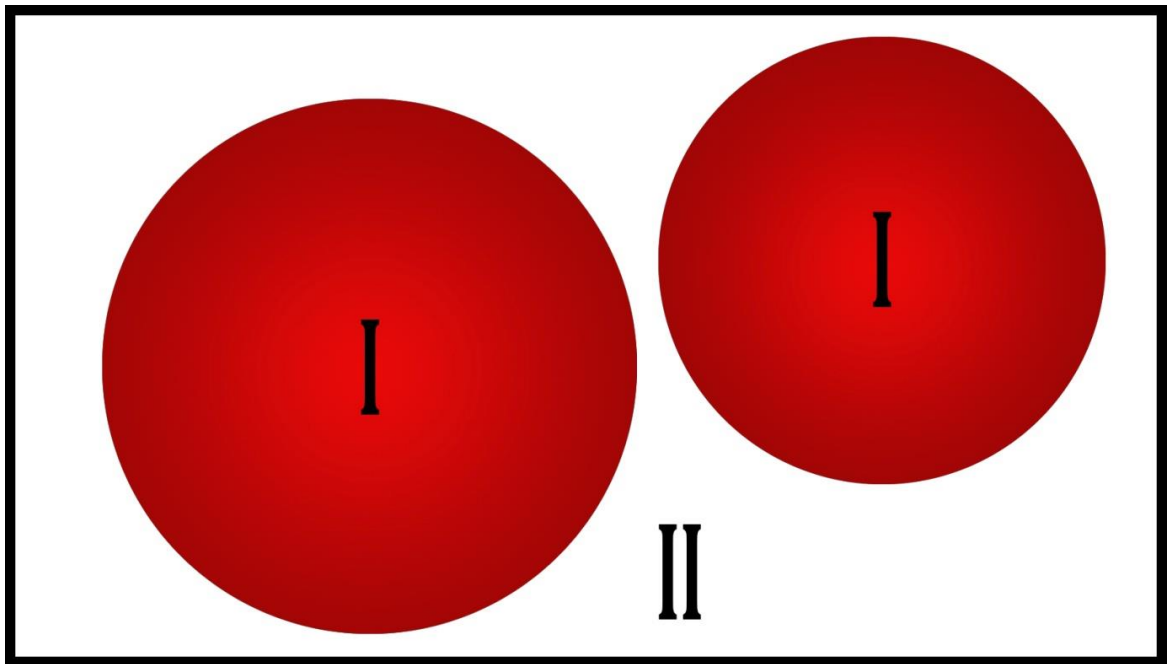


Fig. 2.1 Partitioning of the unit cell into atomic spheres (I) and an interstitial region (II).

equivalent basis function of the interstitial region; u_l and are achieved by numerical integration of the radial Schrodinger Eqn. on a radial mesh inside the sphere.

(ii) In the interstitial zone a plane wave extension is applied

$$\phi_{kn} = \frac{1}{\sqrt{w}} e^{ik_n r} \quad (2.30)$$

where $k_n = k + k_n$, k_n , are the mutual lattice vectors and k is the wave vector inside the first Brillouin zone. Each plane wave is increased by an atomic-like function in every atomic sphere. The solutions to the Kohn-Sham equations are extended in this joint basis set of LAPW's according to the linear dissimilarity technique

$$\psi_k = \sum_n C_n \phi_{k_n} \quad (2.31)$$

and the coefficients C_n , are decided by the Rayleigh-Ritz variation rule. The union of this basis set is controlled by a disconnected parameter $R_{MT} \times K_{max} = 6 - 9$, where R_{MT} is the smallest atomic sphere radius in the unit cell and K_{max} is the magnitude of the largest K vector. Additional (K_n independent) basis functions can be added to improve upon the linearization and to make possible a reliable treatment of semi core and valence states in one energy window .They are called ‘‘local orbitals’’ and consist of a linear combination of 2 radial functions at 2 dissimilar energies and one energy derivative:

$$\phi_{lm}^{LO} = [A_{lm} u_l(\mathbf{r}, E_{1,l}) + B_{lm} u_l(\mathbf{r}, E_{1,l}) + C_{lm} u_l(\mathbf{r}, E_{2,l})] Y_l(\hat{r}) \quad (2.32)$$

The coefficients A_{lm} , B_{lm} , and C_{lm} , are decided by the necessities that ϕ_{lm}^{LO} should be regularized and has zero value and slope at the sphere border. The FP-LAPW technique, in its general form, extends the potential in the following form

$$V(\vec{r}) = \begin{cases} \sum_{lm} V_{lm}(\mathbf{r}) Y_{lm}(\hat{r}) & \text{inside sphere} \\ \sum_K V_K e^{ikr} & \text{outside sphere} \end{cases} \quad (2.33)$$

2.8 Modified Becke Johnson Potential (mBJ)

The density functionals of the local density (LDA) and generalized gradient (GGA) approximations are the standard choice for the exchange–correlation energy $E_{xc} = E_x + E_c$ to perform calculations on periodic solids with the Kohn–Sham method (Kohn and Sham, 1965) of density functional theory (Hohenberg and Kohn, 1964), whose Eqn.s are

$$\left(-\frac{1}{2} \nabla^2 + v_{eff,\sigma}^{KS}(\mathbf{r}) \right) \psi_{i,\sigma}(\mathbf{r}) = \varepsilon_{i,\sigma} \psi_{i,\sigma}(\mathbf{r}) \quad (2.34)$$

where $v_{eff,\sigma}^{KS} = v_{ext} + v_H + v_{xc,\sigma}$ is the Kohn–Sham multiplicative effective potential whose components are the external Hartree, and exchange–correlation ($v_{xc,\sigma} = \delta E_{xc} / \delta \rho_\sigma = v_{x,\sigma} + v_{c,\sigma}$) terms, respectively. In many cases, the LDA and GGA functionals (Perdew *et al.*, 1996, 1997) are able to provide reliable results for the geometry (i.e., equilibrium structure) and electronic structure of solids. Nevertheless, some problems remain with these approximations, and the most notorious is the under estimation of the band gap, which is often too small, or even absent, compared to experimental results (Perdew, 1986). It is also well known that rigorously the Kohn–Sham eigen values should not be used for excitation energies, but it is common practice to do so. Mainly responsible for this deficiency in the band gap is the self-interaction error contained in the LDA and GGA exchange–correlation potentials (Perdew and Zunger, 1981).

There are alternative ways to have an estimate of the experimental band gap. One can use a method which lies outside the KS framework by using a non-multiplicative potential. Hybrid functionals (e.g., HSE (Heyd *et al.*, 2005)), in which a fraction of exact exchange replaces a fraction of the LDA or GGA exchange, also improve the band gap. However, the hybrid methods are more expensive and also not satisfactory in all cases. Another possibility is the LDA+U (Anisimov *et al.*, 1991) method, but it can only be applied to correlated and localized electrons, e.g., $3d$ or $4f$ in transition and rare-earth oxides. Very successful but also very expensive methods are the combination of LDA with dynamical mean-field theory (LDA + DMFT) (Georges *et al.*, 1996) and of course GW (Bechstedt *et al.*, 2009). In fact, with such non-multiplicative potentials (a part of) Δ_{xc} is contained in the CBM – VBM difference.

Nevertheless, if one wants to stay inside the KS framework and still use a computationally cheap semi-local method that leads to KS band gaps which are close to the experimental band gaps, the potential of Becke and Johnson (BJ) (Becke and Johnson, 2006) can be a good starting point. The multiplicative BJ potential reads

$$v_{x,\sigma}^{BJ}(\mathbf{r}) = v_{x,\sigma}^{BJ}(\mathbf{r}) + \frac{1}{\pi} \sqrt{\frac{5}{6}} \sqrt{\frac{t_{\sigma}(\mathbf{r})}{\rho_{\sigma}(\mathbf{r})}}, \quad (2.35)$$

where $\rho_{\sigma} = \sum_{i=1}^{N_{\sigma}} |\psi_{i,\sigma}|^2$ is the electron density, the kinetic-energy density is

given by

$$t_{\sigma} = 1/2 \sum_{i=1}^{N_{\sigma}} \nabla \psi_{i,\sigma}^* \cdot \nabla \psi_{i,\sigma} \quad (2.36)$$

$$v_{x,\sigma}^{BJ}(\mathbf{r}) = -\frac{1}{b_{\sigma}(\mathbf{r})} \left(1 - e^{-x_{\sigma}(\mathbf{r})} - \frac{1}{2} x_{\sigma}(\mathbf{r}) e^{-x_{\sigma}(\mathbf{r})} \right) \quad (2.37)$$

is the Becke-Roussel (BR) (Becke and Roussel, 1989) exchange potential, which was proposed to model the Coulomb potential created by the exchange hole. In Eq. (2.37), x_σ is determined from a nonlinear Eqn. involving ρ_σ , $\nabla\rho_\sigma$, $\nabla^2\rho_\sigma$, and t_σ , and then b_σ is calculated with $b_\sigma = [x_\sigma^3 e^{-x_\sigma} / (8\pi\rho_\sigma)]^{1/3}$. The asymptotic behavior of $v_{x,\sigma}^{BJ}$ is that of the exact KS exchange potential. The $\sqrt{t/\rho}$ term was introduced to reproduce the step structure of the OEP in atoms and can be considered as a kind of screening term.

The BJ exchange potential has been implemented (Tran *et al.*, 2007) self-consistently into the WIEN2k code (Blaha *et al.*, 2001) which is based on the full-potential (linearized) augmented plane-wave and local orbitals method to solve the KS equations for periodic systems. Tran *et al.* (2007) showed that the BJ potential improves over LDA and PBE for the description of band gaps; i.e., the obtained values for CBM – VBM were larger and hence closer to experiment. However, the improvement was moderate. Further improvement has been achieved by a modified version (TB-mBJ) (Tran and Blaha, 2009) of the BJ exchange potential which introduces a parameter to change the relative weights of the two terms in the BJ potential:

$$V_{x,\sigma}^{MBJ}(r) = cV_{x,\sigma}^{BR}(r) + (3c - 2) \frac{1}{\pi} \sqrt{\frac{5}{12}} \sqrt{\frac{2t_\sigma(r)}{\rho_\sigma(r)}} \quad (2.38)$$

where $\rho_\sigma(r)$ is the spin dependent density of states, $t_\sigma(r)$ is the kinetic energy density and $V_{x,\sigma}^{MBJ}(r)$ is the Becke-Roussel potential (BR) (Engel, 2009). The c stands for

$$c = A + B \sqrt{\frac{1}{V_{cell}} \int d^3r \frac{|\Delta\rho(r)|}{\rho(r)}} \quad (2.39)$$

A and B are parameters adjusted to produce the best fit to the experimental values of the semiconductor band gaps. In the WIEN2k code, the kinetic-energy density t_σ is not calculated with Eqn. (2.37) but instead with the equivalent expression

$$t_\sigma = \sum_{i=1}^{N_\sigma} \varepsilon_{i,\sigma} |\psi_{i,\sigma}(\mathbf{r})|^2 - v_{eff,\sigma}^{KS}(\mathbf{r}) \rho_\sigma(\mathbf{r}) + \frac{1}{4} \nabla^2 \rho_\sigma(\mathbf{r}) \quad (2.40)$$

which depends on the potential $V_{eff,\sigma}^{KS}$, entering the Kohn–Sham equations (Eqn. (2.34)). For the evaluation of Eqn. (2.41), the exchange–correlation part of $V_{eff,\sigma}^{KS}$ was taken from the previous iteration of the self-consistent procedure. A Newton algorithm was used to solve the non-linear Eqn. for x_σ in each point of space, and we ensured always obtaining a positive real value (which is unique). The calculations with the mBJ exchange potential are done without correlation or in combination with LDA correlation (Perdew and Wang, 1992).

2.9 Equation of states

The calculated total energies (E) within GGA as function of the volume (V) were used for determination of theoretical lattice constant and bulk modulus. Equilibrium lattice constant, isothermal bulk modulus, its pressure derivative are calculated by fitting the calculated total energy to the Murnaghan’s Eqn. of state (Murnaghan, 1944). A series of total energy calculations as a function of volume can be fitted to an Eqn. of states according to Murnaghan.

$$E(V) = E_0 + \left[\frac{(V_0/V)^{B'_0}}{B'_0 - 1} + 1 \right] - \frac{B_0 V_0}{B'_0 - 1} \quad (2.41)$$

where E_0 is the minimum energy at $T = 0K$, B_0 is the bulk modulus at the equilibrium volume and B_0' is pressure derivative of the bulk modulus at the equilibrium volume. The equilibrium volume is given by the corresponding total energy minimum as shown in Fig. 2.3.

$$\text{Pressure, } P = -\frac{dE}{dV} \text{ and Bulk modulus, } B_0 = -V \frac{dP}{dV} = V \frac{d^2E}{dV^2}$$

2.10 Optical Properties

Interaction of radiation with matter gives various interesting phenomena such as absorption, transmission, reflection, scattering or emission. The study of these properties provides several informations with regard to the behaviour of matter in various energy ranges (Pines, 1963). The electrons of the matter absorb the energy of the incident light and jumps from occupied valence state to the unoccupied conduction state. This kind of transitions provides the understanding of the location of the initial and the final energy bands and symmetry of their associated wave functions (Callaway, 1974a). This is infact related to the response function of the system which is strongly dependent on the frequency of the incident radiation and the wave vector which is given by $\varepsilon(\omega, q)$. In the infrared and higher energy radiation (long wavelength limit) the dielectric function is dependent only on frequency compared to wave vector (Callaway, 1974b) and hence the dielectric function can be written as $\varepsilon(\omega, 0)$ which is the combination of real and imaginary parts and is given by

$$\varepsilon(\omega) = \varepsilon_1(\omega) + i\varepsilon_2(\omega), \quad (2.42)$$

where $\varepsilon_1(\omega)$ and $\varepsilon_2(\omega)$ are the real and imaginary parts of dielectric function. When the electromagnetic radiation falls on crystal it interacts with the electrons of the crystal. We assume that the crystal is free of imperfections, the total Hamiltonian of the electromagnetic radiation on perfect crystal is given by

$$H = \frac{1}{2m} (\vec{P} + e\vec{A})^2 + V(\vec{r}) \quad (2.43)$$

where \vec{P} is the momentum, \vec{A} and $V(\vec{r})$ are the vector potential and periodic crystal potential respectively.

The first order perturbation operator describing the interaction between the radiation and the electrons is

$$H_o(\vec{r}, t) = \frac{e}{m} (\vec{A} \cdot \vec{p}) \quad (2.44)$$

The vector potential for a plane wave can be written as,

$$\vec{A} = \vec{A}_o \hat{e} \exp \left[i(\vec{k} \cdot \vec{r} - \omega t) \right] + c.c. \quad (2.45)$$

where \hat{e} the unit vector of polarization in the direction of the electric field and $c.c.$ is the complex conjugate. The second term is neglected which is the emission term and only the first term is considered which gives the absorption.

The transition probability for an electron going from an occupied valence state $E_v(\vec{k}_v)$ to an empty conduction state $E_c(\vec{k}_c)$ can be written as,

$$w(\omega, t, \vec{k}_v, \vec{k}_c) = \frac{e^2}{m^2 \hbar^2} \left| \int_0^t dt' \int_V d\vec{r} \psi_c(\vec{k}_c, \vec{r}, t) \vec{A} \cdot \vec{p} \psi_v(\vec{k}_v, \vec{r}, t) \right|^2 \quad (2.46)$$

Here, Bloch type eigen functions ψ_c and ψ_v belongs to E_v and E_c respectively and can be written as

$$\psi_v(\vec{k}_v, \vec{r}, t) = \exp\left[-i\hbar^{-1}E_v(\vec{k}_v)t\right] \exp(i\vec{k}_v \cdot \vec{r}) u_v(\vec{k}_v, \vec{r}) \quad (2.47)$$

Here both u_v and u_c are the periodic wave functions with periodicity of the lattice. Combining Eqs. 2.45, 2.46, 2.47, and using

$$\vec{E} = -\frac{\delta \vec{A}}{\delta t} \quad (2.48)$$

We get

$$w(\omega, t, \vec{k}_v, \vec{k}_c) = \frac{e^2 E_o^2}{m^2 \omega^2} \left| \int_0^t dt' \exp\left[i\hbar^{-1}(E_c - E_v - \hbar\omega)t'\right] \vec{e} \cdot \vec{M}_{cv} \right|^2 \quad (2.49)$$

with the matrix element

$$\vec{e} \cdot \vec{M}_{cv} = \int_v d\vec{r} \exp\left[-i(\vec{k}_c - \vec{k}) \cdot \vec{r}\right] u_c^* \vec{e} \cdot \vec{\nabla} \exp(i\vec{k}_v \cdot \vec{r}) u_v \quad (2.50)$$

here the matrix element will vanish unless $\vec{k}_c - \vec{k} = \vec{k}_v + \vec{k}_n$, where \vec{k}_n is the reciprocal lattice vector.

Since $\vec{k} = \frac{2\pi}{\lambda}$ is very small as compared to the linear dimensions of Brillouin

Zone (BZ) it can be neglected. This gives the condition that that only vertical transitions without a change of the wave vector are allowed and is called direct transitions. The integration of Eq. 2.49 over t' gives

$$w(\omega, t, \vec{k}_v, \vec{k}_c) = \frac{e^2 E_o^2}{m^2 \omega^2} \left| \frac{\exp[i(E_c - E_v - \hbar\omega)t/\hbar] - 1}{i(E_c - E_v - \hbar\omega)/\hbar} \vec{e} \cdot \vec{M}_{cv} \right|^2 \quad (2.51)$$

from which we obtain the transition probability per unit time as

$$\vec{W}_{cv} = \frac{\hbar e^2 E_o^2}{2\pi^2 m^2 \omega^2} \int d\vec{k} \left| \vec{e} \cdot \vec{M}_{cv} \right|^2 \delta(E_c - E_v - \hbar\omega) \quad (2.52)$$

The δ function contains the second selection rule and transition probability is different from zero if the initial and final state energy difference is equal to photon energy. We can now obtain the various optical constants as follows: The frequency dependent optical conductivity (σ) given by (Reshak, 2007),

$$\sigma(\omega) = 2W_{cv} \hbar \omega / \vec{E}_0^2 \quad (2.53)$$

The imaginary part of dielectric function is

$$\varepsilon_2(\omega) = \frac{4\hbar^2 e^2}{\pi m^2 \omega^2} \int d\vec{k} \left| \vec{e} \cdot \vec{M}_{cv} \right|^2 \delta(E_c - E_v - \hbar\omega) \quad (2.54)$$

$$\varepsilon_2(\omega) = \frac{4\hbar^2 e^2}{\pi m^2 \omega^2} \int_c ds \frac{\left| \vec{e} \cdot \vec{M}_{cv} \right|^2}{\left| \vec{\nabla}_k (E_c - E_v) \right|_{E_c - E_v = \hbar\omega}} \quad (2.55)$$

The real part of the dielectric function can be calculated using the Kramers-Kronig relations from imaginary part $\varepsilon_2(\omega)$,

$$\varepsilon_1(\omega) = 1 + \frac{2}{\pi} \int_0^\infty \frac{\omega'}{(\omega')^2 - \omega^2} \varepsilon_2(\omega') d\omega' \quad (2.56)$$

The dielectric function is not directly accessible experimentally for the optical measurements, hence they have to be calculated from the other parameters.

They are reflectivity $R(\omega)$, the refractive index $n(\omega)$ and extinction coefficient $k(\omega)$. These experimentally observable quantities are related to real and imaginary parts of the dielectric function as follows:

The optical reflectivity spectra are derived from the Fresnel's formula for normal incidence assuming an orientation of the crystal surface parallel to the optical axis using the relation (Ambrosch *et al.*, 1998; Yu *et al.*, 1999).

$$R(\omega) = \left| \frac{\sqrt{\varepsilon(\omega)} - 1}{\sqrt{\varepsilon(\omega)} + 1} \right|^2 \quad (2.57)$$

While the electron loss-function $\left(-I_m\left(\frac{1}{\varepsilon}\right)\right)$ is given by (Yu *et al.*, 1999, Fox, 2002; Dressel *et al.*, 2001)

$$-I_m\left(\frac{1}{\varepsilon}\right) = L(\omega) = \frac{\varepsilon_2(\omega)}{\varepsilon_1^2(\omega) + \varepsilon_2^2(\omega)} \quad (2.52)(2.58)$$

We calculate the absorption coefficient $I(\omega)$ and real part of optical conductivity $\text{Re}|\sigma(\omega)|$ using the following expression (Ambrosch *et al.*, 1998; Delin *et al.*, 1996)

$$I(\omega) = \alpha(\omega) = 2\omega \left[\frac{\sqrt{\varepsilon_1^2(\omega) + \varepsilon_2^2(\omega)} - \varepsilon_1(\omega)}{2} \right] \quad (2.59)$$

$$\text{Re}|\sigma(\omega)| = \sigma(\omega) = \frac{\omega\varepsilon_1}{4\pi} \quad (2.60)$$

Also, the optical spectra such as the refractive index, $n(\omega)$ and the extinction coefficient, $K(\omega)$, are calculated in terms of the components of the complex dielectric function as follows (Delin *et al.*, 1996; Fox, 2002; Dressel *et al.*, 2001).

$$n(\omega) = \left\{ \frac{\varepsilon_1(\omega)}{2} + \frac{\sqrt{\varepsilon_1^2(\omega) + \varepsilon_2^2(\omega)}}{2} \right\}^2 \quad (2.61)$$

$$K(\omega) = \left\{ \frac{\sqrt{\varepsilon_1^2(\omega) + \varepsilon_2^2(\omega)}}{2} - \frac{\varepsilon_1(\omega)}{2} \right\}^2 \quad (2.62)$$

2.11 The WIEN2k Code

The calculations in this work are performed using the WIEN2k computer code (Blaha *et al.*, 2012). This code contains several sub-programs, few of which are described briefly below. There are two major parts in the program, the initialization and the self-consistent field (SCF) cycle. The flow chart of the code is given in Fig. 2.2.

- **Initialization** (Setting up the unit cell and generating the initial density):

In this sub-program, atomic densities are generated and superimposed to obtain a initial crystal density for the SCF calculation. Additionally, the atomic potentials and optionally, atomic valence densities are created. Information about l , m values of the lattice harmonics representation and number of Fourier coefficients of the interstitial charge density are inserted as input file in this part.

- **LAPW0** (Construction of the effective potential):

The Poisson equation is solved and the total potential is computed as the sum of the Coulomb and the exchange-correlation potential in the LAPW0 program. The electron (spin) density is used as input and the spherical ($l = 0$) and the non-spherical parts of the potential are generated. The exchange-correlation potential is computed numerically on a grid. Additionally, the Hellmann-Feynman force contribution to the force is also determined.

- **LAPW1** (Solving the Kohn-Sham equations of valence electrons):

The Hamiltonian and the overlap matrix are set up in LAPW1. Their diagonalization provides the eigenvalues and eigenvectors. Both the LAPW and the APW+lo methods are supported. For maximum efficiency a mix of both are recommended, i.e. the APW+lo basis functions are used for physically meaningful l values, while LAPW basis functions are employed to describe higher l -values functions.

- **LAPW2** (Construction of the new electron density):

The Fermi-energy is computed. The electronic charge densities are expanded according to the representation of Eq. 2.36 for each occupied state and each k-vector. Afterwards the corresponding (partial) charges inside the atomic spheres are obtained by integration.

- **LCORE** (The treatment of the core electrons):

The potential and the charge density of the core electrons are computed.

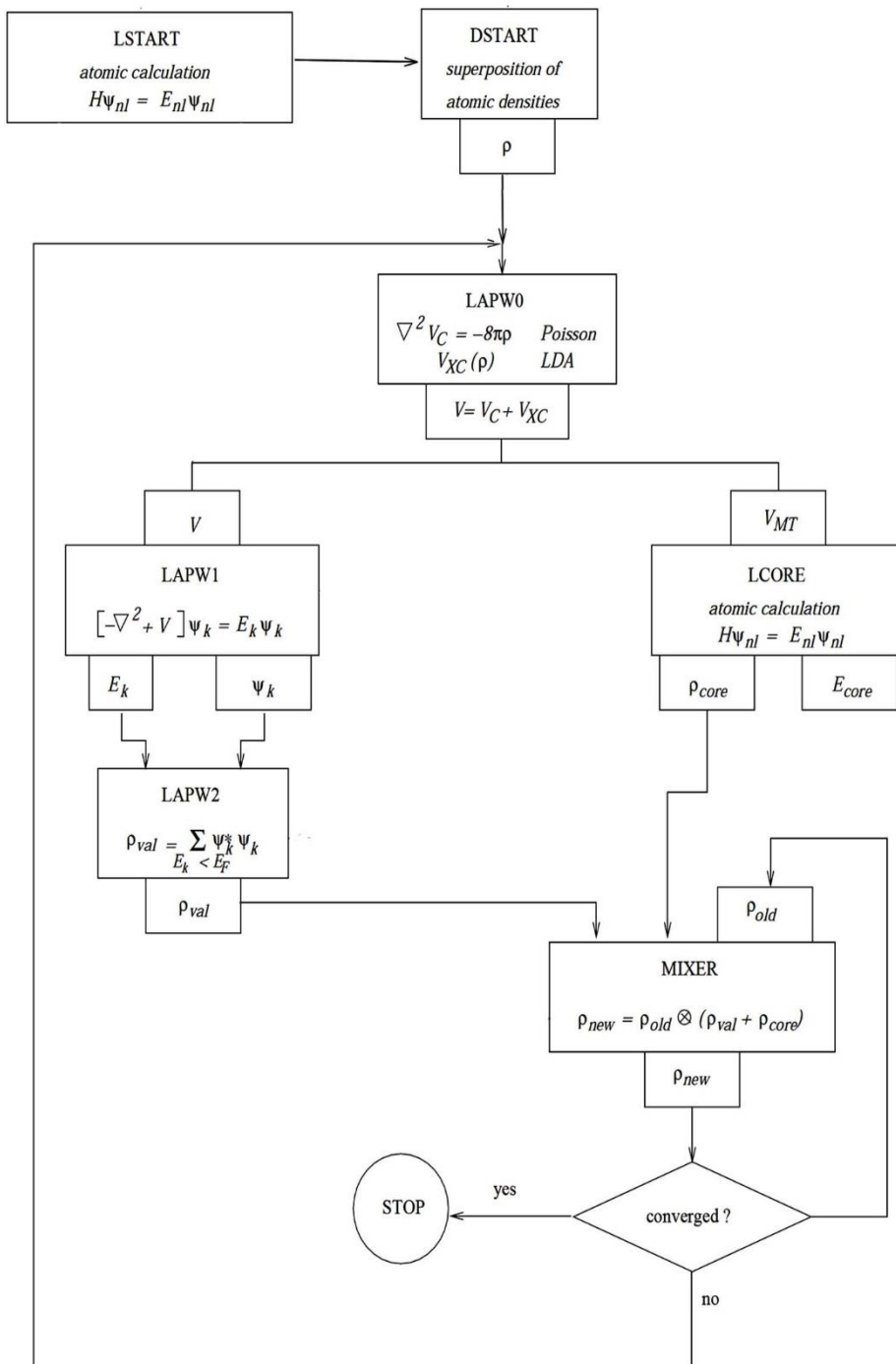


Fig. 2.2: Flow chart of WIEN2k code

- **LMIXER** (Generating the input density for the next iteration):

The electron densities of core, semi-core, and valence states are combined to yield the total new density. Taking only the new densities would, however, lead to instabilities in the iterative SCF process. To have a stable SCF cycle new and old densities need to be mixed, to obtain a new density.

$$n_{new}^{m+1} = (1 - \alpha)n_{new}^m + \alpha n_{old}^m \quad (2.63)$$

here α is a mixing parameter. In the WIEN2k code this is done (mainly) using the Broyden scheme. The total energy and the atomic forces are computed in mixer, as well.

It is well known that for localized electrons LDA and GGA methods are not accurate enough for a proper description of some of the strongly correlated systems. Thus other methods like LDA+U and Orbital polarization are also implemented in this program. In WIEN2k (Blaha *et al.*, 2012) the effective Coulomb- exchange interaction ($U_{\text{eff}} = U - J$) is used for the LDA+U calculations (Anisimov *et al.*, 1991, 1997). This particular scheme is used in WIEN2k to include double-counting corrections, however, it neglects multiple terms. It should be mentioned that the +U was used on top of GGA or LSDA parametrization of the exchange-correlation functional. A significant difference was observed using one or the other of the parameterizations.

3

Study of Electronic and Optical properties of Double Perovskites A_2MgWO_6 ($A = Ba, Sr$)

In this chapter, the study of the electronic and optical properties of cubic double perovskites A_2MgWO_6 ($A = Ba$ and Sr) by using the generalized gradient approximation (GGA) potential. The combination of the elements for the formation of the perovskite in this study is : (a) the element A are Ba and Sr which are Alkaline Earth elements (b) The combination of the elements B and B' is Mg and W respectively which are transition elements. The result of density of states (DOS), electronic band structures and optical properties have been studied for Ba_2MgWO_6 and Sr_2MgWO_6 using the Wien2k program (Blaha *et al.*, 2012).

3.1 Crystal structure

All atomic positions are in fractional coordinates (Wyckoff, 1935). Fig. 3.1 shows that the (100) plane of the corresponding conventional unit cell which was displayed by XCrySDen (Kokalj, 2003). The structural optimization based on Murnaghan's equation of state (Murnaghan, 1994) was performed to obtain the relax structure with minimum energy, the obtained optimized lattice parameters are summarized in Table 3.1. The structural optimization defines the energy versus volume plot for A_2MgWO_6 ($A = Ba$ and Sr) which are given in Figs. 3.2 and 3.3. The optimized lattice constants were used to calculate the electronic structure and optical properties.

The double perovskites compound A_2MgWO_6 (where A are Ba and Sr) contain four atoms in the unit cell which forms the base of fcc lattice. The crystal structure is shown in Fig. 3.1 and found to crystalize in the cubic phase with space group Fm-3m (No. 225). The Wycokff's atomic positions of the atoms are given by A=Ba, Sr (8c)(0.25, 0.25, 0.25), Mg (4b)(0.5, 0.5, 0.5), W (4a)(0,0,0), and O (24e)(u,0,0), respectively.

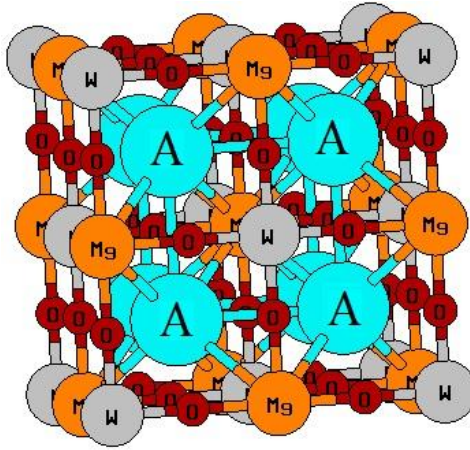


Fig. 3.1. Crystal structure of A_2MgWO_6 (A = Ba, Sr)

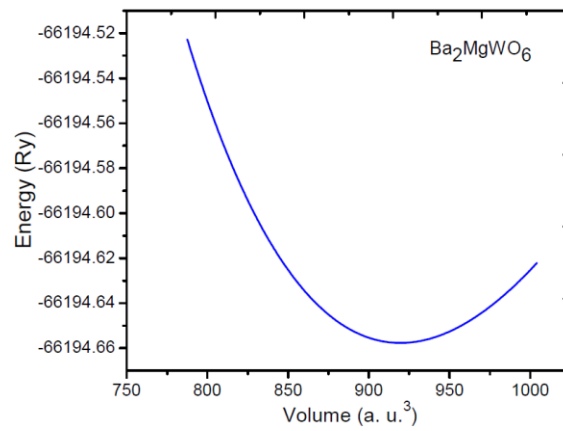


Fig. 3.2. Volume optimization of Ba_2MgWO_6

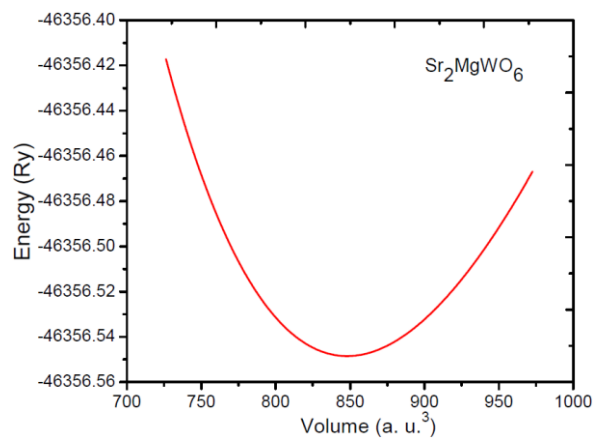


Fig. 3.3. Volume optimization of Sr_2MgWO_6

Table 3.1. Calculated lattice constant (a), internal atomic parameters u, bulk modulus B (in GPA) and pressure derivative of bulk modulus (B') of A₂MgWO₆ (A = Ba, Sr)

Compound	Calculated (a)	Previous (a)	u	B(GPA)	B'
Ba ₂ MgWO ₆	8.1685	8.112 ^a	0.2551	157.1005	4.3944
Sr ₂ MgWO ₆	7.9510	7.9524 ^b	0.2556	166.1450	4.3527

^a(Filipev *et al.*, 1974), ^b(Patwe *et al.*, 2005)

3.2 Computational details

In this method, the space is divided into non-overlapping muffin-tin (MT) spheres separated by an interstitial region. The basis functions are expanded into spherical harmonic functions inside the muffin-tin sphere and the Fourier series in the interstitial region. The convergence of basis set was controlled by a cutoff parameter $R_{\text{MT}} \times K_{\text{max}} = 7$ where R_{MT} is the smallest of the MT sphere radii and K_{max} is the largest reciprocal lattice vector used in the plane wave expansion. The cutoff energy which defines the separation of valence and core states was chosen as -6.0 Ry. For k-point sampling, a 12 x 12 x 12 k-point mesh in the first Brillouin zone was used. The self-consistent calculations were considered to be converged until the integrated charge difference between the last two iterations was less than 10^{-4} eV. The theoretically obtained lattice parameters have been used here for DOS, energy bands calculations etc.

3.3 Results of Density of states (DOS)

In this section, we present the results of total density of states (DOS) and the partial density of states (PDOS) in the case of double perovskites $A_2\text{MgWO}_6$ ($A = \text{Ba}$ and Sr). For the combinations of the elements, we have chosen the alkaline earth elements A as Ba and Sr, transition metals B as Mg and B' as W.

3.3.1 Density of states for Ba_2MgWO_6

In this section, we present the results of density of states (DOS) calculated in the case of Ba_2MgWO_6 double perovskites using the GGA potential. The optimized lattice constants given in Table 3.1 were used to calculate the electronic structures of Ba_2MgWO_6 perovskites.

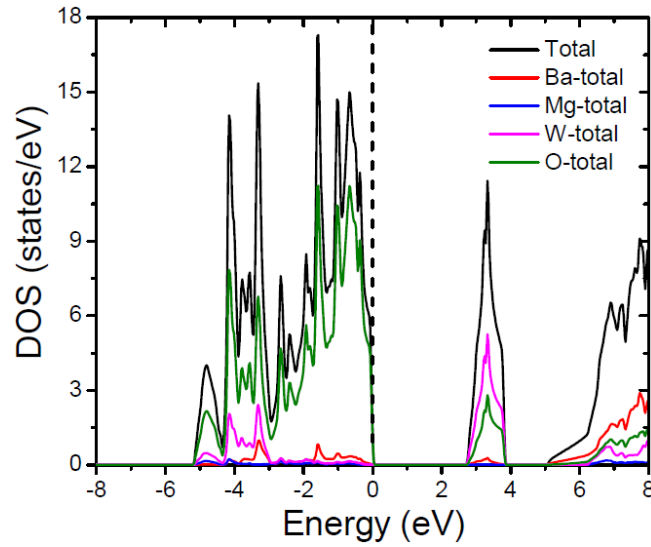


Fig. 3.4. Total DOS plot for Ba_2MgWO_6

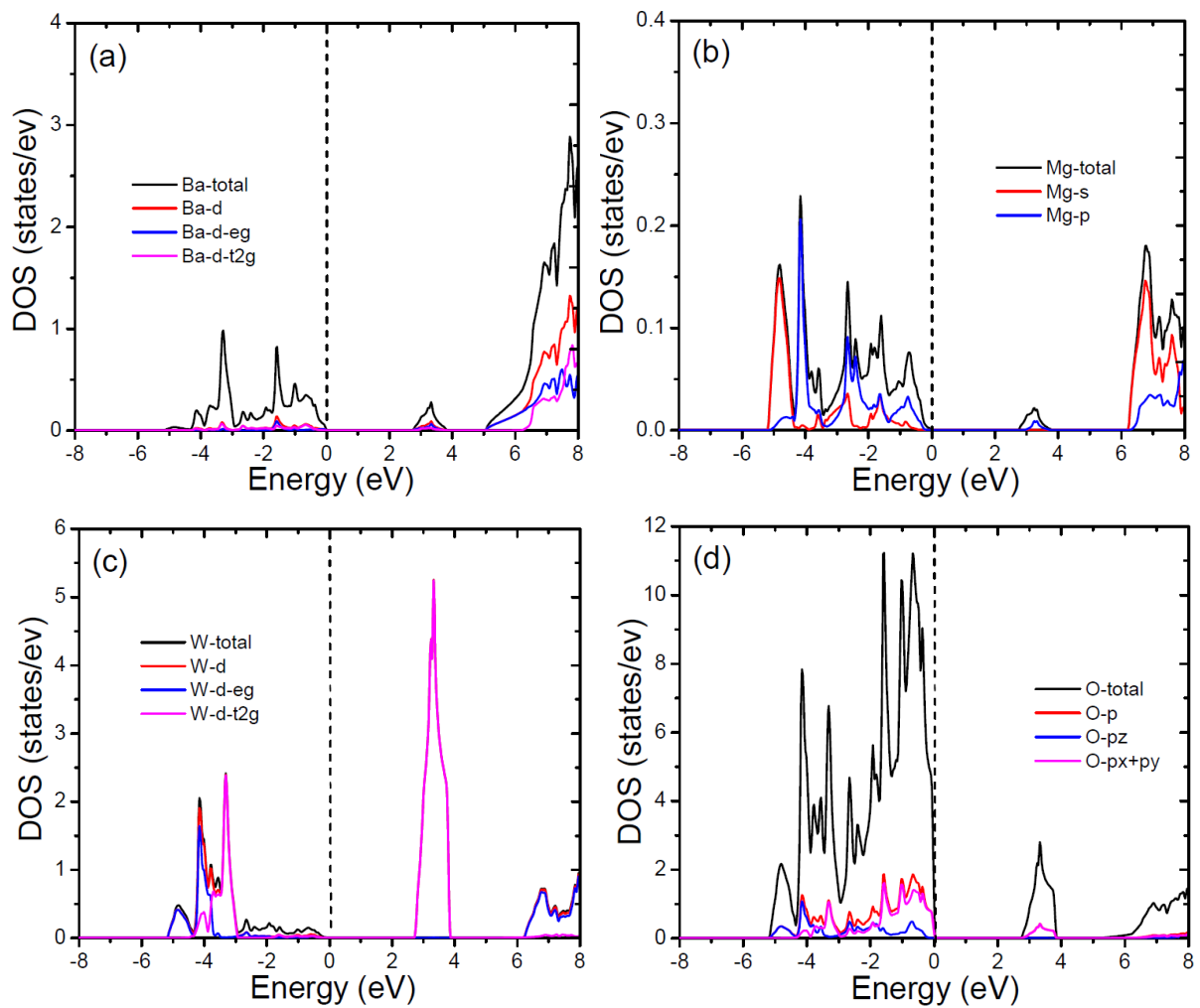


Fig. 3.5. TDOS and PDOS plot for individual atom of Ba_2MgWO_6

The total density of states (TDOS) and partial density of states (PDOS) of Ba_2MgWO_6 and the individual atoms Ba, Mg, W and O are given in Fig. 3.4 and 3.5 respectively. It is seen from Fig. 3.4 that there is maxima in TDOS of Ba_2MgWO_6 which is about ~ 17 states/eV that occurs at -1.5 eV below Fermi level ($E_F = 0$) in valence band. From the plots of TDOS of individual atoms, it is seen that only the TDOS of O atom is maximum and coincides almost with TDOS in the valence band. The other atoms Ba and Mg except W are having negligible contribution to TDOS since minor contribution from W at ~ -3 eV in the valence band as seen in the plots. In the conduction band, the maxima in the TDOS of Ba_2MgWO_6 is 11.5 states/eV which occurs at around 3.5 eV energy contributed by W atom above the Fermi level. Ba and O atoms give several trend above the Fermi level except W who are having negligible contribution in the conduction region. We observe a gap between the valence and the conduction band and the value of this energy band gap is 2.753 eV.

To find out exactly which atoms or the electrons from different states do contribute to the TDOS, we have also plotted the PDOS of each individual atoms along with their respective TDOS. These are shown for all the atoms in Fig 3.5. In Fig 3.5(a), TDOS and PDOS of Ba atom is plotted. We find that in the valence band, contribution to TDOS is by the $d-t_{2g}$ -state electrons of Ba atom. It is seen also that PDOS contribution by Ba atom in valence band is very negligible as it doesn't make much impact to DOS. From TDOS and PDOS plots in Figs. 3.5(b) for the case of Mg atom, there are almost negligible contributions to TDOS and PDOS by all the electron states in the valence band regions. From Fig. 3.5(c), we have the maximum contribution by W atom, we we can see a sharp peak about 2.5 state/eV occurs at -3.5 eV by W $d-t_{2g}$ state and below that similar peak are observed same contributed by W-d state. Also, from Fig. 3.5(d), there

are contribution to TDOS by the p and p_x+p_y state electrons of O near the Fermi level in the valence region respectively.

From the conduction region given in Figs. 3.5(a-d), we can see that a sharp peak at 3.4 eV which is about 5.5 state/eV contributed by d- t_{2g} state of W atom. Beside that there are virtually no contribution to TDOS and PDOS by the other atom Ba, Mg and O atoms since there contribution are quietly negligible. Hence, we can say that maximum contribution comes from W atom in the conduction band.

3.3.2 Density of states for Sr_2MgWO_6

The total density of states (TDOS) and partial density of states (PDOS) of Sr_2MgWO_6 are given in Figs. 3.6 and 3.7. It was obtained that various bands are observed in the energy range of -8 eV to 8 eV. It is very similar to previous Ba_2MgWO_6 that the maximum contribution from TDOS of Sr_2MgWO_6 by O atom, which is about ~ 18 states/eV and occurs at -3.8 eV below Fermi level ($E_F = 0$) in valence band and also minor attributed by W atom near the semi core region. From the plots of TDOS of individual atoms, we can see that only the TDOS of O atom is maximum and coincides almost with TDOS except W atom which a short trend at ~ -4 eV of Sr_2MgWO_6 . Also similar to the case of Ba_2MgWO_6 compound, the other atoms Ba and Mg are having negligible contribution to TDOS in the valence band.

In the conduction band, the maxima in the TDOS of Sr_2MgWO_6 is 11 states/eV which occurs at 7.5 eV which is contributed by Sr-atom above the Fermi level. Sr and W atoms occupy the major contribution in the conduction band. The other atoms Mg and O are having negligible contribution to TDOS compared to Sr and W atom, hence in the conduction band; it is W atom

which contributes to TDOS near Fermi level and above that Sr atom. We observe a gap between the valence and the conduction band and the value of this energy band gap is 2.731 eV.

The PDOS plot of Sr_2MgWO_6 are given in Fig. 3.7 to further clarify the TDOS plot. We find that in the valence band, contribution to TDOS is by the d- t_{2g} -state electrons of W atom but near Fermi level, it is O-p and O- p_x+p_y state electron that gives contribution in the valence band. From TDOS and PDOS plots in Figs. 3.7(a) and 3.7(b) for the case of Sr and Mg atoms, their contribution are negligible by all their electron states as we can see in the valence band regions. From Figs. 3.7(a-d), it is seen that in the conduction band region, it is the Sr-d and W-d- t_{2g} state electrons which are responsible for the occurrence of maxima in the conduction band.

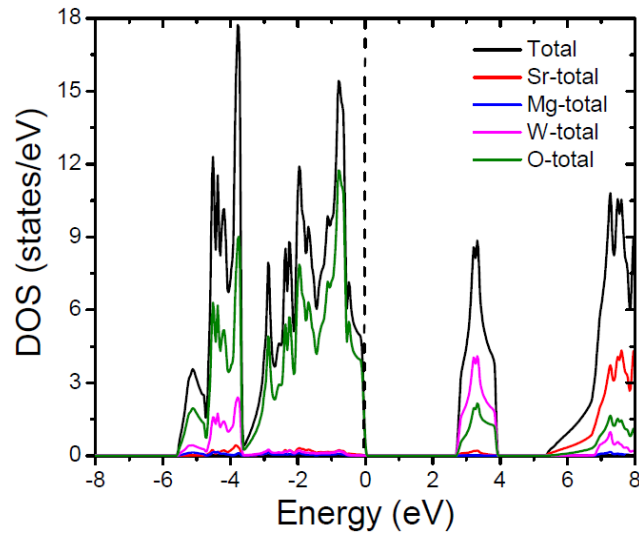


Fig. 3.6. Total DOS plot for Sr_2MgWO_6

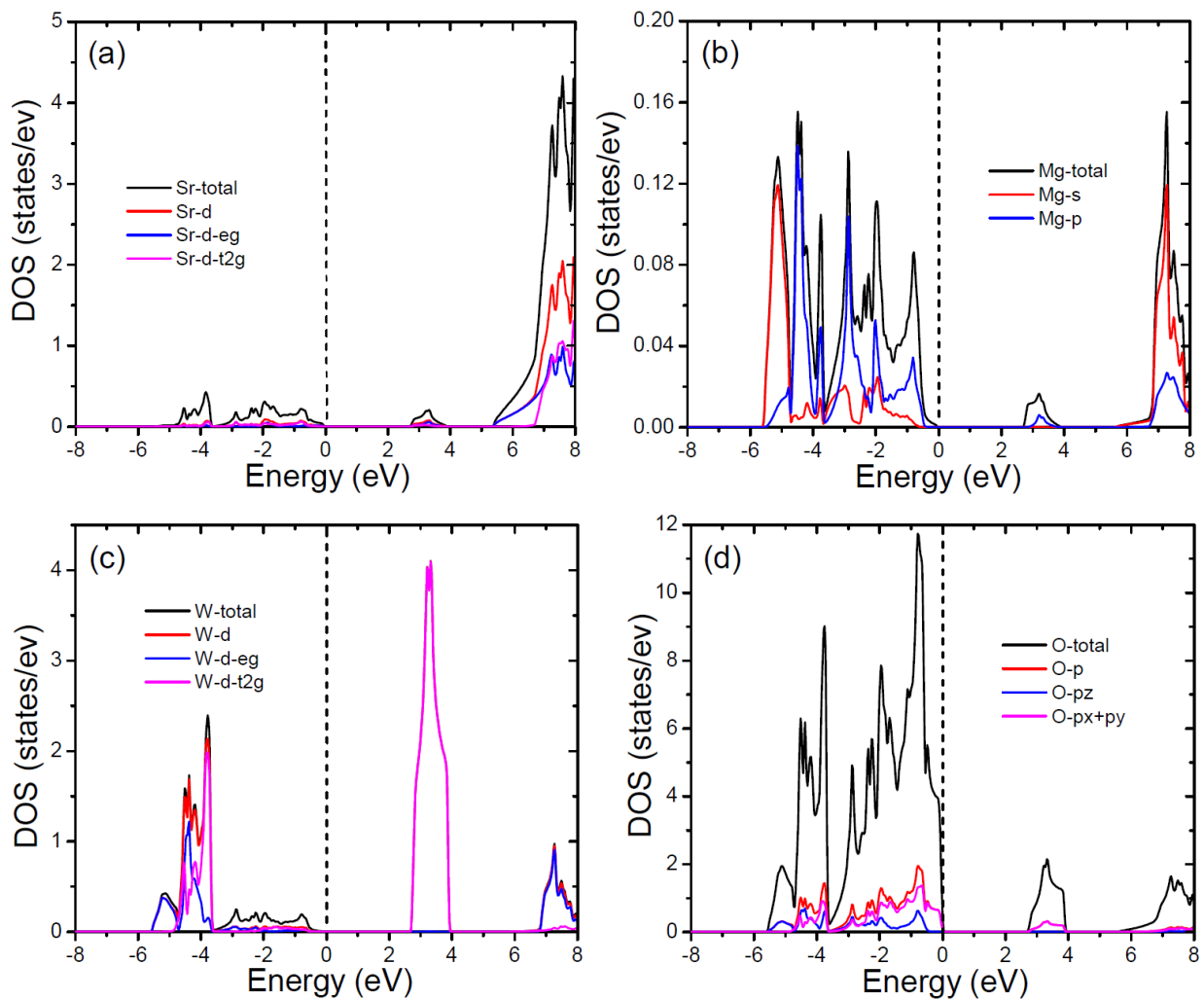


Fig. 3.7. TDOS and PDOS plot for individual atom of Sr_2MgWO_6

3.4 Energy bands of Ba_2MgWO_6 and Sr_2MgWO_6

The band structure of A_2MgWO_6 ($\text{A} = \text{Ba}$ and Sr) is plotted along high symmetry directions $W-L-\Gamma-X-W-K$ in the irreducible part of Brillouin zone as shown in Fig. 3.8. The Fermi level is set to be at zero energy. Both of these compounds were found to have indirect band gap along Γ -X direction. The calculated band gaps from GGA approximation are 2.753 eV and 2.731 eV for Ba_2MgWO_6 and Sr_2MgWO_6 respectively. Looking at the band gap value and the DOS peaks at the lowest of the conduction band, it seems that both these compounds may exhibit semiconducting nature. GGA exchange functional tends to underestimate the band gaps. So the calculated GGA value may be less than the experimentally created real crystals. Recently, many complex functional have been developed to compute for the accurate band gap results. Our results are in good agreement to the available theoretical results (Brik, 2012; Guo *et al.*, 2013). The Fig. 3.8 gives the band structure plot of A_2MgWO_6 , for both of the compounds, the conduction band minima (CBM) lies along the X symmetry point and the valance band maxima (VBM) along Γ symmetry point. Thus, an indirect band gap along Γ - X direction is observed in the irreducible part of the first Brillouin zone. In the conduction band along the Γ symmetry point, VCM is observed, which is mainly formed by the p states of O atom. The p_x and the p_y orbitals contributes the most. The bands in the CBM are formed by the hybridization of p states of O atom and the d states of atom W. The dt_{2g} states of atom W contributes the most of CBM. Thus, the band gap of compounds A_2MgWO_6 can be explained as due to the hybridization of p_x+p_y states of O atoms with $d-t_{2g}$ states of atom W mixed with some s states of atom Mg.

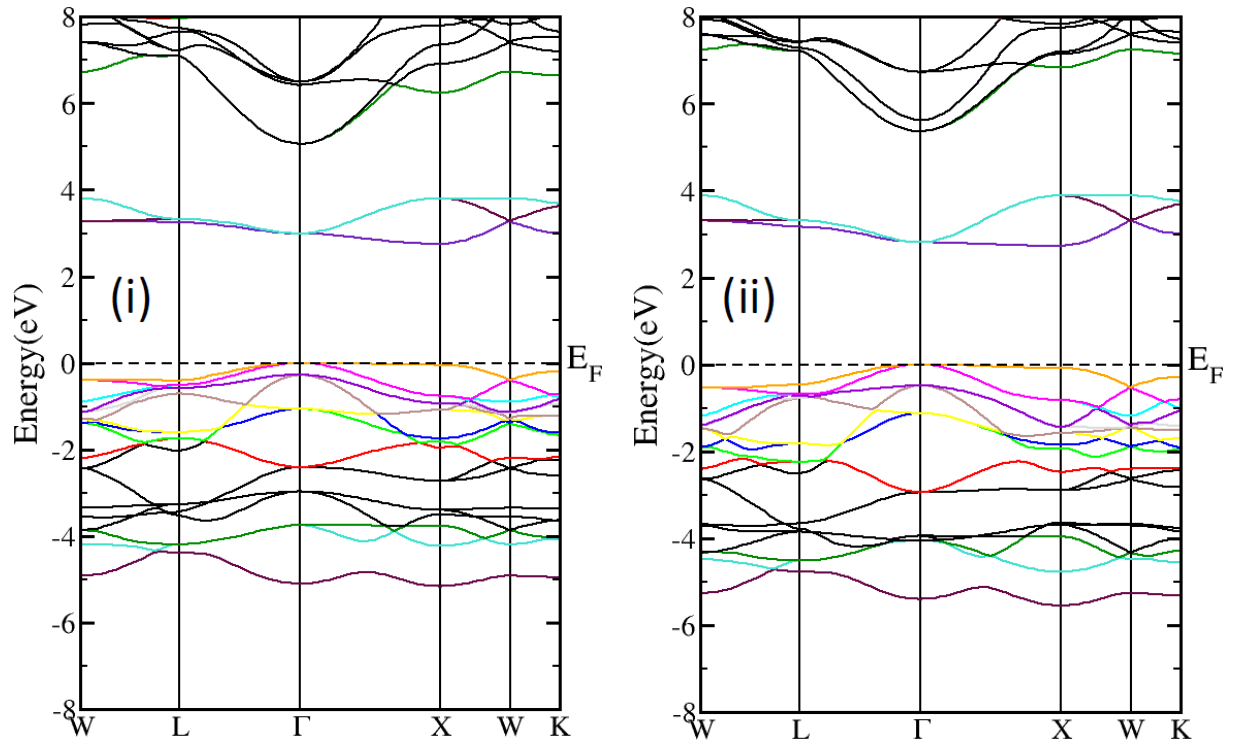


Fig. 3.8. Band structure plot for (i) Ba_2MgWO_6 and (ii) Sr_2MgWO_6

3.5. Results of Optical properties for A_2MgWO_6

The variation of the calculated dielectric function, absorption coefficient, refractive index, and reflectivity for Ba_2MgWO_6 and Sr_2MgWO_6 as a function of photon energy within GGA are shown in Figs. 3.9 and 3.10. Both the compounds Ba_2MgWO_6 and Sr_2MgWO_6 are having cubic symmetry and hence, the principal tensor component ϵ_{xx} , ϵ_{yy} and ϵ_{zz} will be equal. Therefore only one component of the dielectric function has to be calculated i.e $\epsilon_{xx} = \epsilon_{yy} = \epsilon_{zz}$.

The calculated value of the real and imaginary parts of the electronic dielectric function for Ba_2MgWO_6 and Sr_2MgWO_6 are shown in Figs. 3.9(a) and 3.9(b). The detail analysis of the imaginary part $\epsilon_2(\omega)$ curve shows that the first optical critical point of the dielectric function occurs at 4.585 eV for Ba_2MgWO_6 and for Sr_2MgWO_6 , it occurs at 4.001 eV. This point is called $\Gamma_v - X_c$ splitting, which gives us the threshold of direct optical transitions between the lowest conduction band minima and the highest valence band maxima and is called the fundamental absorption edge. Beyond this point, as the energy increases, the curve also increases rapidly. The main reason behind is that the number of points contributing towards the imaginary $\epsilon_2(\omega)$ increases instantaneously. The highest peak of $\epsilon_2(\omega)$ spectrum for Ba_2MgWO_6 situated at 4.176 eV and for Sr_2MgWO_6 situated at 3.986 eV. For the real part ϵ_1 spectrum, the highest peak are observed with a magnitude of 8.73 situated at 3.442 eV for Ba_2MgWO_6 and for Sr_2MgWO_6 , a magnitude of 9.04 situated at 3.496 eV. The various peaks observed in the optical spectra was originated from the transitions between the occupied states in the valence band to the unoccupied states in the conduction band. The optical transitions of the compounds in the energy range 0-12 eV corresponds mainly to the transition from O-2p to W-d states whereas the higher energy

peaks corresponds to transition from the semi-core electrons in the valence band to unoccupied states in the conduction band.

The calculated reflectivity $R(\omega)$ behavior of Ba_2MgWO_6 and Sr_2MgWO_6 are given in Figs. 3.10(a) and 3.10(b). From the reflectivity profile of Ba_2MgWO_6 clearly shows the location of peaks at energy of 4.258, 7.877, 8.231, 9.347, 9.945 eV and for Sr_2MgWO_6 , peaks are at 4.013, 8.204, 9.836 eV. The resulted plots from these compounds clearly show that the maximum value of reflectivity are originated from the inter-band transitions. Therefore, we can say these compounds possess semiconducting behavior since the reflectivity $R(\omega)$ values do not approach the unity toward zero energy. A detail analysis of the plots, we find that the reflectivity spectrum is almost flat in the low energy region, but in higher energies, the reflectivity peaks increase rapidly with some oscillations. The obtained low value of reflectivity in these compounds implies that it becomes a strong candidate for the potential applications in the area of transparent coatings in the visible and deep UV region.

From Fig. 3.10(c) and 3.10(d), the calculated peak of the absorption for Ba_2MgWO_6 and Sr_2MgWO_6 . It is seen that from Ba_2MgWO_6 , the absorption spectrum has four peaks located at energy of 4.204, 7.904, 8.231, 9.020 eV and for Sr_2MgWO_6 , we have obtained the peaks at 4.013, 5.047, 8.122, 9.455 eV. We have obtained that for both the compounds Ba_2MgWO_6 and Sr_2MgWO_6 , the peaks obtained in the absorption spectra clearly matches with the peaks of imaginary part of the dielectric function $\varepsilon_2(\omega)$. From the absorption spectrum, it shows that at the lower energies the absorption coefficient decreases which is a well-known behavior of semiconductors and insulators.

Table 3.2 The calculated dielectric constant $\varepsilon_1(0)$, reflectivity $R(\omega)$, and absorption coefficient $I(\omega)$ for Ba_2MgWO_6 and Sr_2MgWO_6 .

Compound	$\varepsilon_1(0)$	$R(\omega)$	$I(\omega)$
Ba_2MgWO_6	4.58	1.16	2.95
Sr_2MgWO_6	4.01	0.12	2.19

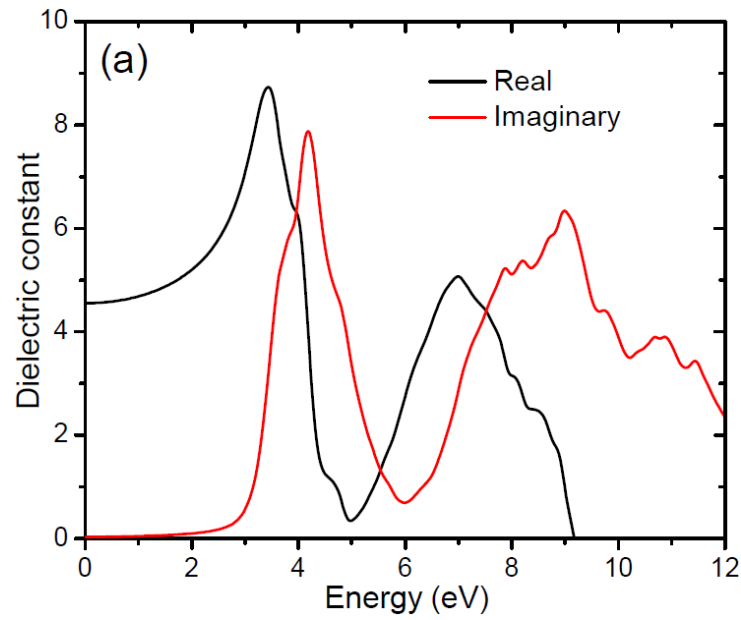


Fig. 3.9(a). The optical spectrum of the dielectric constant as a function of the photon energy of Ba_2MgWO_6

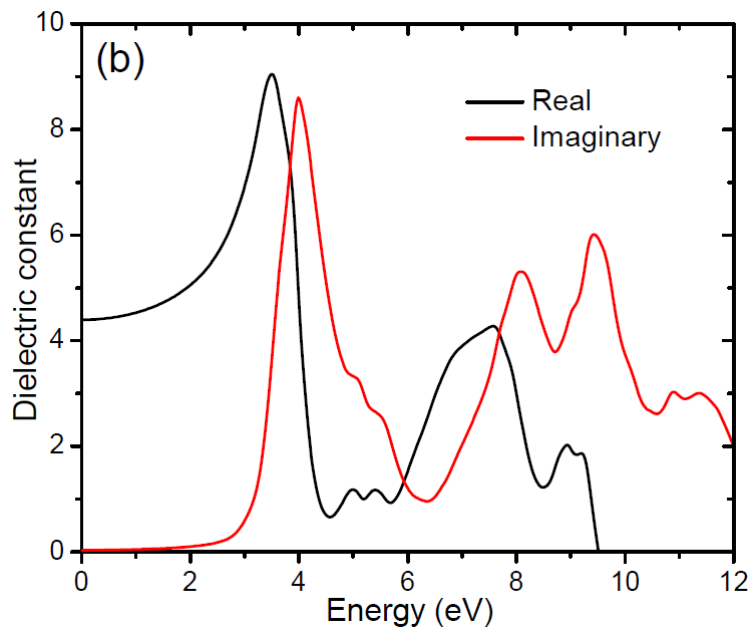


Fig. 3.9(b). The optical spectrum of the dielectric constant as a function of the photon energy of Sr_2MgWO_6

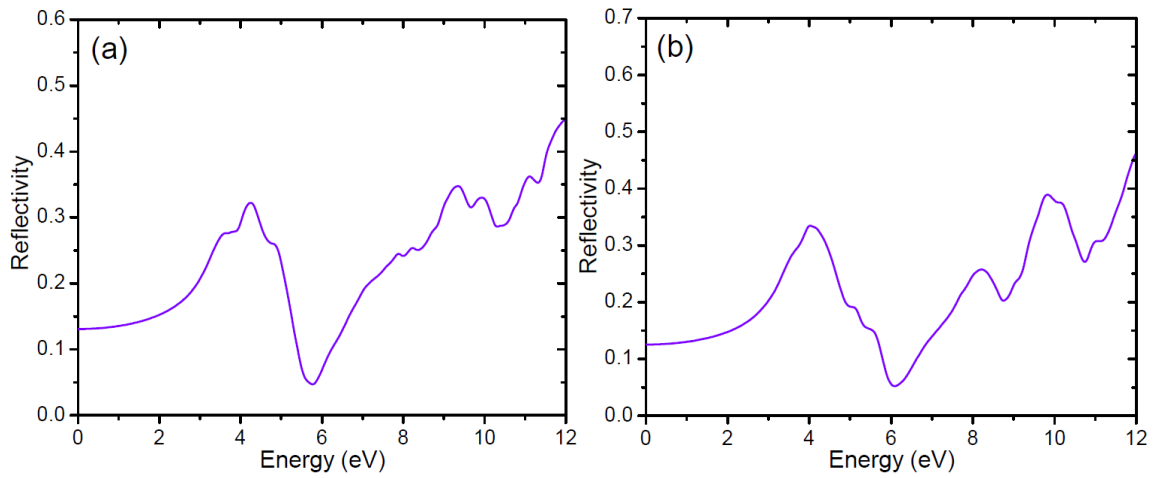


Fig. 3.10. Reflectivity spectra of (a) Ba_2MgWO_6 and (b) Sr_2MgWO_6

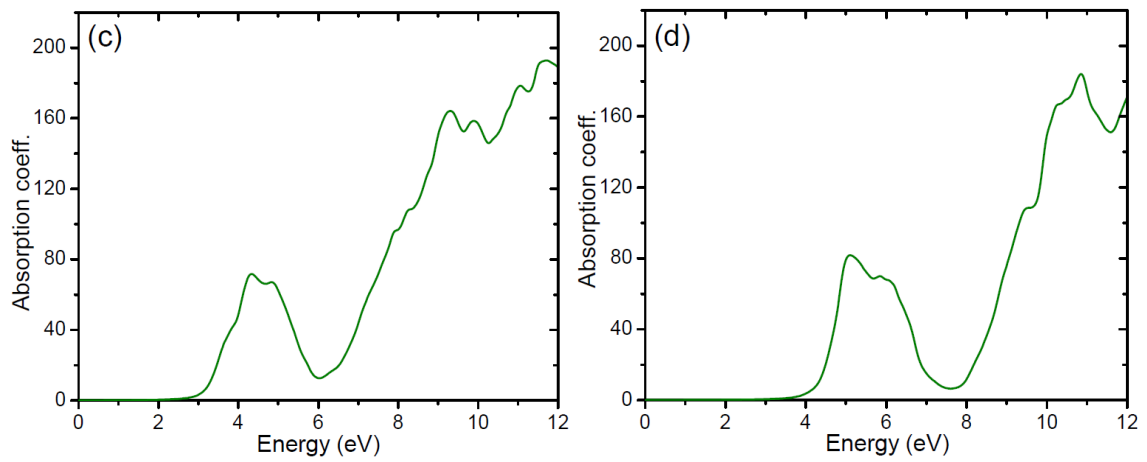


Fig. 3.10. Absorption spectra of (c) Ba_2MgWO_6 and (d) Sr_2MgWO_6

4

Study of Electronic and Optical properties of Double Perovskites $Pb_2ScB'O_6$ ($B' = Sb, Ta$)

In this chapter, we will present the results of calculations of the electronic and optical properties for the $Pb_2ScB'O_6$ ($B' = Sb, Ta$). We have chosen the combinations of alkaline earth element as $AA' = Pb$ and transition metals such that B as Sc and B' as Sb and Ta respectively. The results of electronic and optical properties of these systems will be discussed here in the context of FP-LAPW model within density functional theory. The exchange correlations potentials used for the calculation is by using the GGA and mBJ potential, hence the results obtained is presented for both of these methods. The computational details used in this chapter had been already discussed in section 3.2 of Chapter-3. The only difference with the previous calculations is that in the case of $Pb_2ScB'O_6$, we have used $k=4000$ points.

4.1 Crystal Structure

All atomic positions are in fractional coordinates (Wyckoff, 1935). Fig. 4.1 shows that the (100) plane of the corresponding conventional unit cell which was displayed by XCrySDen (Kokalj, 2003). The structural optimization based on Murnaghan's equation of state (Murnaghan, 1994) was performed to obtain the relaxed structure of the crystal with minimum energy. From this minimum energy, we obtained the optimized lattice parameters, which are summarized in Table 4.1. The structural optimization defines the obtained energy versus volume plot for

$\text{Pb}_2\text{ScB}'\text{O}_6$ ($\text{B}' = \text{Sb}$ and Ta) as given in Figs. 4.2 and Fig. 4.3 respectively. With this, the optimized lattice constants were used to calculate the electronic structure and optical properties.

The double perovskite compound $\text{Pb}_2\text{ScB}'\text{O}_6$ ($\text{B}' = \text{Sb}$ and Ta) crystalizes in cubic phase forming face-centred cubic crystal structure with space group $Fm-3m$ having with four atoms per unit cell as shown in Fig. 4.1. The atomic positions in the unit cell are as: Pb (0.25, 0.25, and 0.25), Sc (0.5, 0.5, and 0.5), B' (0, 0, 0) and O (u, 0, 0) which is shown in Fig. 4.1.

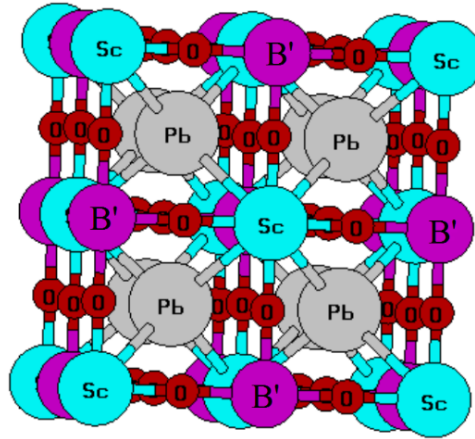


Fig. 4.1. Unit cell structure of double perovskite oxide $\text{Pb}_2\text{SbB}'\text{O}_6$ ($\text{B}' = \text{Sb}$ and Ta)

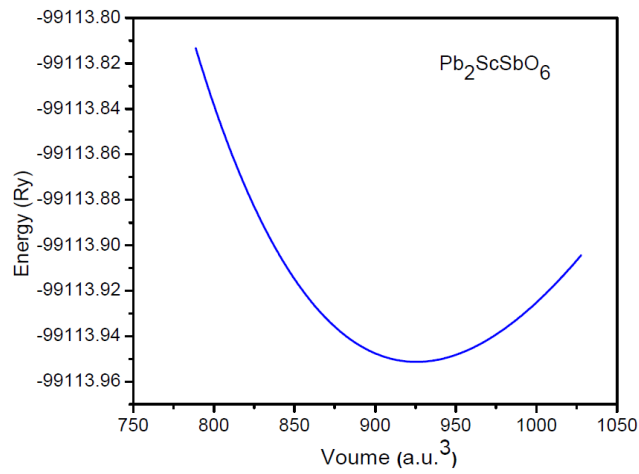


Fig. 4.2. Volume optimization of $\text{Pb}_2\text{ScSbO}_6$

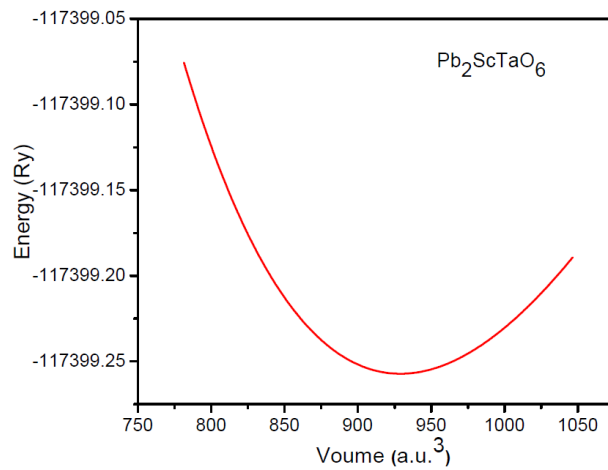


Fig. 4.3. Volume optimization of $\text{Pb}_2\text{ScTaO}_6$

Table 4.1. Calculated lattice constant (a), internal atomic parameters u, bulk modulus B (in GPA) and pressure derivative of bulk modulus (B') of $\text{Pb}_2\text{ScB}'\text{O}_6$ (B' = Sb, Ta)

Compound	Calculated (a)	Previous (a)	u	B(GPA)	B'
$\text{Pb}_2\text{ScSbO}_6$	8.1866	8.1050 ^a	0.2551	147.7090	4.5160
$\text{Pb}_2\text{ScTaO}_6$	8.1967	8.1488 ^b	0.2556	165.4635	4.3416

^a(Larregola *et al.*, 2009), ^b(Kishi, 1998)

4.2 Results of Density of State (DOS)

In this section, the results of calculations of total density of states (TDOS) and partial density of state (PDOS), in the case of double perovskite $\text{Pb}_2\text{ScB}'\text{O}_6$ ($\text{B}' = \text{Sb}$ and Ta). For the combinations of the elements, we have chosen the transition metal AA' as Pb , transition metals B as Sc and B' with $\text{B}' = \text{Sb}$ and Ta .

4.2.1. Density of States for $\text{Pb}_2\text{ScSbO}_6$

In this section, we present the results of density of states (DOS) calculated in the case of $\text{Pb}_2\text{ScSbO}_6$ double perovskites using the GGA and mBJ potentials. The optimized lattice constants given in Table 4.1 were used to calculate the electronic structures of $\text{Pb}_2\text{ScSbO}_6$ perovskites. In Fig. 4.4, the plots of total density of states (TDOS) in the case of $\text{Pb}_2\text{ScSbO}_6$ and individual atoms Pb , Sc , Sb and O are shown. It is seen from the plots that maxima in TDOS of $\text{Pb}_2\text{ScSbO}_6$ is 16 states/eV which occurs at -2.0 eV below Fermi level E_F in valence band. From the plots of TDOS of individual atoms, it is seen that only the TDOS of O atom is maximum and coincides almost with TDOS of $\text{Pb}_2\text{ScSbO}_6$ in valence band. The other atoms Pb , Sc and Sb are having negligible contribution to TDOS in the valence band as seen in the plots. In the conduction band, the maxima in the TDOS of $\text{Pb}_2\text{ScSbO}_6$ is 20 states/eV which occurs at 5 eV energy above the Fermi level. The TDOS contribution is maximum for Sc atom which occurs at 5.5 eV energy above the Fermi level. The other atoms Pb , Sb and O are having negligible contribution to TDOS compared to Sc atom, hence in the conduction band, it is Sc atom which contributes maximum to TDOS of $\text{Pb}_2\text{ScSbO}_6$. We observe a gap between the valence and the conduction band and the value of this energy band gap is 2.712 eV.

In Fig. 4.4(b), we show the TDOS plots of $\text{Pb}_2\text{ScSbO}_6$ but using the mBJ potential. It is seen that TDOS shows similar trends for both the valence and conduction band regions as in the case of GGA. For example, the first maxima in TDOS of value around 18 states/eV occurs at -1.0 eV below the Fermi level. Here also the contribution to this maxima in TDOS is due to O atom. In the conduction band, the maxima in TDOS occurs at around 6 eV above the Fermi level. In this case also contribution to this maxima is due to Sc atom as the maxima of TDOS of Sc atom is nearest to the TDOS of $\text{Pb}_2\text{ScSbO}_6$ compound. However the energy band gap in this case is very wide and is equal to 3.842 eV. This is obvious as mBJ potential when included in FP-LAPW model, it usually overestimates the magnitude of energy band gap.

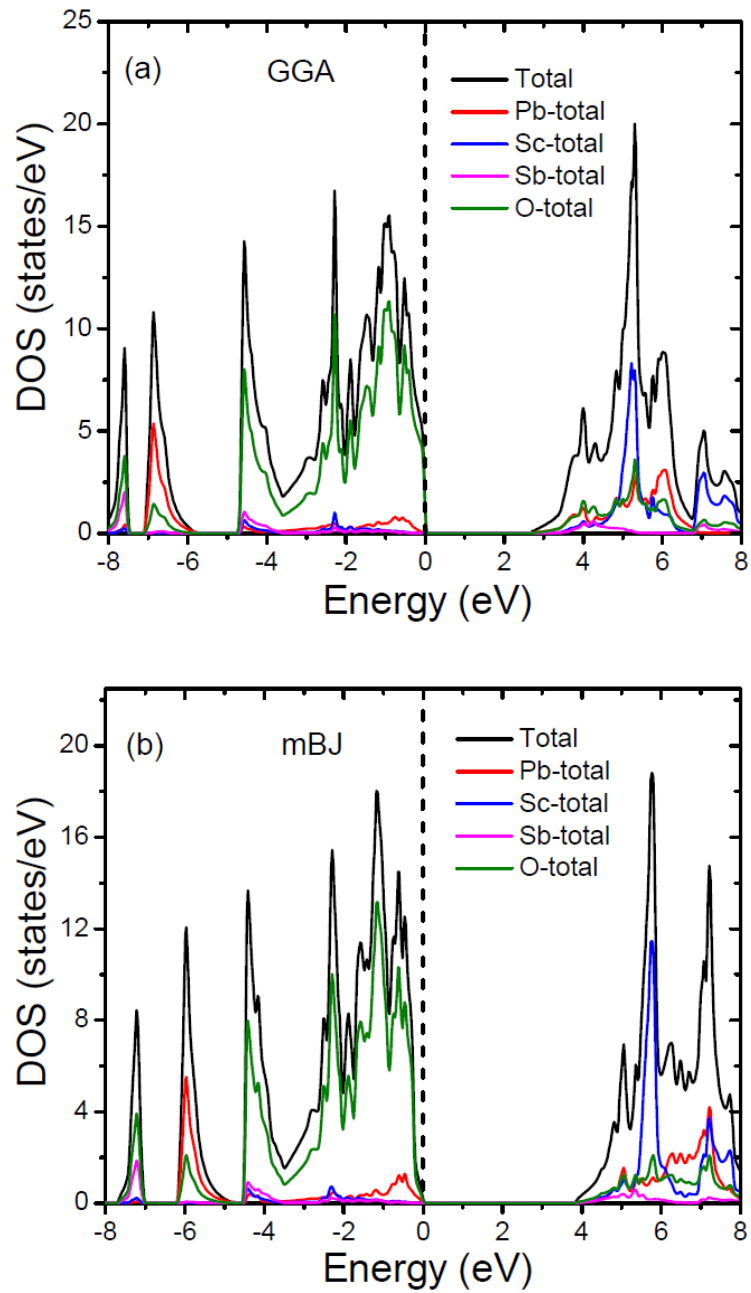


Fig. 4.4. Total DOS of $\text{Pb}_2\text{ScSbO}_6$ and individual atoms Pb, Sc, Sb and O with (a) GGA and (b) mBJ. Energy = 0 refers to Fermi level (E_F).

To find out exactly which atoms or the electrons from different states do contribute to the TDOS, we have also plotted the PDOS of each individual atoms along with their respective TDOS. These are shown for all the atoms in Fig 4.5 for both GGA and mBJ method. In Fig 4.5(a), using GGA, TDOS and PDOS of Pb atom is plotted. We find that in the valence band, contribution to TDOS is by the s-state electrons of Pb atom but from the core states below -6 eV and hence it is not relevant. It is seen from Fig. 4.5(b) that PDOS contribution by s and p state electrons of Pb atom in valence band is negligible. If we just look at the TDOS and PDOS plots in Figs. 4.5(c & d) for the case of Sc atom, there are almost negligible contributions to TDOS and PDOS by all the electron states of Sc in the valence band regions for both the cases of GGA and mBJ. However, there are contribution to TDOS by the p state electrons of Sb and O which are ~ 1 states/eV and 2.1 states/eV respectively.

Referring now again to Fig. 4.5(e-h) in the conduction band region for both the GGA and mBJ cases, we find that there are virtually no contribution to TDOS and PDOS by the Sb and O atoms or their respective electrons in other levels. From Fig. 4.5(c & d) it is seen that for both the GGA and mBJ cases, it is the Sc-d- t_{2g} state electrons, which are responsible to the occurrence of maxima in PDOS at ~ 5 eV above the Fermi level. This is a confirmation to the occurrence of maxima in TDOS as shown in Fig. 4.4(a & b) at 5.5 eV above the Fermi level.

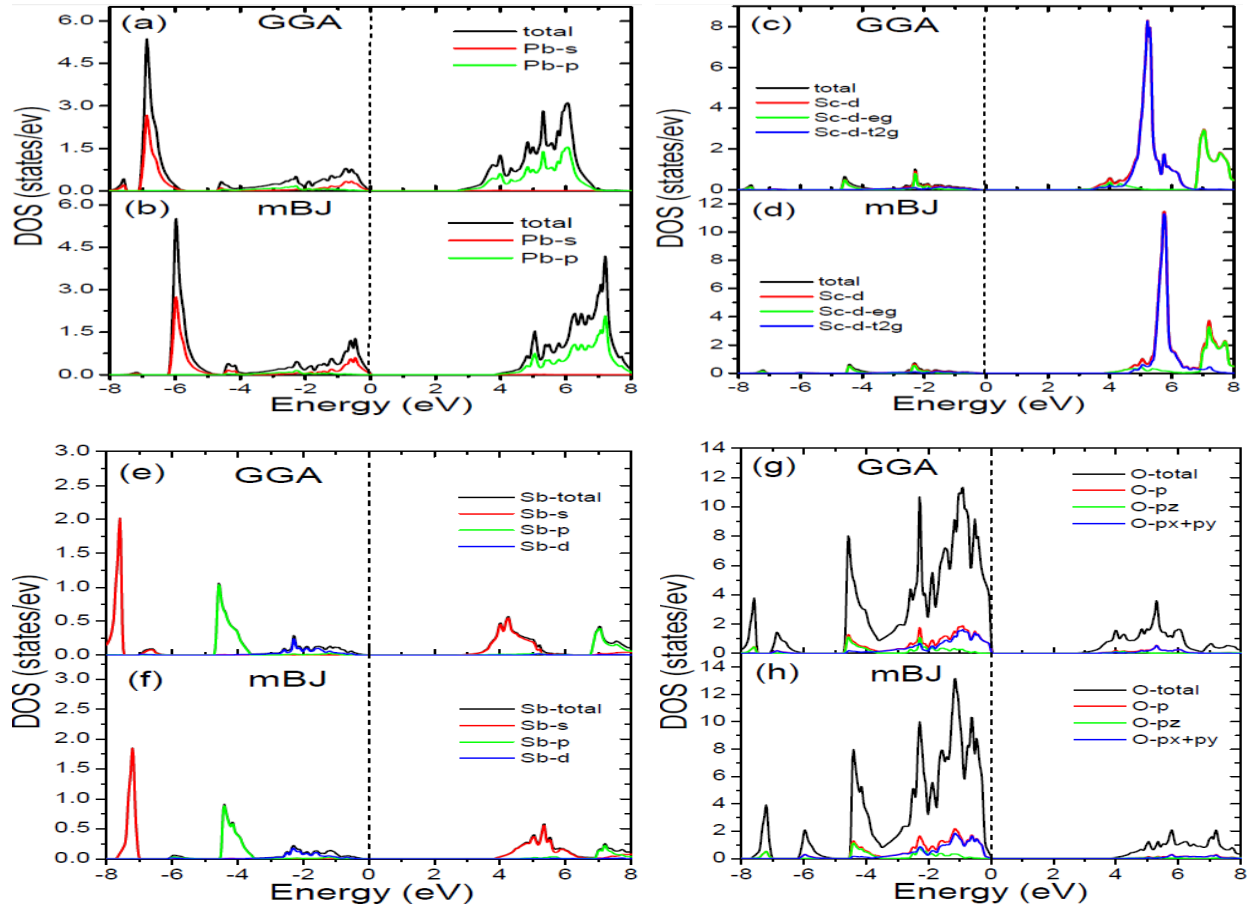


Fig. 4.5. TDOS and PDOS of Pb, Sc, Sb and O atoms in $\text{Pb}_2\text{ScSbO}_6$ perovskite using (e) GGA and (f) mBJ method. Energy equal zero is Fermi level.

4.2.2. Density of States for $\text{Pb}_2\text{ScTaO}_6$

In this section, we have presented the result of TDOS and PDOS for $\text{Pb}_2\text{ScTaO}_6$ using GGA and mBJ potential. Fig. 4.6 shows the plots of total density of states (TDOS) in the case of $\text{Pb}_2\text{ScTaO}_6$ and the individual atoms Pb, Sc, Ta and O for GGA and mBJ potentials. It is seen from Fig. 4.6(a) that in the case of GGA, there is maxima in TDOS of $\text{Pb}_2\text{ScTaO}_6$, which is about ~ 19 states/eV and occurs at -1.0 eV below Fermi level E_F in valence band. From the plots of TDOS of individual atoms, it is seen that only the TDOS of O atom is maximum and coincides almost with TDOS of $\text{Pb}_2\text{ScTaO}_6$. Here also just like in the case of $\text{Pb}_2\text{ScSbO}_6$ perovskite, the other atoms Pb and Ta are having negligible contribution to TDOS in the valence band as seen from the plots. The Pb atom has contribution to TDOS but in the core region below -6 eV and hence is omitted. In the conduction band, the maxima in the TDOS of $\text{Pb}_2\text{ScTaO}_6$ is 12 states/eV which occurs at 6.1 eV energy above the Fermi level. The TDOS contribution is maximum for Sc atom which occurs at 5.5 eV energy above the Fermi level. The other atoms Pb, Ta and O are having negligible contribution to TDOS compared to Sc atom, hence in the conduction band, it is Sc atom which contributes to TDOS of $\text{Pb}_2\text{ScTaO}_6$. We observe a gap between the valence and the conduction band and the value of this energy band gap is 2.657 eV.

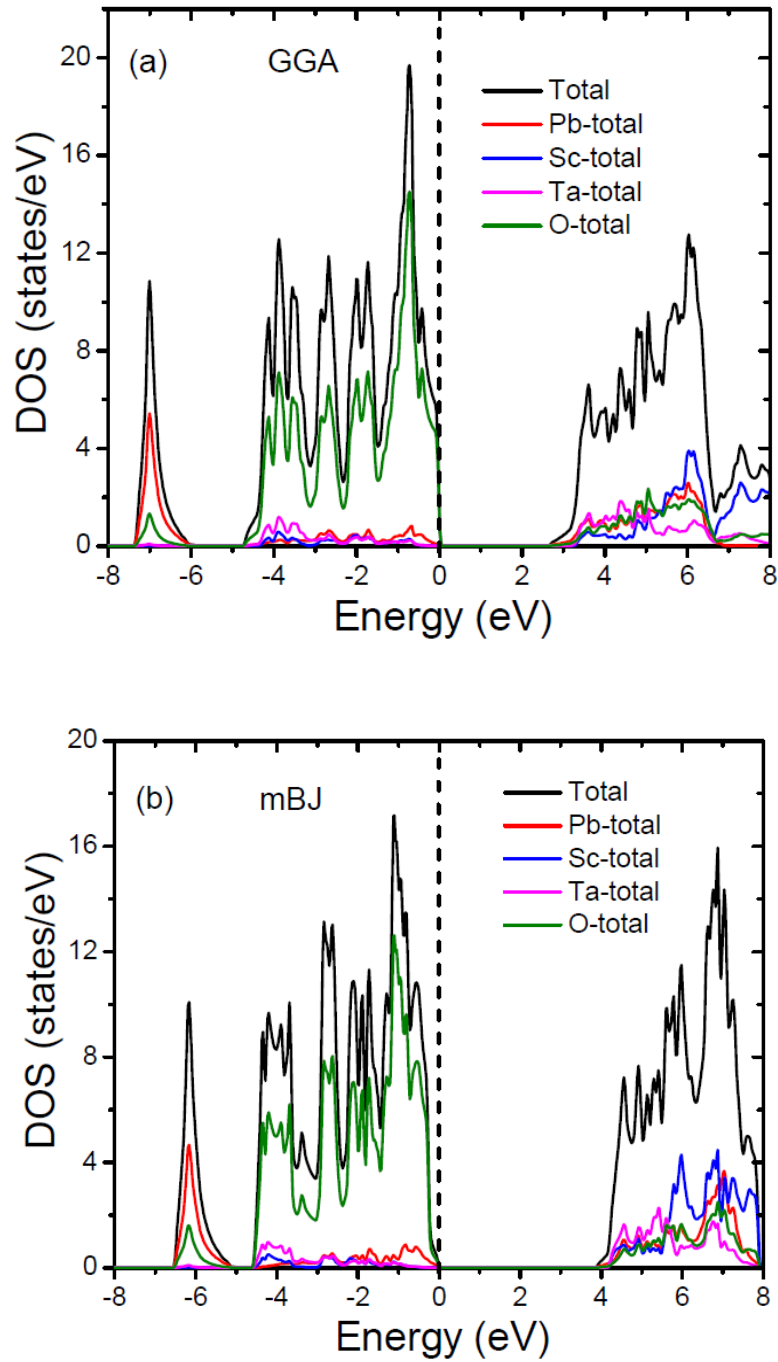


Fig. 4.6. Total DOS of $\text{Pb}_2\text{ScTaO}_6$ and individual atoms Pb, Sc, Ta and O with (i) GGA and (ii) mBJ. Energy = 0 refers to Fermi level (E_F).

In Fig. 4.6(b), we show the TDOS plots of $\text{Pb}_2\text{ScTaO}_6$ but using the mBJ potential. It is seen that TDOS shows similar trends for both the valence band and conduction band regions. For example, the first maxima in TDOS of ~ 17 states/eV occurs at -1.0 eV below the Fermi level. Also the contribution to maxima in TDOS is due to O atom. In the conduction band, the maxima in TDOS occurs at around 7 eV above the Fermi level. Contribution to this maxima is due to Sc atom as the maxima of TDOS of Sc atom is nearest to the TDOS of $\text{Pb}_2\text{ScTaO}_6$ compound. However the energy band gap in this case is very wide and is equal to nearly 3.889 eV just like in the case of $\text{Pb}_2\text{ScSbO}_6$. This is obvious whenever mBJ potential is included in FP-LAPW model, it overestimates the magnitude of energy band gap.

Just like before in the case of $\text{Pb}_2\text{ScSbO}_6$ here also we will try to find out exactly which of the atoms or the electrons from different states do contribute to the TDOS of $\text{Pb}_2\text{ScTaO}_6$. This is possible only when we plot the PDOS of individual atoms which are shown in Fig. 4.7 for both the GGA and mBJ methods. In Fig 4.7(a), using GGA, TDOS and PDOS of Pb atom is plotted. We find that in the valence band, contribution to TDOS is by the s-state electrons of Pb atom but from the core states and hence it is not relevant. It is seen from Fig. 4.7(b) that PDOS contribution by s and p state electrons of Pb atom in valence band is negligible in mBJ case also. However in the conduction band region, it is the p-state electrons which contributes to the maxima in the TDOS of Pb atom. This is found to be same both in the case of GGA and mBJ methods. If we just look at the TDOS and PDOS plots in Fig. 4.7(c, d, g & h) for the case of Sc and O atoms respectively in the valence band regions for both the case of GGA and mBJ, there are almost negligible contributions to TDOS and PDOS by all the electron states. However in the case of Ta atom as shown in Fig. 4.7(e & f), there is a maxima in TDOS occurring at around -4 eV below the Fermi level both in GGA and mBJ cases. This is true as it is evident from TDOS plots in Fig. 4.6(a & b)

which showed occurrence of maxima of ~ 10 states/eV at -4 eV below Fermi level for Ta atom in both the GGA and mBJ cases. This is attributed to the Ta-d and Ta- d_{eg} electron states which is contributing to the origin of this maxima in the valence band. From Fig. 4.7(a-h), it is seen that in the conduction band region, it is the Sc-d and Sc $d-t_{2g}$ state electrons which are responsible for the occurrence of maxima in the conduction band. This is true for both the GGA and mBJ potentials with only the difference that the energy band gap is wider in the case of mBJ.

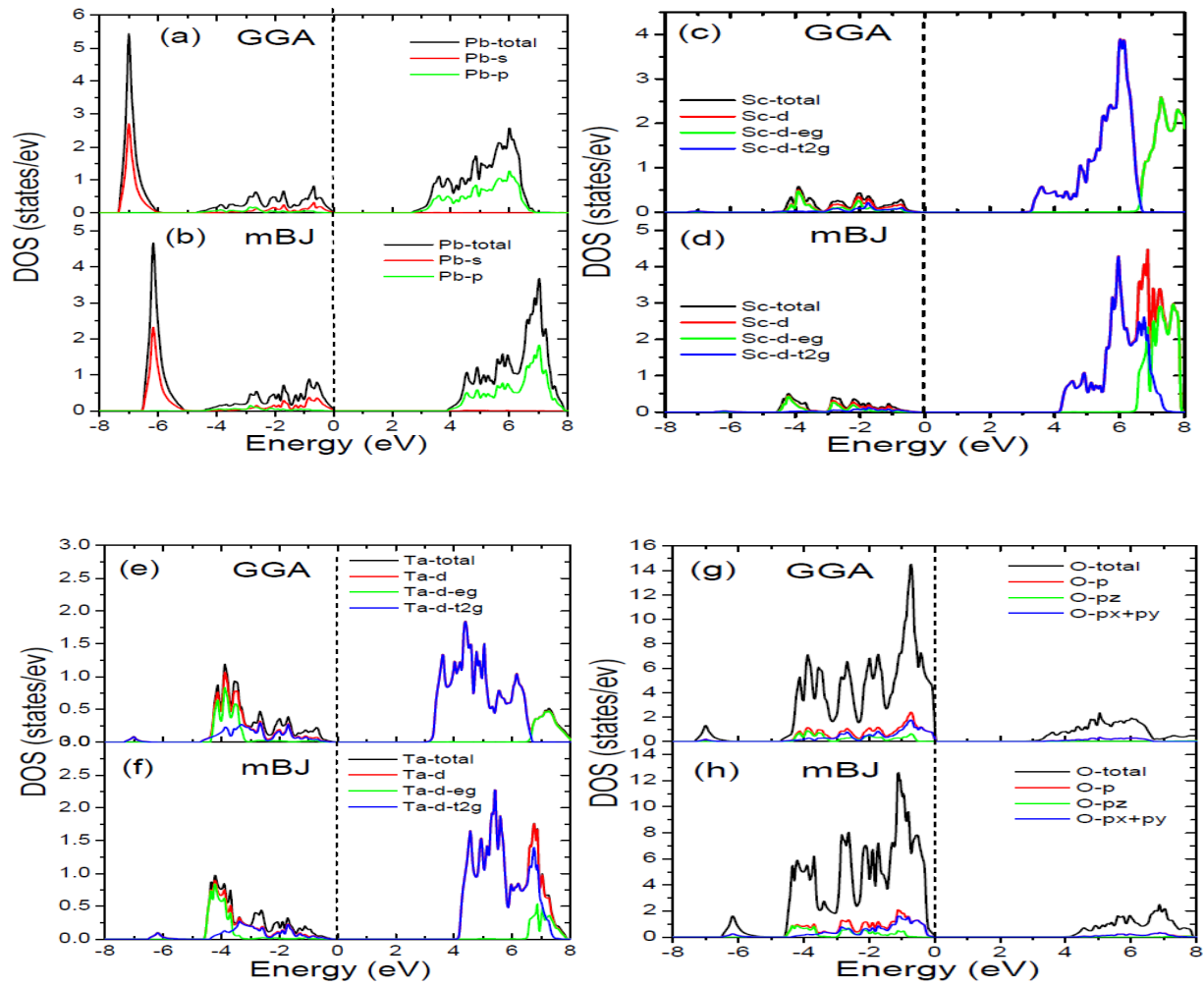


Fig. 4.7. TDOS and PDOS of Pb, Sb, Ta and O atoms in $\text{Pb}_2\text{ScTaO}_6$ perovskite using (i) GGA and (ii) mBJ method. Energy equal zero is Fermi level.

4.3. Energy bands in $\text{Pb}_2\text{ScB}'\text{O}_6$ ($\text{B}' = \text{Sb}, \text{Ta}$)

In Fig. 4.8 and Fig. 4.9, we show the energy band structures drawn in the case of $\text{Pb}_2\text{ScSbO}_6$ and $\text{Pb}_2\text{ScTaO}_6$ perovskites by considering the (a) GGA and (b) mBJ potential respectively. From the energy bands plot of the $\text{Pb}_2\text{ScSbO}_6$ perovskite as shown in Fig. 4.8(a), it is seen that the contribution to maxima in the valence bands using GGA is due to Sb-p states electrons. In the conduction bands, the contribution to maxima of the energy bands are due to Sc- d_{t2g} state electrons. This is as evident from DOS studies. But the occurrence of minima in energy bands at X symmetry point is due to Sc- d_{eg} electrons lying at X symmetry point. In the conduction bands contribution to maximum energy bands at the symmetry point X is due to Sc- d_{t2g} and Ta- d_{t2g} state electrons. Similar features had been obtained for $\text{Pb}_2\text{ScSbO}_6$ perovskite using mBJ as shown in Fig 4.8 (b) in which the bands are all from the X symmetry point and the transition is direct type. The only difference is with the width of the energy band gap which is wider in this case than in the case of GGA. The energy band gaps calculated for $\text{Pb}_2\text{ScSbO}_6$ are 2.712 eV (GGA) and 3.842 eV (mBJ) respectively.

In Fig. 4.9, we show the plots of energy bands for $\text{Pb}_2\text{ScTaO}_6$ perovskite using both GGA and mBJ. Here also the maxima in the valence bands are due to Ta-d and Ta- d_{eg} state electrons lying at -4 eV below the Fermi level. In the conduction bands, it is the Sc- d_{t2g} and Ta- d_{t2g} electrons which contributes maximum to the bands. Here also similar trends are seen in the case of mBJ potential. The only difference with GGA is that it is a wider band gap. The energy band gaps calculated are 2.657 eV (GGA) and 3.889 eV (mBJ) respectively and is direct at the symmetry point X.

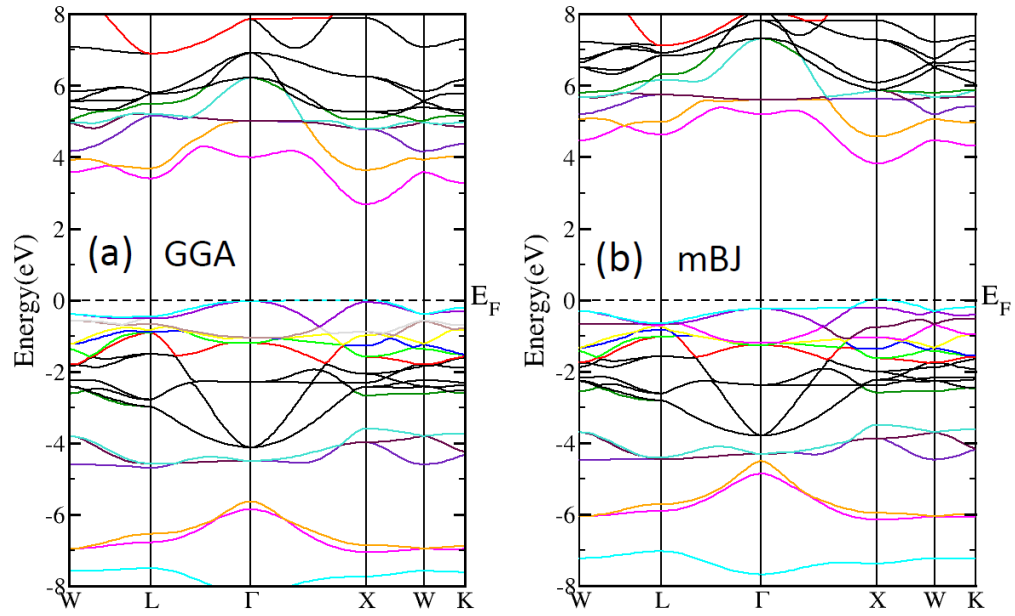


Fig. 4.8. Band structure plots for $\text{Pb}_2\text{ScSbO}_6$ using GGA and mBJ.

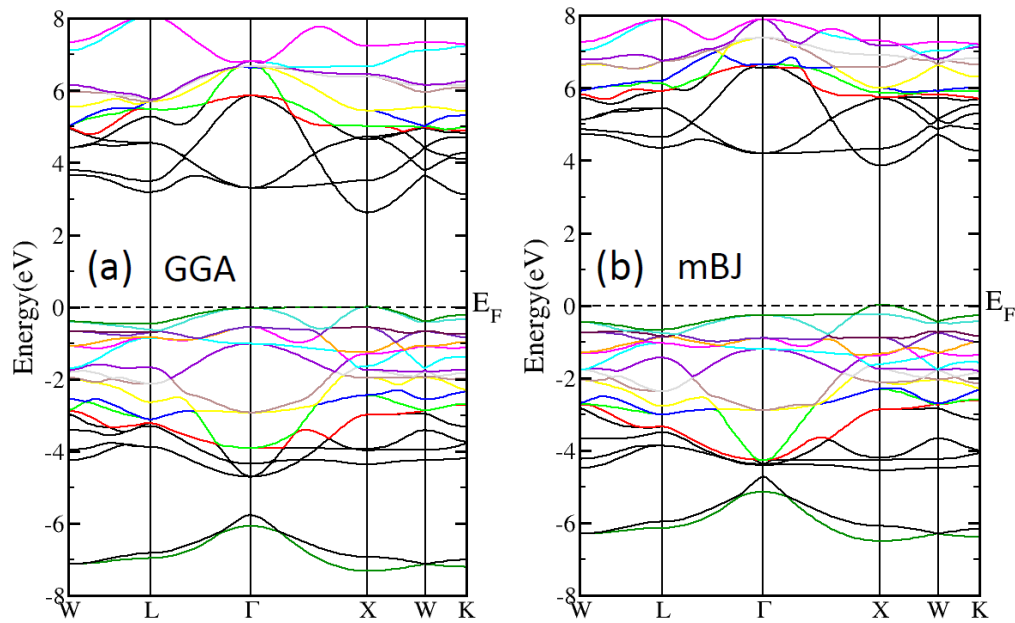


Fig. 4.9. Band structure plots for $\text{Pb}_2\text{ScTaO}_6$ using GGA and mBJ.

From the band structures plot, it is seen that both the compounds show that the top of valence band and the bottom of conduction band lies at X symmetry point and hence is a direct band gap. It means that a direct recombination takes place with the release of the energy equal to the energy band gap. The efficiency factor of a direct band gap semiconductor is higher than those of indirect band. Therefore, this material is the best candidate for applications comprising the emission of photons through radiative recombination of electrons and holes and thereby it means that they are suitable for LED, lasers and optical sources.

4.4 Results of Optical properties for $\text{Pb}_2\text{ScB}'\text{O}_6$ ($\text{B}' = \text{Sb, Ta}$)

Referring to Fig. 4.9(a), here we have the plots of the variation of real $\varepsilon_1(\omega)$ and imaginary parts $\varepsilon_2(\omega)$ of the dielectric constants as a function of incident photon energy using GGA. Like its behavior in solids, the real dielectric constant $\varepsilon_1(\omega)$ increases with the increase in photon energy then attains a maximum value at 4 eV photon energy indicating normal dispersion phenomena. With increase in photon energy beyond 4 eV, it decreases and become zero at ~ 7 eV showing anomalous type dispersion. Beyond 7 eV photon energy, $\varepsilon_1(\omega)$ becomes negative and ultimately tends towards zero value. $\varepsilon_2(\omega)$ is zero in the range 0 - 3.5 eV after which it increases and showed maxima at 6.0 eV. With the further increase in photon energy beyond 6.0 eV, $\varepsilon_2(\omega)$ showed a decrease with the further increase in photon energy. The behavior by $\varepsilon_1(\omega)$ and $\varepsilon_2(\omega)$ in mBJ method are similar to results obtained by GGA method as shown in Fig. 4.10(b). The only difference is that the occurrence of peaks takes place at different photon energies. For example, for $\varepsilon_1(\omega)$ peak value occurred at 6 eV and at $\varepsilon_2(\omega)$ maxima occurs at 7 eV photon energies.

It is interesting to note that the first peak in $\varepsilon_1(\omega)$ coincides with the transition at the point X between the top of the valence band and the bottom of the conduction band. This is possible only in the case of mBJ as the gap is wider. The major difference between the $\varepsilon_1(\omega)$ spectra of the compounds appear to occur in the region where $\varepsilon_1(\omega)$ is negative. These correspond to direct interband transitions which originate from the top of the valence band at the X-point to the lowest conduction band. The imaginary part of the dielectric function for the compounds are also shown in Figure 4.10(b) for both GGA and mBJ cases. The onset of the absorption edge in $\text{Pb}_2\text{ScSbO}_6$ occurs at 2.5 eV when ε_2 just rises from zero value. This correspond to direct optical band gap at X symmetry point and there is a sharp increase in the slope of ε_2 beginning at the optical band gap and rising to the main peak. The global peak in ε_2 occurring at 6 and 7 eVs respectively for GGA and mBJ methods respectively. There is another small peak in ε_2 which arises due to direct transitions from the top of the valence band at the L-point to the next higher conduction band. Similar is the case for mBJ method for $\text{Pb}_2\text{ScSbO}_6$.

In Fig. 4.11(a) and 4.11(b), we show the plots of reflectivity in the case $\text{Pb}_2\text{ScSbO}_6$ for GGA and mBJ methods. We note that by both the methods, the reflectivity is small in the low photon energy up to 2 eV. This is indicative of the nature that interband transition do not take place in far infrared (IR) spectrum as this a wide band insulator. However, there is 20 % to 50 % reflectivity in the photon range 6 - 10 eV indicating that they reflect more in ultra violet region. However, beyond 10 eV, reflectivity decreases in both the cases making the compound good for applications in visible and ultra violet region. The low values of reflectivity also shows that its applications is possible in the field of anti-reflection coating and deep UV region etc.

The onset of absorption involves a sharp increase in the spectra of ε_2 at energy corresponding to the energy band gap. For $\text{Pb}_2\text{ScSbO}_6$ this pertains to 2.5 eV (GGA) and 3.5 eV (mBJ) from Fig. 4.11(c) and calculated values from energy bands gaps are 2.712 eV and 3.84 eV respectively. This means that the values of band gaps from Fig. 4.11(d) for GGA and mBJ are agreeing with the calculated results. The calculated value of reflectivity $R(\omega)$ and optical absorption coefficient $I(\omega)$ for both the compounds with GGA and mBJ potentials are tabulated in Table 4.2.

Table 4.2. The calculated dielectric constant $\varepsilon_1(0)$, reflectivity $R(\omega)$, and optical absorption coefficient $I(\omega)$ for $\text{Pb}_2\text{ScSbO}_6$ and $\text{Pb}_2\text{ScTaO}_6$ with GGA and mBJ exchange potentials (XC).

Compounds	XC	$\varepsilon_1(0)$	$R(\omega)$	$I(\omega)$
$\text{Pb}_2\text{ScSbO}_6$	GGA	5.80	0.17	2.70
	mBJ	4.10	0.12	3.75
$\text{Pb}_2\text{ScTaO}_6$	GGA	6.45	1.19	2.50
	mBJ	4.50	0.13	3.80

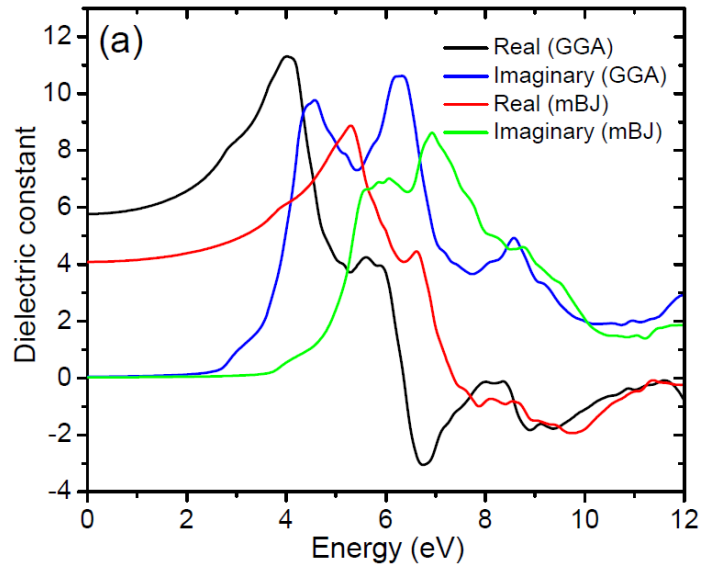


Fig. 4.10(a). The optical spectrum of the dielectric constant as a function of the photon energy of $\text{Pb}_2\text{ScSbO}_6$

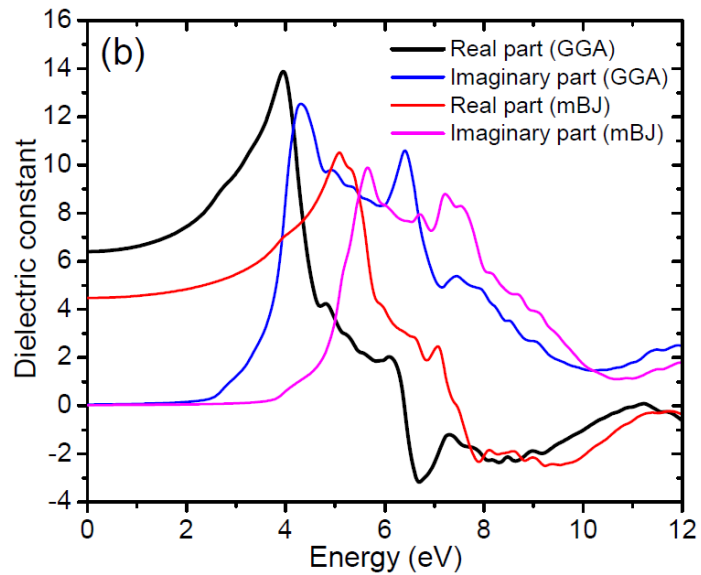


Fig. 4.10(b). The optical spectrum of the dielectric constant as a function of the photon energy of $\text{Pb}_2\text{ScTaO}_6$

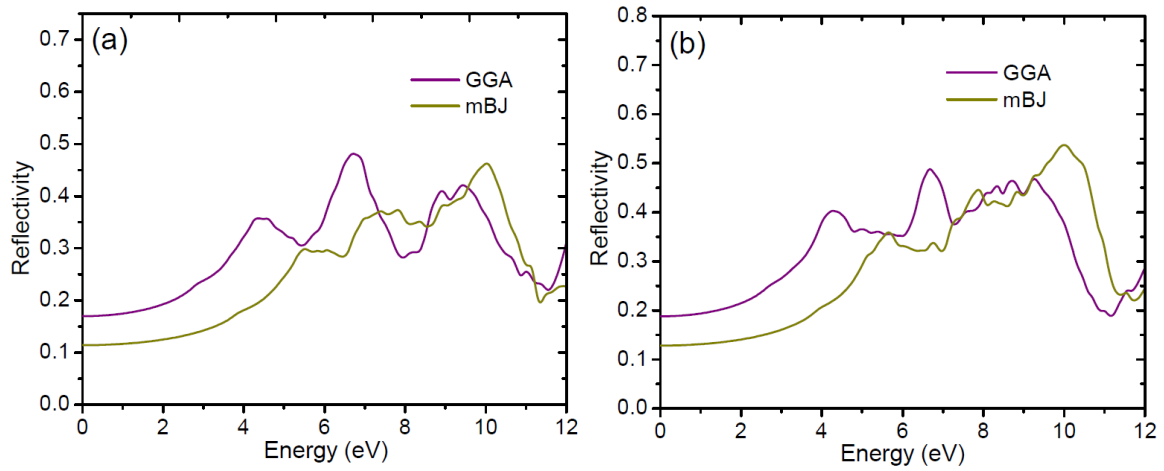


Fig. 4.11. Reflectivity spectra of (a) $\text{Pb}_2\text{ScSbO}_6$ and (b) $\text{Pb}_2\text{ScTaO}_6$

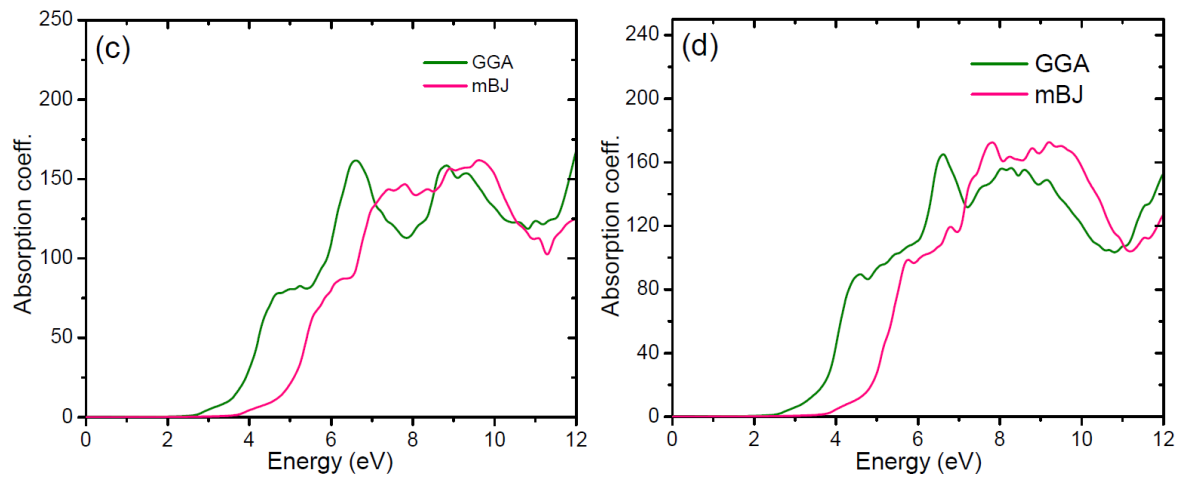


Fig. 4.11. Absorption spectra of (c) $\text{Pb}_2\text{ScSbO}_6$ and (d) $\text{Pb}_2\text{ScTaO}_6$

5

Study of Electronic and Optical properties of Double Perovskites $Ba_2VB'O_6$ ($B' = Nb$ and Mo)

In this chapter, we will present the results of calculations of the electronic, magnetic and optical properties of double perovskites $Ba_2VB'O_6$ ($B' = Nb$ and Mo). In this context, we will also present the structural parameters like lattice constants calculated by volume optimization. We have chosen alkaline earth elements AA' as Ba , and transition metals BB' such that B as V , B' as Nb and Mo respectively. The results of electronic, magnetic and optical properties of these systems will be discussed here in the context of FP-LAPW model within density functional theory. Magnetic properties is studied by plotting the density of states and energy bands of the perovskites for the spin up and down of the electrons. The exchange correlations potentials had been calculated by using the GGA and mBJ potential. We have calculated these properties for Ba_2VNbO_6 within GGA, and for Ba_2VMoO_6 by using mBJ by considering the spins up and down for the electrons. The computational details used in this chapter had been already discussed in section 3.2 of Chapter-3. The only difference with the previous calculations is that in the case of $Ba_2VB'O_6$, we have used $k = 2000$ points.

5.1 Crystal Structure

All atomic positions are in fractional coordinates (Wyckoff, 1935). Fig. 5.1 shows that the (100) plane of the corresponding conventional unit cell which was displayed by XCrySDen (Kokalj, 2003). The structural optimization based on Murnaghan's equation of state (Murnaghan,

1994) was performed to obtain the relaxed structure of the crystal with minimum energy. From this minimum energy, we obtained the optimized lattice parameters which are summarized in Table 5.1. The structural optimization defines the obtained energy versus volume plot for $\text{Ba}_2\text{VB}'\text{O}_6$ ($\text{B}' = \text{Nb}$ and Mo) as given in Figs. 5.2 and 5.3 respectively. With this, the optimized lattice constants were used to calculate the electronic structure, optical and magnetic properties.

The perovskite $\text{Ba}_2\text{VB}'\text{O}_6$ ($\text{B}' = \text{Nb}$ and Mo) crystallizes in cubic phase with $Fm\bar{3}m$ space group. The Ba, V, B' and O atoms occupy the $8c$, $4a$, $4b$ and $24e$ Wyckoff position in the unit cell with Ba (0.25, 0.25, 0.25), V (0, 0, 0), B' (0.5, 0, 0) and O (u, 0, 0), see Fig. 5.1.

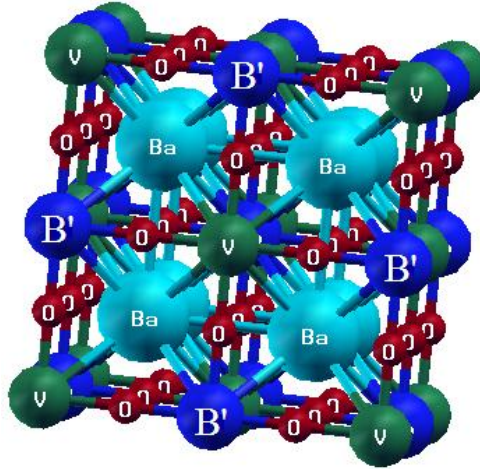


Fig. 5.1. Unit cell structure of double perovskite oxide $\text{Ba}_2\text{VB}'\text{O}_6$ ($\text{B}' = \text{Nb}$ and Mo)

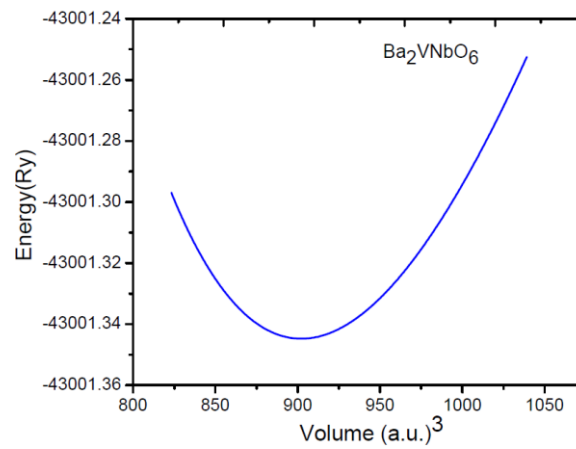


Fig. 5.2. Volume optimization for Ba_2VNbO_6

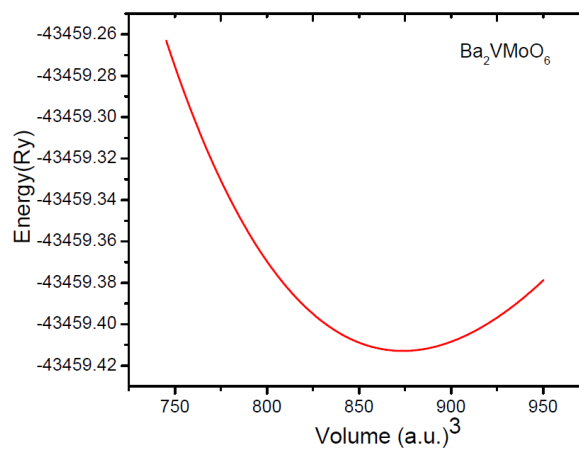


Fig. 5.3. Volume optimization for Ba_2VMoO_6

Table 5.1 Calculated lattice constant (a), internal atomic parameters u, bulk modulus B (in GPA) and pressure derivative of bulk modulus (B') of Ba₂VB'O₆ (B' = Nb, Mo)

Compounds	Calculated (a)	Previous (a)	u	B(GPA)	B'
Ba ₂ VNbO ₆	8.1164	7.9559 ^a	0.2513	170.0401	4.7950
Ba ₂ VMoO ₆	8.0305	7.9478 ^a	0.2516	174.2414	4.5078

^a(Musa, 2012)

5.2 Results of Density of states (DOS)

In this section, we present the results of total density of states (DOS) and the partial density of states (PDOS) in the case of double perovskites $Ba_2VB'O_6$ ($B' = Nb$ and Mo) considering the spins of the electrons. For the combinations of the elements, we have chosen the alkaline earth elements Ba, transition metals V and B' with $B' = Nb$ and Mo .

5.2.1 Density of states for Ba_2VNbO_6

The double perovskite Ba_2VNbO_6 is a magnetic system and hence we have calculated the DOS and PDOS for this system considering the spin up and spin down of the electrons using the GGA. In Fig. 5.4, we have shown the plots of TDOS considering the spin up and spin down of the electrons. For spin up case, we find that in the energy range from -3 eV to -5 eV in the valence band, contribution to the maxima in the TDOS are by O atoms. At the Fermi level (energy=0) in spin up case, there is maxima in TDOS which appears due to contribution by the V atoms. In the conduction band, above the Fermi level at 2 eV, there is contribution by the Nb atom to the TDOS maxima of the perovskite. Also it is found that in the energy range +5 eV to 7 eV, contribution to the occurrence of maxima in TDOS of the perovskite is due to Ba atom only. The occurrence of maxima in TDOS at the Fermi level indicate the metallic behavior in spin up case.

For spin down case for Ba_2VNbO_6 perovskite, the plots of DOS is also shown in Fig. 5.4. From the plots of DOS, we find that in the valence band, there are maxima occurring in TDOS at the energies -3 eV, -5 eV and -6 eV respectively. Contribution to these maxima are by O atom. In the conduction band, there are maxima in TDOS at 2 eV and 7 eV respectively which are due to the V and Ba atoms. However we find the occurrence of energy gap of 2.3 eV between the valence and the conduction bands in the spin down case. This is indicative of the behavior of the perovskite as a semiconductor but with a wide band gap.

The plots of PDOS in the case of spins up and down for the perovskite Ba_2VNbO_6 are shown in Fig. 5.5 for individual atoms Ba, V, Nb and O respectively. The PDOS in fact supports the results of the TDOS as shown in Fig. 5.4. In the valence band as shown in Fig. 5.5(a), contribution by Ba atom to PDOS is nil in spin up and down case, whereas in the conduction band Ba-d electrons are contributing to the PDOS in both spin up and down case. V atom has maxima in the PDOS at the Fermi level which is due to V- $d_{t_{2g}}$ electrons. In the conduction band, V-d electron contributes to PDOS at ~ 2 eV above the Fermi level for both the spins. We find from Fig. 5.5(c) that in the valence band, it is the $d-t_{2g}$ electron of Nb which contributes to maximum in PDOS at ~ -5 eV for both spin up and down cases. Whereas in the conduction band also for both the spins, it is the Nb- $d_{t_{2g}}$ electron which contributes to the maxima in PDOS at 2 eV. From Fig. 5.5(d), we find that both for the spins in the valence and the conduction bands, O atom has very negligible contribution to PDOS.

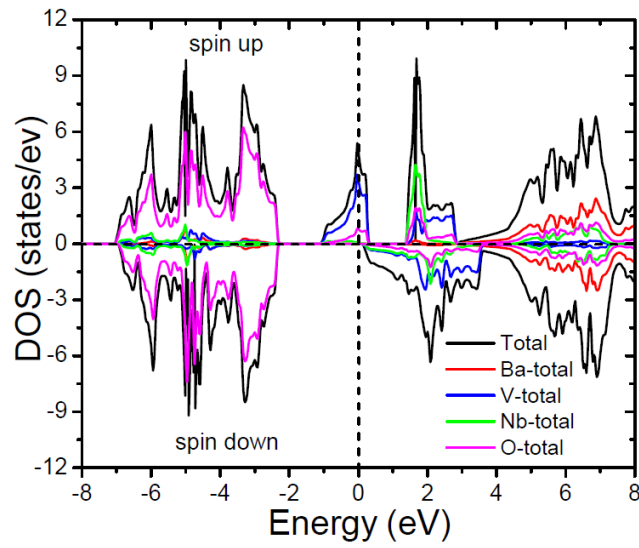


Fig. 5.4. Total DOS plot for Ba_2VNbO_6

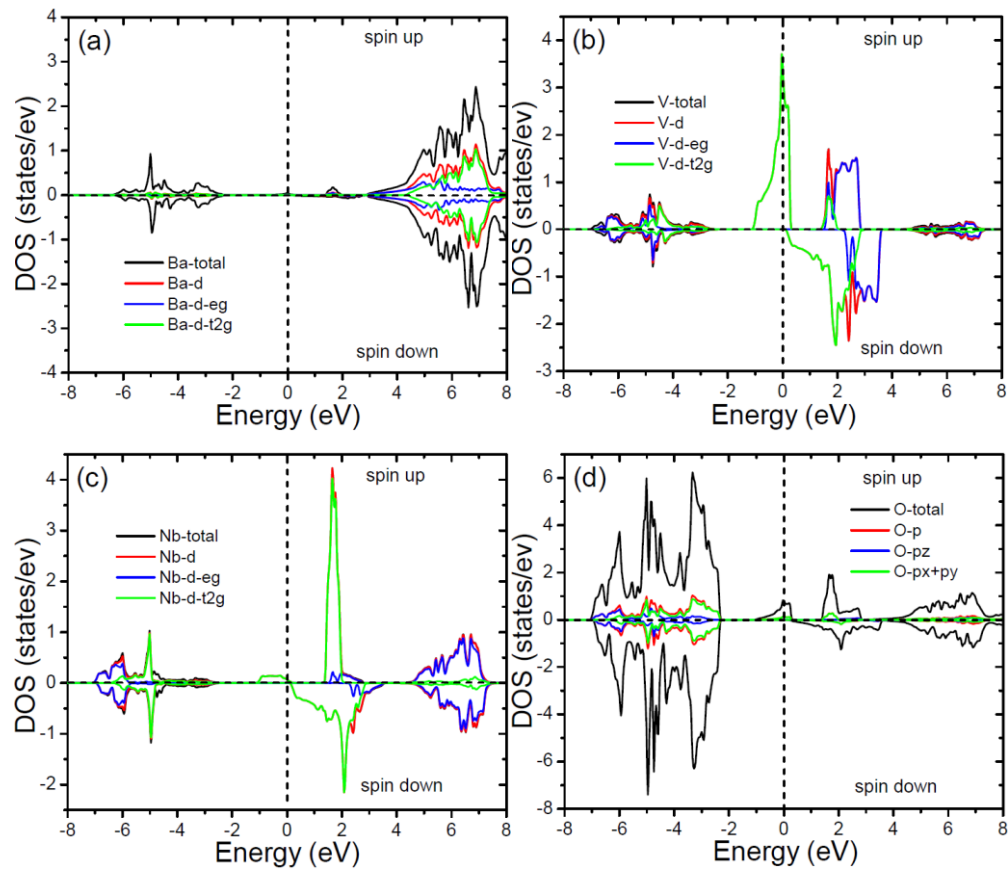


Fig. 5.5. TDOS and PDOS plot for individual atom of Ba_2VNbO_6

5.2.2 Density of states for Ba₂VMoO₆

In this section, we discuss the results of calculations of DOS and PDOS in the case of perovskite Ba₂VMoO₆. Here also we have used the FP-LAPW method but by using the mBJ potential. In Fig. 5.6, we have shown the plots of TDOS by considering the spin up and spin down of the electrons. For spin up case, we find that the maximum contribution in the TDOS ranging from -3 eV to -5 eV in the valence band are by O atoms. At the Fermi level (energy=0) in spin up case, we see that the Fermi is cover by DOS which appears due to contribution by the V atoms. In the conduction band, above the Fermi level at 0.2 eV, there is contribution to the TDOS maxima by the Mo atom. Also it is found that in the energy range +5 eV to +7 eV, contribution to the occurrence of maxima in TDOS by Ba atom only. The occurrence of maxima in TDOS at the Fermi level indicate the metallic behavior in spin up case.

For spin down case, the plots of DOS for Ba₂VMoO₆ is shown in Fig. 5.6, we find that in the valence band, there are maxima occurring in TDOS at the energy range from -3 eV to -6 eV, contribution to these maxima are by O atom. In the conduction band, we find that there are maxima in TDOS at 1 eV, 3 eV and 6 eV respectively which are due to the Mo, V and Ba atoms. In the spin down channel, we find the occurrence of energy gap of 2.6 eV between the valence and the conduction bands in the spin down case. This is indicates that the behavior of these system as a semiconductor with a very wide band gap.

The plots of PDOS in the case of spins up and down for the perovskite Ba₂VMoO₆ are shown in Fig. 5.7 for individual atoms Ba, V, Mo and O respectively. In the valence band as shown in Fig 5.7(a), no contribution by Ba atom to PDOS in spin up and down case, where as in the conduction band Ba-d electrons are contributing to the PDOS in both spin up and down case between the energy ranges from 6 eV to 7 eV. V atom has maxima in the PDOS at the Fermi level

which is due to V- d_{t_2g} electrons. In the conduction band, V-d electron contributes to PDOS at ~ 4 eV above the Fermi level for both the spins. From Fig. 5.7(c) that in the valence band, it is the d- t_{2g} electron of Mo which contributes to maximum in PDOS at ~ -5.5 eV for both spin up and down cases. Whereas in the conduction band, in the spin up channel, it is the Nb- d_{t_2g} electron which contributes to the maxima in PDOS at ~ 0.2 eV and at 1 eV in spin down channel. From Fig. 5.7(d), we find that both for the spins in the valence and the conduction bands, O atom has very negligible contribution to PDOS.

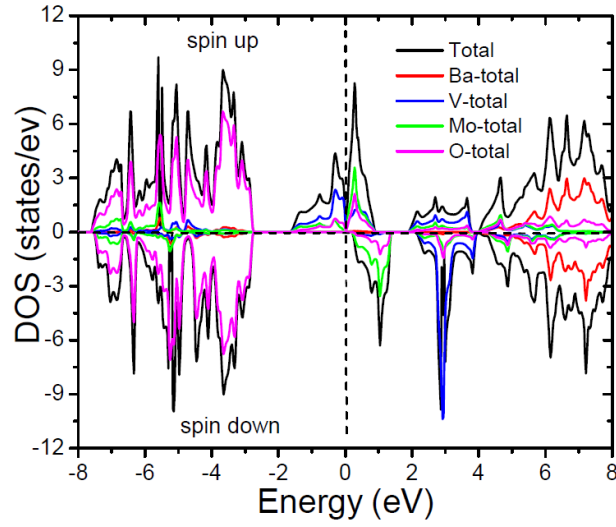


Fig. 5.6. Total DOS plot for Ba₂VMoO₆

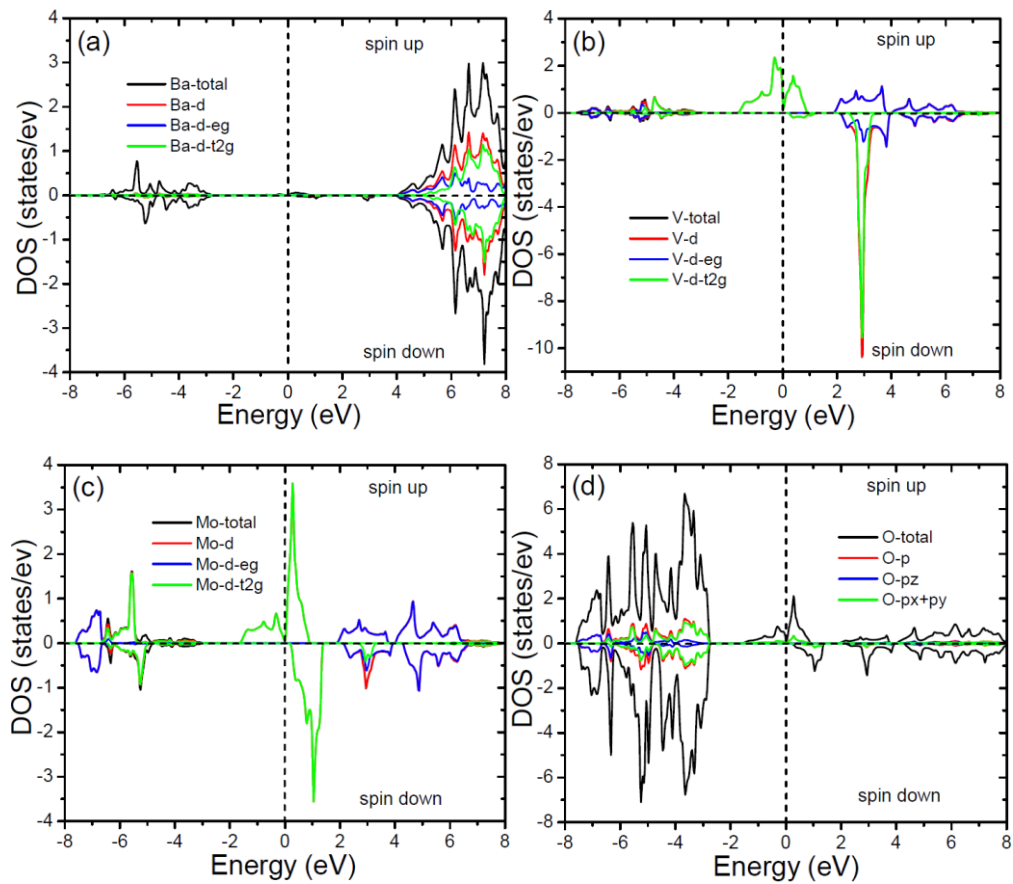


Fig. 5.7. TDOS and PDOS plot for individual atom of Ba₂VMoO₆

5.3. Energy Bands in $\text{Ba}_2\text{VB}'\text{O}_6$ ($\text{B}' = \text{Nb}, \text{Mo}$)

In this section, we discuss the results of the energy bands for the perovskites of Ba and V with the transition metals combinations Nb and Mo. The various parameters involved in the calculations of energy bands are already discussed in section 5.3. The energy bands are calculated for the spin up and down cases for the system which are shown in Figs. 5.8 and 5.9.

In Fig. 5.8(i and ii), we show the plots of energy bands in the case of Ba_2VNbO_6 for spins up and down. In Fig. 5.8(i), in the spin up case in the valence band, the maxima in the energy band is at -2.5 eV below the Fermi level (Fermi level is set at 0 eV) at the symmetry point Γ . The contribution to this maxima in the energy band is due to O-p electron states which is evident from the PDOS plots as given in Fig. 5.5(d). We also find from the energy bands in Fig. 5.8 (i) that there is a maxima in conduction band above the Fermi level at +0.4 eV. This band is coinciding with the maxima in TDOS and PDOS as shown in Figs. 5.4 and 5.5 respectively, which is due to V- d_{t_2g} electron states. This is indicative of the metallic behavior of the electrons in the solid.

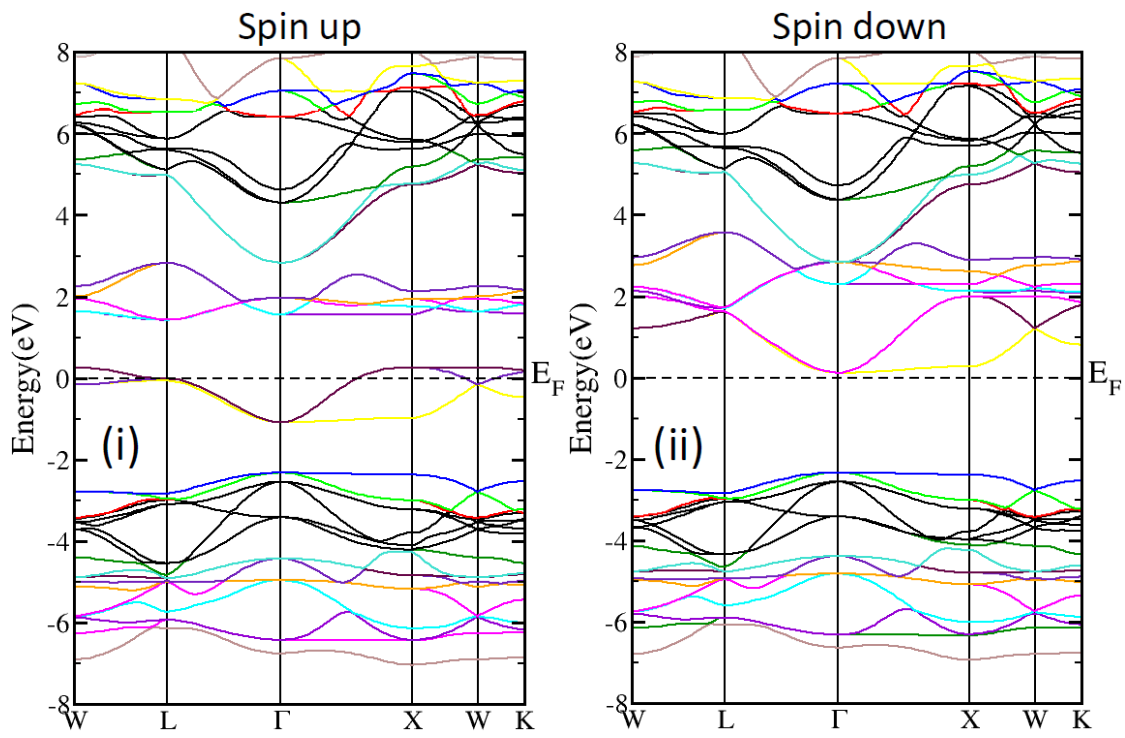


Fig. 5.8. Band structure plot for Ba_2VNbO_6 calculated using GGA

In Fig. 5.8(ii) we show the plots of energy bands in the case of Ba_2VNbO_6 for spin down. Here also we find that in the valence band, the maxima in the energy band is at -2.5 eV below the Fermi level (Fermi level is set at 0 eV) at the symmetry point Γ . The contribution to this maxima in the energy band is due to O-p electron states which is evident from the PDOS plots as given in Fig. 5.5(d). We also find from the energy bands in Fig. 5.8(ii) that there is a minimum in conduction band at 0.1 eV above the Fermi level at the symmetry point Γ . This is indicative of a semiconducting behavior of the electrons in the solid and hence an energy band gap exist. The value of the energy band gap is 2.6 eV and it is a direct band gap at the symmetry point Γ .

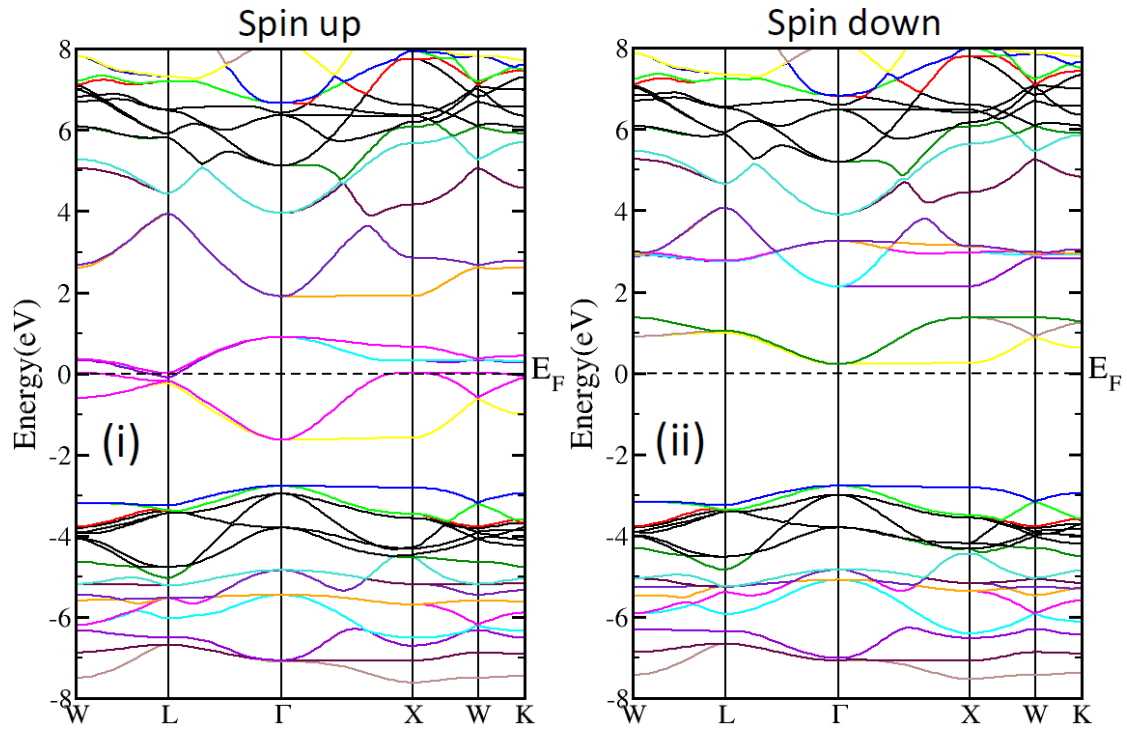


Fig. 5.9. Band structure plot for Ba_2VMoO_6 using mBJ potential

In Fig. 5.9(i and ii), we again show the plots of energy bands in the case of Ba_2VMoO_6 for spins up and down. In Fig. 5.9(i), in the spin up case in the valence band, the maxima in the energy band is at -2.3 eV below the Fermi level (Fermi level is set at 0 eV) at the symmetry point Γ . The contribution to this maxima in the energy band is due to O-p electron states which is evident from the PDOS plots as given in Fig. 5.7(d). We also find that there is a maxima in conduction band above the Fermi level at 1 eV. This band is coinciding with the maxima in TDOS and PDOS as shown in Fig. 5.6 and 5.7 respectively, which is due to V- d_{t_2g} electron states. This is indicative of the metallic behavior of the electrons in the solid.

In Fig. 5.9(ii), we show the plots of energy bands in the case of Ba_2VMoO_6 for spin down. Here also we find that in the valence band, the maxima in the energy band is at -2.8 eV below the Fermi level (Fermi level is set at 0 eV) at the symmetry point Γ . The contribution to this maxima in the energy band is due to O-p electron states which is evident from the PDOS plots as given in Fig. 5.7(d). We also find from the energy bands in Fig. 5.9(ii) that there is a minimum in conduction band at 0.1 eV above the Fermi level at the symmetry point Γ . This is indicative of a semiconducting behavior of the electrons in the solid and hence an energy band gap exist. The value of the energy band gap is 2.5 eV and it is a direct band gap at the symmetry point Γ .

5.4 Magnetic moments of $\text{Ba}_2\text{VB}'\text{O}_6$

To investigate the magnetic nature of $\text{Ba}_2\text{VB}'\text{O}_6$ ($B' = \text{Nb}, \text{Mo}$), we carried out the spin polarized DFT calculations with GGA scheme. We found that these compounds possess half metallic nature. The main source of magnetization in these compounds is the unfilled V-3d orbital. From the study of the PDOS as shown in Fig. 5.5(b) and 5.7(b), we find that it is the V-3 d_{t_2g} state electrons which is the responsible for ferromagnetism in these perovskite. The magnetic moments

of each of these compounds as well as their individual atomic magnetic moment are given in Table 5.2. Our calculations reveal that the magnetic moments for Ba_2VNbO_6 and Ba_2VMoO_6 are 2.00049 and 3.00018 μB , respectively. In each compound, the magnetic moments of all the spheres that is assumed in the FP-LAPW model have the same direction. Hence, in the two type of compounds, the vanadium contributes largely to the magnetisation of the perovskites.

Table 5.2 Magnetic moments (in μB) of the interstitial region, individual atoms and total magnetic moment for the double perovskites $\text{Ba}_2\text{VB}'\text{O}_6$ ($\text{B}' = \text{Nb}, \text{Mo}$)

Compounds	m^{Inst}	m^{Ba}	m^{V}	$m^{\text{Nb}\backslash\text{Mo}}$	m^{O}	m^{Total}
Ba_2VNbO_6	0.3858	0.0047	1.5097	0.1488	-0.0089	2.0004
Ba_2VMoO_6	0.5141	0.0017	1.7491	0.7117	0.0036	3.0001

5.5 Results of Optical properties for Ba₂VB'O₆

Optical properties describe the interaction of electromagnetic radiations with a material and dielectric function plays key role in the investigation of the optical properties of compounds. The optical properties of solids are a major topic, both in basic research as well as for industrial applications. In research part the origin and nature of different excitation processes is of fundamental interest, while the industries can make use of them in many opto-electronic devices. The dielectric function of an anisotropic material is a complex symmetric second-order tensor which describes the linear response of an electronic system to an applied external electric field. It is expressed as $\varepsilon(\omega) = \varepsilon_1(\omega) + i\varepsilon_2(\omega)$, where ε_1 and ε_2 are the real and imaginary components of the dielectric function, respectively. The calculations of this frequency dependent dielectric function require the precise values of energy eigenvalues and electron wavefunctions. These are natural outputs of a band structure calculation.

The knowledge of both the real and imaginary parts of the dielectric function allows the calculation of important optical functions such as reflectivity $R(\omega)$ and optical absorption coefficient $I(\omega)$. The compounds Ba₂VNbO₆ and Ba₂VMoO₆ are having cubic symmetry. For cubic symmetry, the principal tensor component ε_{xx} , ε_{yy} and ε_{zz} will be equal. Hence only one component of the dielectric function has to be calculated i.e, $\varepsilon_{xx} = \varepsilon_{yy} = \varepsilon_{zz}$.

In Fig. 5.10(a) and Fig. 5.10(b) represents real part $\varepsilon_1(\omega)$ of dielectric function of Ba₂VNbO₆ and Ba₂VMoO₆ compound. From our calculation, we have found maximum value of $\varepsilon_1(\omega)$ at 0.012 eV for Ba₂VNbO₆ and at 0.4 eV for Ba₂VMoO₆ then it starts to decreases abruptly. From the plot in real part of dielectric function with photon energy, we have found the minimum value of $\varepsilon_1(\omega)$ at 5.6 eV for Ba₂VNbO₆ and at 0.8 eV for Ba₂VMoO₆. From Fig. 5.10(a) and Fig.

5.10(b), the imaginary part $\varepsilon_2(\omega)$ of dielectric function for Ba_2VNbO_6 and Ba_2VMoO_6 in the approach of GGA. From this calculation, we have found the maximum value of $\varepsilon_2(\omega)$ at 0.01 eV for Ba_2VNbO_6 and at 0.6 eV Ba_2VMoO_6 .

The important optical constants like reflectivity $R(\omega)$ and optical absorption coefficient $I(\omega)$, are shown in Fig. 5.11 (a-d). From Fig. 5.11 (a) the reflectivity profiles of Ba_2VNbO_6 clearly show the location of peaks at energy of 1.5 eV and 5.2 eV. From Fig. 5.11 (b), for Ba_2VMoO_6 peaks are observed at energy of 0.5 eV, 3.5 eV and 4.5 eV. The low value of reflectivity in these compounds makes sure its potential applications in the area of transparent coatings in the visible and deep UV region.

The calculated absorption for Ba_2VNbO_6 and Ba_2VMoO_6 are shown in Figs. 5.11(c) and (d). From Fig. 5.11(c), for Ba_2VNbO_6 the absorption spectrum has two peaks located at energy of 1.8 eV and 5.2 eV. However, from Fig. 5.11(d), for Ba_2VMoO_6 four peaks are located at energy of 0.5, 4.5, 6.1, and 8.2 eV. It is clear that for both the compounds the peaks obtained in the absorption spectrum matches with the peaks of imaginary part of the dielectric function $\varepsilon_2(\omega)$, which indicates that the origin of absorption is due to the imaginary part of the dielectric function. From the absorption spectrum it is clear that at the lower energies the absorption coefficient decreases rapidly which is a well know behavior for semiconductors.

Table 5.3. The calculated dielectric constant $\varepsilon_1(0)$, reflectivity $R(\omega)$, and absorption coefficient $I(\omega)$ for Ba_2VNbO_6 and Ba_2VMoO_6

Compound	$\varepsilon_1(0)$	$R(\omega)$	$I(\omega)$
Ba_2VNbO_6	18.5	0.16	0.09
Ba_2VMoO_6	32.6	0.88	0.25

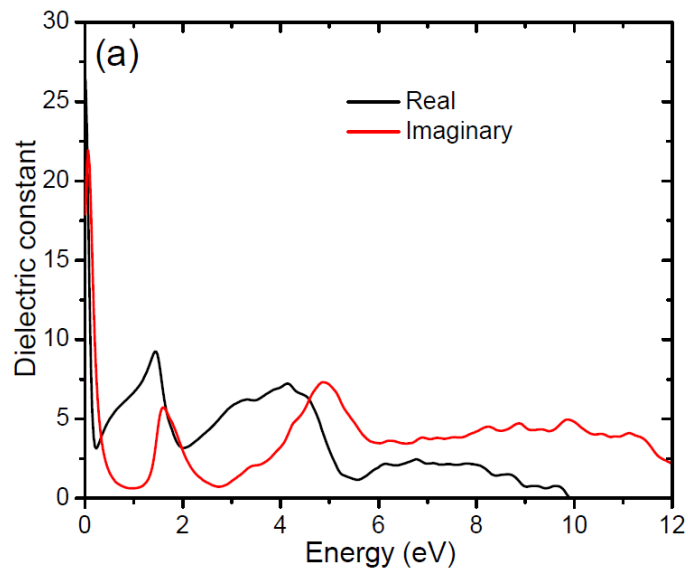


Fig. 5.10(a). The optical spectrum of the dielectric constant as a function of the photon energy of Ba_2VNbO_6 using GGA potential

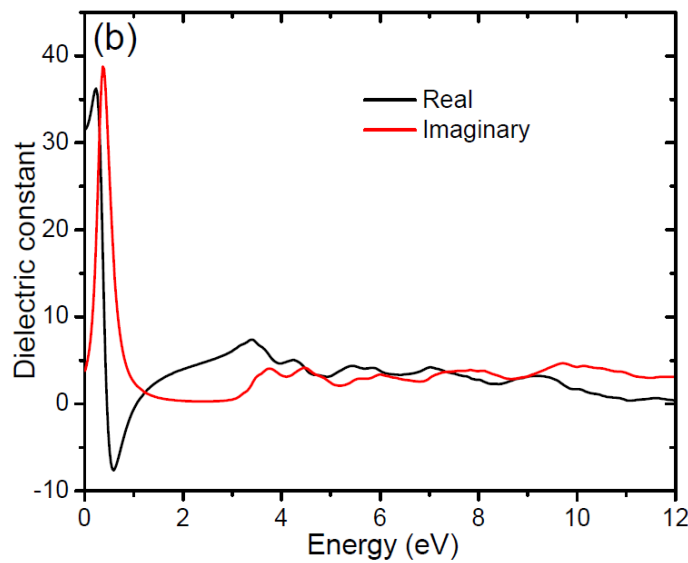


Fig. 5.10(b). The optical spectrum of the dielectric constant as a function of the photon energy of Ba_2VMoO_6 using mBJ potential

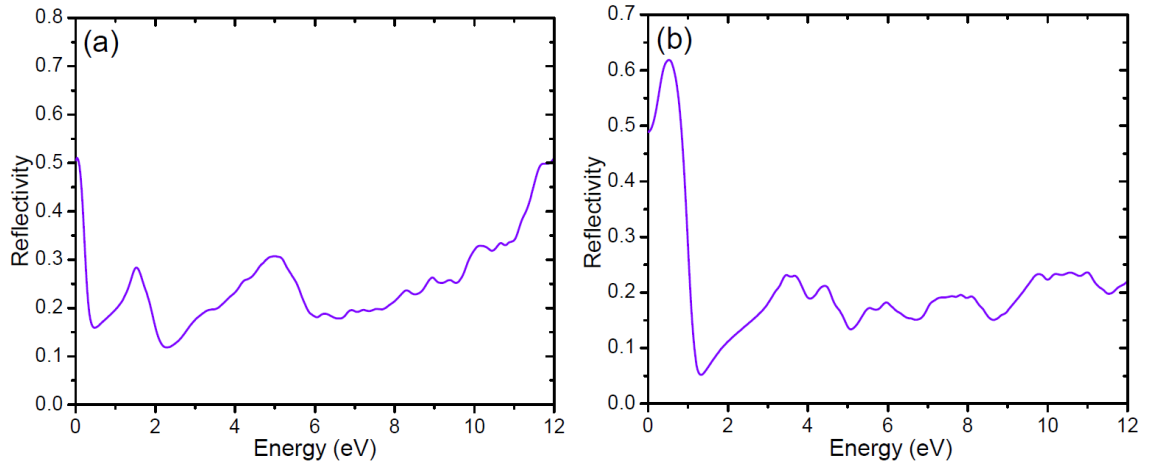


Fig. 5.11. Reflectivity spectra of (a) Ba₂VNbO₆ and (b) Ba₂VMoO₆

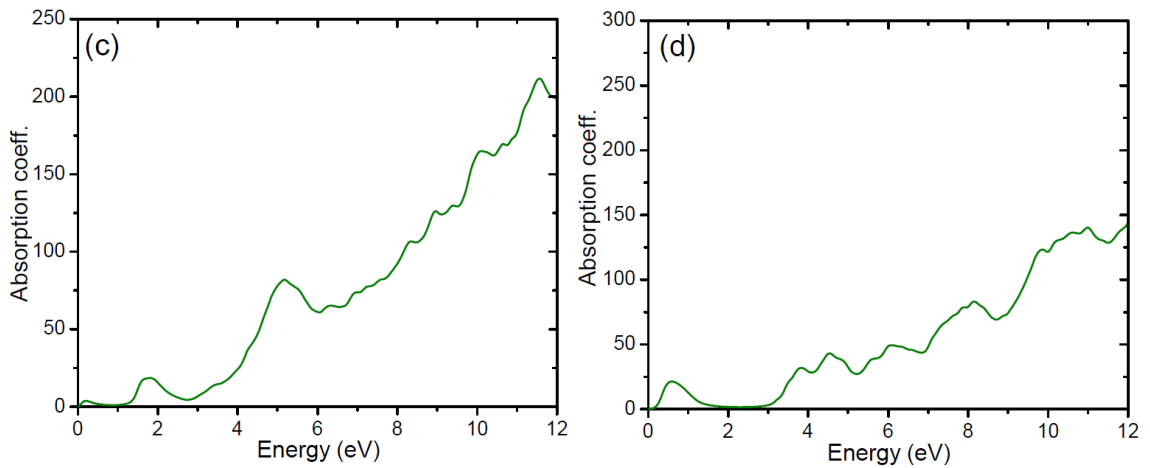


Fig. 5.11. Absorption spectra of (c) Ba₂VNbO₆ and (d) Ba₂VMoO₆

6

Study of Electronic and Optical properties of Double Perovskites $La_2CrB'O_6$ ($B' = Co, Ni$)

In this chapter, the study of electronic structures, magnetic and optical properties will be presented for the combination of double perovskite systems $La_2CrB'O_6$ ($B'=Co, Ni$). We have chosen the combinations of rare earth elements A, $A' = La$, and transition metals $B = Cr$ and $B' = Co, Ni$ respectively. The electronic configuration of lanthanum is La: $[Xe]6s^25d^1$ and it is seen that probably the d-state electrons will be taking part in the electronic transitions. However this will be possible to understand from interaction of other electrons of the elements in the perovskite which we will understand from the study of the total and partial density of states (DOS). The results of total and partial density of states, energy bands and also the optical properties of these systems will be discussed here in the context of FP-LAPW model within density functional theory. This method had been already discussed in Chapter-2. The exchange correlations potentials used for the calculation is GGA. The computational details used in this chapter had been already discussed in section 3.2 of Chapter-3. The only difference with the previous calculations is that in the case of $La_2CrB'O_6$, we have used $k=2000$ points. We have used here also the Wien2k code (Blaha *et al.*, 2012) as used in the earlier chapters.

6.1 Crystal Structure

All atomic positions are in fractional coordinates as given by (Wyckoff, 1935). Fig. 6.1 shows that the (100) plane of the corresponding conventional unit cell which was displayed by

XCrySDen (Kokalj, 2003). The structural optimization based on Murnaghan's equation of state (Murnaghan, 1994) have been done as usual to obtain the relaxed structure of the crystal with minimum energy. From this minimum energy, we obtained the optimized lattice parameters which are summarized in Table 6.1. The structural optimization defines the obtained energy versus volume plot for $\text{La}_2\text{CrB}'\text{O}_6$ ($\text{B}' = \text{Co}$ and Ni) as given in Fig. 6.2 and Fig. 6.3 respectively. With this, the optimized lattice constants were used to calculate the electronic structure, optical and magnetic properties.

The double perovskite compounds $\text{La}_2\text{CrB}'\text{O}_6$ ($\text{B}' = \text{Co}, \text{Ni}$) crystallize in body centered tetragonal structure with space group $I4/m$, the atomic position of La atom is at (0, 0.5, 0.75), Cr atom is at (0, 0, 0), B' atom is at (0, 0, 0.5), O is at (0, 0, u) see Fig. 6.1.

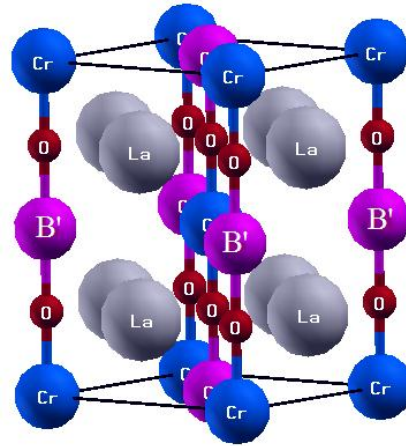


Fig. 6.1. Unit cell structure of double perovskite oxide $\text{La}_2\text{CrB}'\text{O}_6$ ($\text{B}' = \text{Co}$ and Ni)

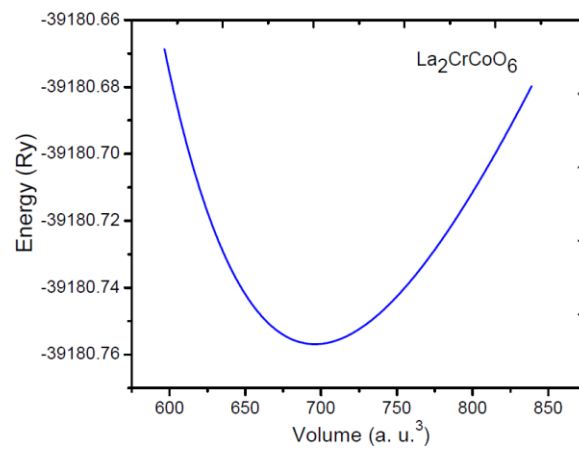


Fig.6.2. Volume optimization of $\text{La}_2\text{CrCoO}_6$

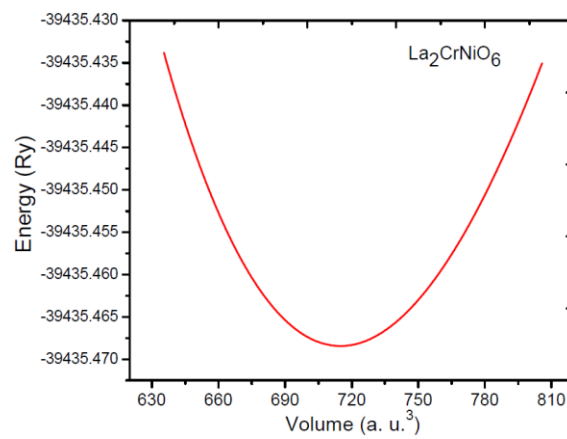


Fig.6.3. Volume optimization of $\text{La}_2\text{CrNiO}_6$

Table. 6.1 Calculated lattice constant (a), internal atomic parameters u, bulk modulus B (in GPA) and pressure derivative of bulk modulus (B') of $\text{La}_2\text{CrB}'\text{O}_6$ (B' = Co, Ni)

Compounds	a(Å)	Previous	c(Å)	Previous	c/a(Å)	u	B(GPA)	B'
$\text{La}_2\text{CrCoO}_6$	4.1916	5.4461 ^a	5.9227	7.7018 ^a	1.4142	0.2522	108.617	5.5986
$\text{La}_2\text{CrNiO}_6$	4.2140	5.4735 ^a	5.9595	7.7406 ^a	1.4142	0.2467	102.094	4.5120

^a(Lui *et al.*, 2012)

6.2 Results of Density of states (DOS)

In this section, we present the results of total density of states (DOS) and the partial density of states (PDOS) in the case of double perovskites $\text{La}_2\text{CrB}'\text{O}_6$ ($\text{B}' = \text{Co}$ and Ni) considering the spins of the electrons. For the combinations of the elements, we have chosen the rare earth element La and transition metals Cr and $\text{B}' = \text{Co}$ and Ni .

6.2.1 Density of states for $\text{La}_2\text{CrCoO}_6$

The double perovskite $\text{La}_2\text{CrCoO}_6$ is a magnetic system and hence we have calculated the DOS and PDOS for this system considering the spin up and spin down of the electrons using the GGA. In Fig. 6.4, we have shown the plots of TDOS considering the spin up and spin down of the electrons. For spin up case, we can see that in the valence region, maxima in DOS occurs at -1.28 eV below the Fermi level (energy = 0) which is due to the contribution of Co atom. In the conduction band from spin up channel, above the Fermi level at 2 eV, there is contribution by the La atom to the TDOS maxima of the perovskite.

For spin down case for $\text{La}_2\text{CrCoO}_6$ perovskite, the plots of DOS is also shown in Fig. 6.4. From TDOS plot, we find that in the valence band, there is a maxima occurring in TDOS at 0.42 eV below the Fermi level (Fermi level=0) which is due to the contribution of Co atom. In the conduction band, there are maxima in TDOS at 2 eV which are due to the La atom. At Fermi level, we see that in both the spin up and spin down channel, the Fermi level is covered by the DOS resulting in a metallic behavior in both spin channels.

The plots of PDOS in the case of spins up and down for the perovskite $\text{La}_2\text{CrCoO}_6$ are shown in Fig. 6.5 for individual atoms La, Cr, Co and O respectively. We find that the PDOS in fact supports the results of the TDOS as shown in Fig. 6.4. In the valence band as shown in Fig 6.5 (a), contribution by La atom to PDOS is nil in spin up and down case, where as in the

conduction band, La-f electron state are contributing to the maxima in PDOS from both spin up and down case at 2 eV. Cr atom has maxima in the PDOS at the Fermi level, which is due to Cr-d electrons. In the valence band, Cr-d electron contributes to the maxima in PDOS at ~ -1.8 eV above the Fermi level for spin up channel and from the spin down channel in the conduction band, it contributes to PDOS at ~ 2.5 eV above the Fermi level. We also find from Fig. 6.5(c) that in the valence band, it is the d state electron of Co, which contributes to maximum in PDOS at ~ -1.2 eV for spin up and at ~ -0.4 for spin down cases. But in the conduction band, for both the spins, the contribution to PDOS by Co atom was nil, as it is highly negligible. From Fig. 6.5(d), we find that both for the spins in the valence and the conduction bands, O atom has very negligible contribution to PDOS.

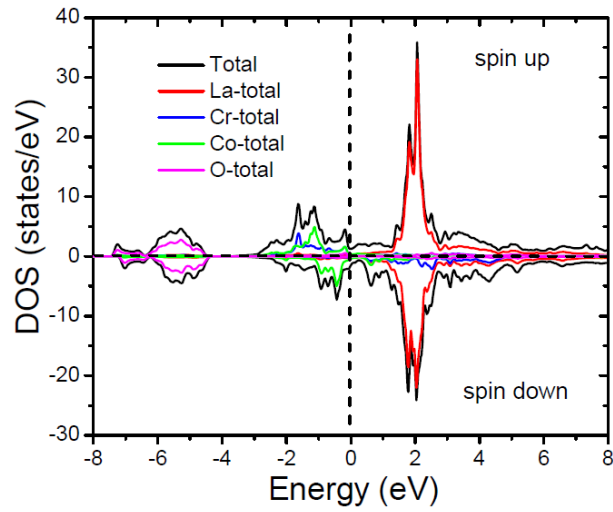


Fig. 6.4. Total DOS plot for $\text{La}_2\text{CrCoO}_6$

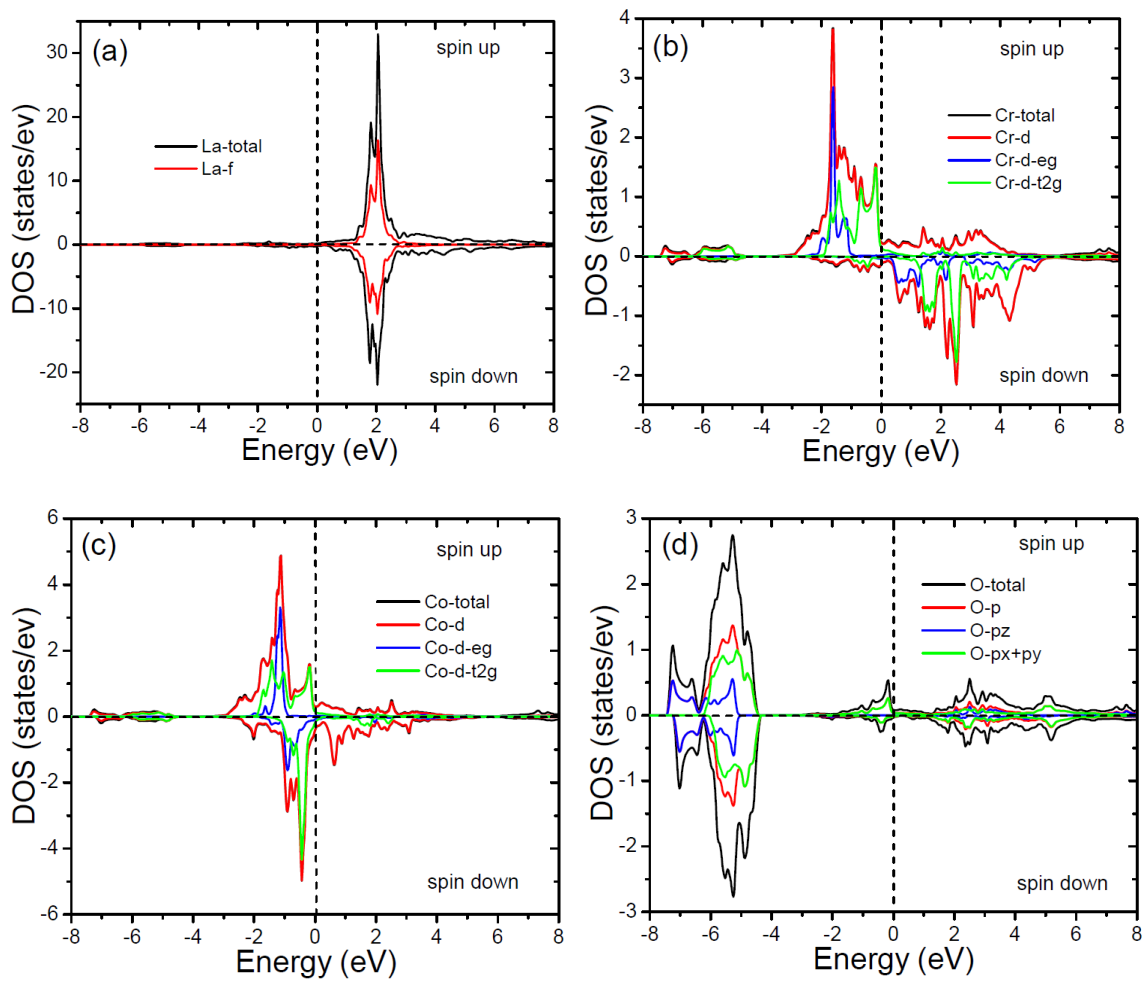


Fig. 6.5. TDOS and PDOS plot for individual atom of $\text{La}_2\text{CrCoO}_6$

6.2.2 Density of states for $\text{La}_2\text{CrNiO}_6$

In this section, we discuss the results of calculations of DOS and PDOS in the case of magnetic double perovskite $\text{La}_2\text{CrNiO}_6$ by considering the spin up and spin down of the electrons using the GGA. In Fig. 6.6, we have shown the plots of TDOS considering the spin up and spin down of the electrons. For spin up case, we can see that in the valence region, maxima in DOS occurs at -1.5 eV below the Fermi level ($E_F = 0$) which is the contribution of Ni atom. Whereas in the conduction band, it was the La atom which contributes to the maxima in TDOS at 2 eV.

For the spin down case, we find the maxima in TDOS at -1.3 eV below Fermi level, which is due to the occurrence of Ni atom. Whereas in the conduction band, just like the previous case of $\text{La}_2\text{CrCoO}_6$, it is the La atom which contributes to the maxima in TDOS. From both spin up and spin down, we have find that the Fermi level is covered by DOS which mainly contributed by Cr and Ni atoms. Thus, we find that it exhibit metallic properties.

The plots of PDOS in the case of spins up and down for the perovskite $\text{La}_2\text{CrNiO}_6$ are shown in Fig. 6.7 for individual atoms La, Cr, Ni and O respectively. In the valence band as shown in Fig 6.7 (a), in spin up and down case, contribution by La atom to PDOS is negligible where as in the conduction band, La-f electrons are contributing to the maxima in PDOS at 2 eV in both spin up and down case. From Fig. 6.7 (b), in the spin up channel, we find that in the energy range from -0.2 eV to -1.8 eV, Cr electron makes considerable contributes to the PDOS below the Fermi level and in the spin down channel, also Cr-d electron contributes to PDOS at ~ 2.5 eV above the Fermi level. We find from Fig. 6.7 (c) that in the valence band, it is the Ni-d electron which contributes to maximum in PDOS at ~ -1.7 eV for both spin up and down cases. But no contribution from Ni atom in the conduction band for both the spins. From Fig. 6.7 (d), we find that for both

the spins in the valence and the conduction bands, O atom has very negligible contribution to PDOS near the Fermi level.

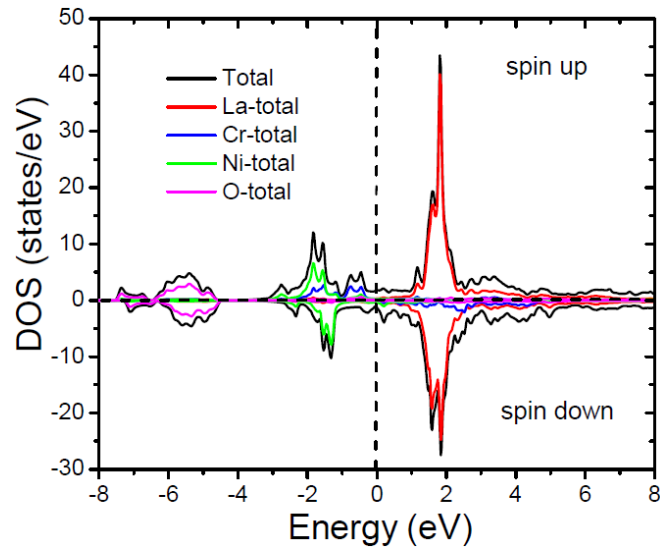


Fig. 6.6. Total DOS plot for $\text{La}_2\text{CrNiO}_6$

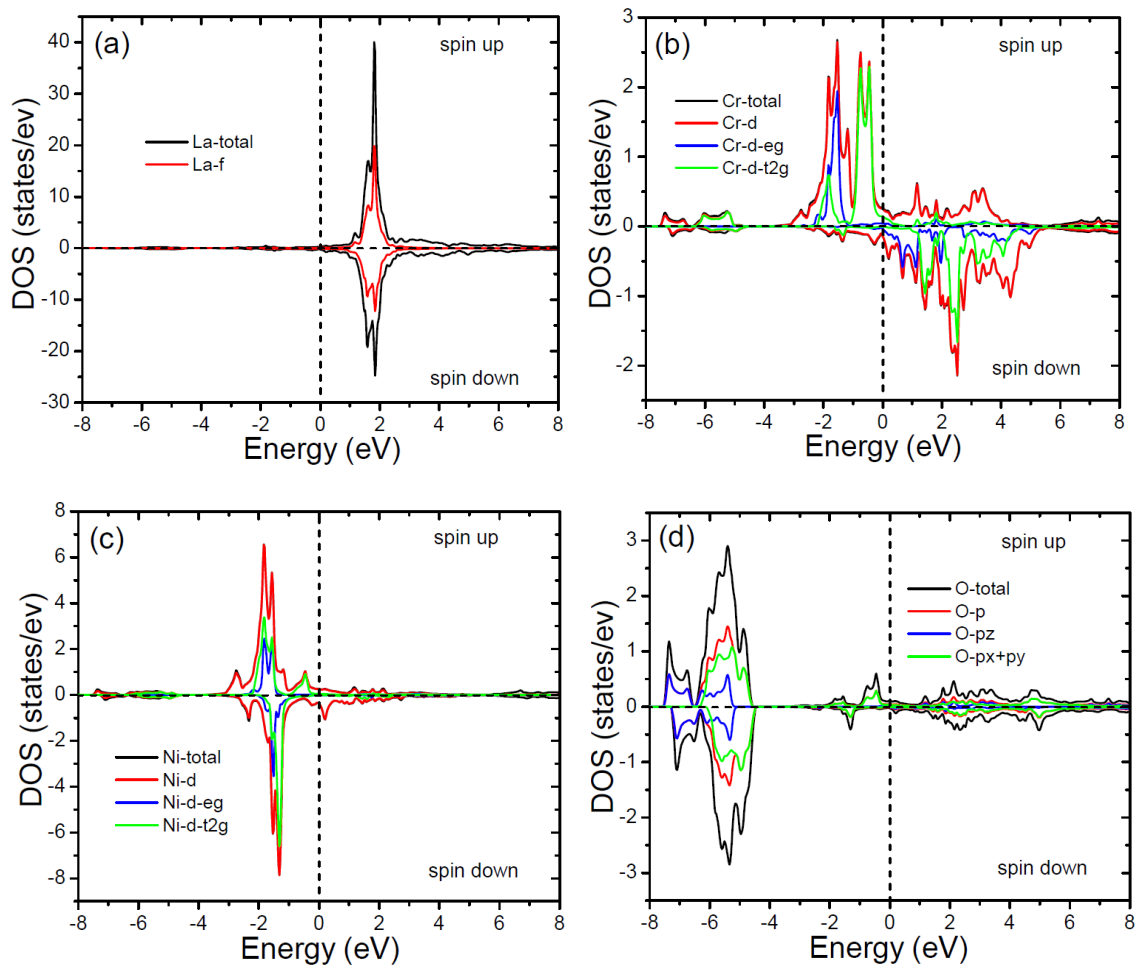


Fig. 6.7. TDOS and PDOS plot for individual atom of $\text{La}_2\text{CrNiO}_6$

6.3. Energy bands of $\text{La}_2\text{CrB}'\text{O}_6$

Here, the lattice constants obtained by volume optimization were used to study the electronic properties which are given in Table 6.1. From Table 6.1, we have for $\text{La}_2\text{CrCoO}_6$, $a = 4.1916$ and $c = 5.9227$; for $\text{La}_2\text{CrNiO}_6$, $a = 4.2140$ and $c = 5.9595$. In Fig. 6.8 and Fig. 6.9, we have shown the band structure plots for $\text{La}_2\text{CrCoO}_6$ and $\text{La}_2\text{CrNiO}_6$. The contribution of different electronic states in the valance and the conduction band determines the electronic property of the material.

From Fig. 6.8 and Fig. 6.9, we can clearly see that no band gap is observed, implying that $\text{La}_2\text{CrCoO}_6$ and $\text{La}_2\text{CrNiO}_6$ are showing a metallic behavior. From PDOS plot, we observe that from Figs. 6.5(b) and 6.7(b) for $\text{La}_2\text{CrCoO}_6$ and $\text{La}_2\text{CrNiO}_6$ for both the spins, that at the Fermi level, there is maximum number of band lines, which is the contribution from Cr atom. This is indicative of the metallic nature in both the case of $\text{La}_2\text{CrCoO}_6$ and $\text{La}_2\text{CrNiO}_6$ without a band gap.

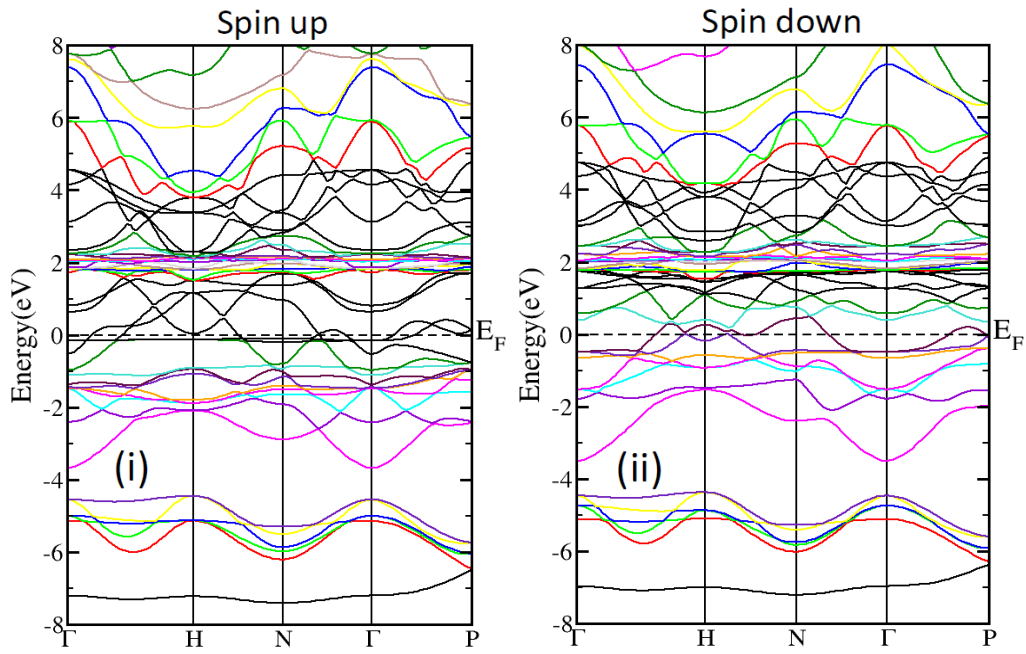


Fig. 6.8. Band structure plot for $\text{La}_2\text{CrCoO}_6$

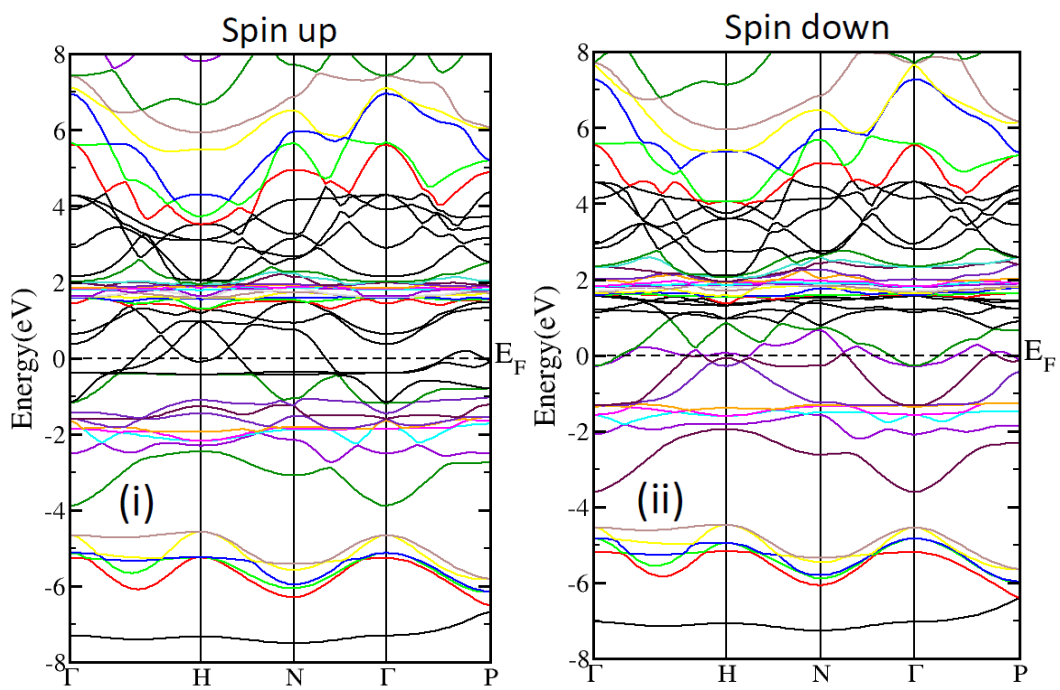


Fig. 6.9. Band structure plot for $\text{La}_2\text{CrNiO}_6$

6.4. Magnetic moments of $\text{La}_2\text{CrB}'\text{O}_6$

To investigate the magnetic nature of double perovskite $\text{La}_2\text{CrB}'\text{O}_6$ ($\text{B}' = \text{Co}, \text{Ni}$), we carried out the spin polarized DFT calculations with GGA scheme. We found that these compounds possess half metallic nature. The main source of magnetization in these compounds is the unfilled Co-3d orbital. Further investigation of the Co-3d state shows that it is the partially filled d- e_g orbital which is responsible for ferromagnetism in these compounds. The total magnetic moments of each of these compounds as well as their individual atomic magnetic moments are given Table 6.2. Our calculations reveal that the magnetic moments for $\text{La}_2\text{CrB}'\text{O}_6$ ($\text{B}' = \text{Co}, \text{Ni}$) are 3.5920 and 3.6699 μB , respectively. In each compound, the magnetic moments of all the spheres that is assumed in the FP-LAPW model have the same direction. Hence, in the two types of double perovskites, the chromium contributes largely in the total spin magnetic moment.

Table 6.2. Magnetic moments (in μB) of the interstitial region, individual atoms and total magnetic moment for the double perovskites $\text{La}_2\text{CrB}'\text{O}_6$ ($\text{B}' = \text{Co}, \text{Ni}$)

Compounds	m^{Inst}	m^{La}	m^{Cr}	$m^{\text{Co/Ni}}$	m^{O}	m^{Total}
$\text{La}_2\text{CrCoO}_6$	0.1151	-0.8750	2.8039	0.8054	0.0212	3.5920
$\text{La}_2\text{CrNiO}_6$	0.4130	-0.2746	2.7853	0.4448	0.0407	3.6699

6.5 Results of Optical Properties for $\text{La}_2\text{CrB}'\text{O}_6$

Interaction of electromagnetic radiations with a material plays key role in understanding the optical response of a system. The variation of dielectric function as a function of incident radiation give ideas about the optical properties of solids. The dielectric function of an anisotropic material is a complex symmetric second-order tensor, which describes the linear response of an electronic system to an applied external electric field. It is expressed as $\varepsilon(\omega) = \varepsilon_1(\omega) + i\varepsilon_2(\omega)$, where are the real and imaginary components of the dielectric function, respectively. The calculations of this frequency dependent dielectric function require the precise values of energy eigenvalues and electron wavefunctions. These are natural outputs of a band structure calculation.

The knowledge of both the real and imaginary parts of the dielectric function allows the calculation of reflectivity $R(\omega)$ and optical absorption coefficient $I(\omega)$ using the standard expression (Delin *et al.*, 1996, Yu *et al.*, 1999). The compounds $\text{La}_2\text{CrCoO}_6$ and $\text{La}_2\text{CrNiO}_6$ are having tetragonal symmetry which permit only two principal diagonal non-zero second order dielectric tensor components $\varepsilon_{xx}(\omega)$ and $\varepsilon_{zz}(\omega)$ along a and c crystallographic axis.

The variations in the real and imaginary parts of the electronic dielectric function for $\text{La}_2\text{CrCoO}_6$ and $\text{La}_2\text{CrNiO}_6$ along xx and zz directions are shown in Figs. 6.10 (a) and (b). From Fig. 6.10 (a), the real part of the dielectric function shows sharp peaks at 0.2 eV and 0.05 eV along xx direction and at 0.1 eV and 0.02 eV along zz direction for $\text{La}_2\text{CrCoO}_6$ and $\text{La}_2\text{CrNiO}_6$ in the visible region of the spectrum. After attaining maxima in the real and imaginary parts of the electronic dielectric functions, the peaks reduces gradually and tends towards minimum value which is obtained at 2.2 eV and 1.9 eV along xx direction; and at 2.1 eV and 2.8 eV along zz direction respectively for $\text{La}_2\text{CrCoO}_6$ and $\text{La}_2\text{CrNiO}_6$. This is due to the inter-band transition between the VCM and the CBM.

In Fig.6.11 (a) and (b), we show the plots of the two components $R_{xx}(\omega)$ and $R_{zz}(\omega)$ of the reflectivity of the perovskites $\text{La}_2\text{CrCoO}_6$ and $\text{La}_2\text{CrNiO}_6$. The plots clearly show that the reflectivity is about 45 % to 50 % at about 10.40 eV along xx and zz direction, which has in fact originated from the inter-band transitions. From the plots, one can notice that the reflectivity spectrum is nearly flat in the low energy region, but at higher energies, the reflectivity peaks increase rapidly with some oscillations.

The calculated linear absorption of the incident radiation along a and c axis for $\text{La}_2\text{CrCoO}_6$ and $\text{La}_2\text{CrNiO}_6$ are shown in Fig. 6.11 (c) and (d) respectively. It is clear from the figures that for both the compounds the maxima in absorption coefficient occurs at ~ 10 eV. This in fact coincides with the occurrence of maxima in imaginary parts of dielectric constants for both directions at ~ 10 eV. This is true from the optical properties of the compounds. From 6.11 (c) and (d), it is obvious that both the compounds show the maximum absorption at photon energies ~ 10 eV where almost minimum reflection takes place i.e. 45% to 50 %. However $\text{La}_2\text{CrCoO}_6$ shows higher absorption coefficient than $\text{La}_2\text{CrNiO}_6$. The threshold of the absorption spectra of $\text{La}_2\text{CrCoO}_6$ and $\text{La}_2\text{CrNiO}_6$ are located in 0.08 eV and 0.09 along xx direction, while it occurs at 0.11 eV and 0.12 eV

Table 6.3. The calculated dielectric constant $\epsilon_1(0)$, reflectivity $R(\omega)$, and absorption coefficient $I(\omega)$ for $\text{La}_2\text{CrCoO}_6$ and $\text{La}_2\text{CrNiO}_6$

Compound	$\epsilon_{1xx}(0)$	$\epsilon_{1zz}(0)$	$R_{xx}(\omega)$	$R_{zz}(\omega)$	$I_{xx}(\omega)$	$I_{zz}(\omega)$
$\text{La}_2\text{CrCoO}_6$	36.50	35.44	0.53	0.520	0.08	0.11
$\text{La}_2\text{CrNiO}_6$	72.25	52.75	0.63	0.58	0.09	0.12

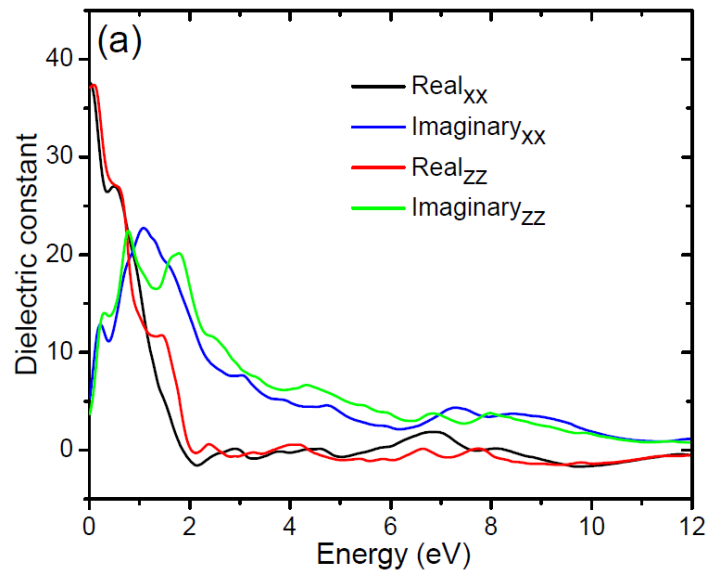


Fig. 6.10(a). Variation of dielectric constant as a function of photon energy of La₂CrCoO₆ along xx and zz directions.

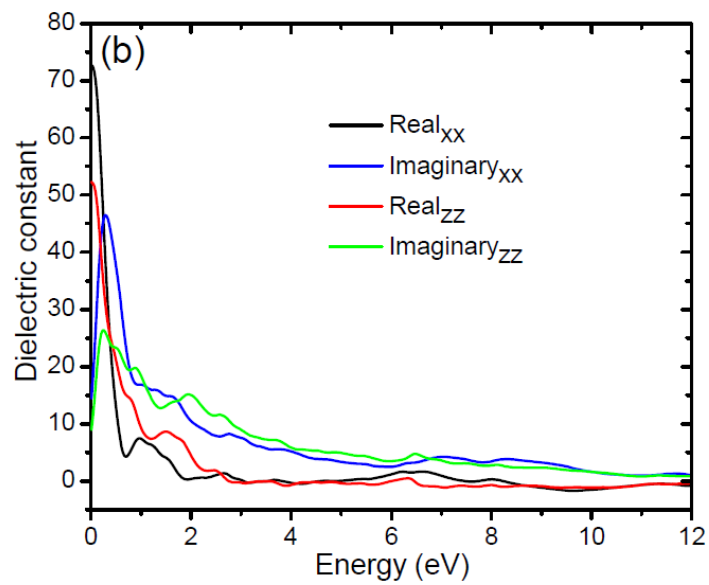


Fig. 6.10(b). Variation of dielectric constant as a function of photon energy of La₂CrNiO₆ along xx and zz directions.

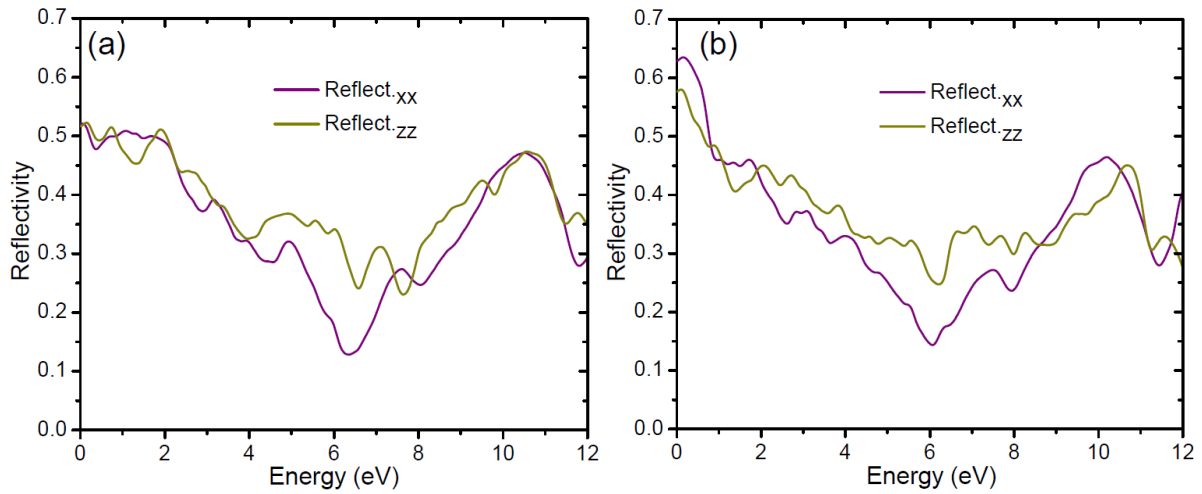


Fig. 6.11. The calculated reflectivity of (a) $\text{La}_2\text{CrCoO}_6$ and (b) $\text{La}_2\text{CrNiO}_6$ along xx and zz directions.

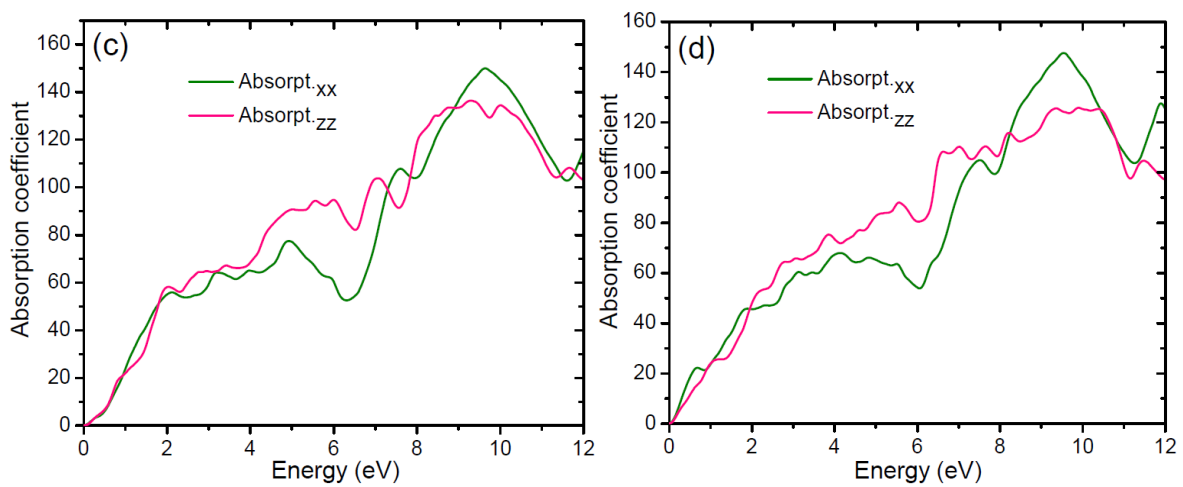


Fig. 6.11. The calculated absorption coefficient of (c) $\text{La}_2\text{CrCoO}_6$ and (d) $\text{La}_2\text{CrNiO}_6$ along xx and zz directions.

Conclusion

In this thesis we present the study of structural, electronic and optical properties of double perovskite $AA'BB'O_6$ type using self-consistent full-potential linearized augmented plane wave (FP-LAPW) method on the base of density functional theory (DFT). In this thesis, the combinations of the alkaline earth, transition and rare earth elements A and A' are : Ba, La, Pb, Sr, and the transition metals B are Cr, Mg, Sc, V with B' as Co, Nb, Ni, Mo, Sb, Ta and W. The methodology followed had been discussed in detail in chapter 2. The electronic properties studied in this thesis are concerned with calculation of density of states (DOS) and energy band structures. The results of the optical parameters like isotropic complex dielectric function, reflectivity and optical absorption of the double perovskite as a function of photon energy is also presented in the thesis. All these study had been done by using FP-LAPW method of DFT by using wien2k code.

In chapter 3, we discuss the electronic structure and optical properties of double perovskites A_2MgWO_6 ($A = Ba, Sr$) by using GGA approximation potential. We found that A_2MgWO_6 is a semiconductor with indirect type of transition. The lowest energy in the conduction and highest band in the valence region lies in Γ -X symmetry direction. Energy band gap obtained from our calculation is 2.753 eV for Ba_2MgWO_6 and 2.731 eV for Sr_2MgWO_6 , which indicates that it is a wide band gap semiconductor. This will probably have application in optoelectronic devices.

Chapter 4, we discussed the electronic and optical properties of the cubic double perovskites $Pb_2Sc B'O_6$ ($B' = Sb, Ta$), using the GGA and mBJ approximations based on FP-LAPW

method. We obtained a direct band gap in GGA and mBJ along X-X symmetry direction around the Fermi level and a semiconducting behavior in both the perovskite systems. However it is an insulating semiconductor with wide band gaps of 2.712 eV (GGA); 3.842 eV (mBJ) for $\text{Pb}_2\text{ScSbO}_6$ and 2.657 eV (GGA); 3.889 eV (mBJ) for $\text{Pb}_2\text{ScTaO}_6$. The energy band gaps are wider in mBJ than in GGA. This is a general trend found in mBJ method. Further from the absorption coefficient results, calculated band gaps are nearly of same magnitudes that are obtained from energy band plots for both the perovskites.

Finally, the results of the dielectric function, optical reflectivity and absorption coefficient confirm the usefulness of the cubic double perovskites $\text{Pb}_2\text{ScB}'\text{O}_6$ ($\text{B}' = \text{Sb, Ta}$) compound for applications in the optoelectronic devices in the low and UV spectrum.

In Chapter 5, we discuss the structural, electronic, optical and magnetic properties of Ba_2VNbO_6 and Ba_2VMoO_6 respectively by using GGA and mBJ potentials respectively. From the plots of DOS, for Ba_2VNbO_6 , we find that in the valence band, contribution to the maxima in the TDOS are by O-p atoms for both the spin up and spin down. At the Fermi level (energy=0) in spin up case, there is maxima in TDOS which appears due to contribution by the V d_{t2g} atoms. In the conduction band in spin up case, near the Fermi level, there is contribution by the Nb atom to the TDOS maxima of the perovskite and above that, it was Ba-d atom which contributes to the maxima in DOS for both spin up and spin down. The occurrence of maxima in TDOS at the Fermi level indicate the metallic behavior in spin up case. Whereas in the spin down channel for Ba_2VNbO_6 , we find that in the valence band, there are maxima occurring in TDOS at the energy range from -3 eV to -6 eV, contribution to these maxima are by O atom. In the conduction band, we find that there are maxima in TDOS at 1 eV, 3 eV and 6 eV respectively which are due to the Mo, V and Ba atoms. Here, we find the occurrence of energy gap of 2.6 eV between the valence and the

conduction bands in the spin down case. This indicates that the behavior of these system as a semiconductor.

There is similar trends in the values of TDOS and PDOS in the systems Ba_2VMoO_6 as calculated by using the mBJ potential. The only differences found in the calculated energy band gap in spin down cases are 2.6 eV with a little wider band gap in the same Γ symmetry direction.

From reported optical results for Ba_2VNbO_6 and Ba_2VMoO_6 , we conclude that for both the compounds is optically isotropic. The optical properties further revealed that the compounds has low absorption rate and are thus favorable for transparent properties.

In Chapter 6, we have described results obtained for electronic, optical and magnetic properties of $\text{La}_2\text{CrB}'\text{O}_6$ ($\text{B}' = \text{Co}, \text{Ni}$) perovskites by using GGA approximation potential. For the compound $\text{La}_2\text{CrCoO}_6$ and $\text{La}_2\text{CrNiO}_6$, we get the same trend and result from both the cases. In the conduction band for both spin up and spin down, La-f atom contributes to the maxima in DOS for both the system. At Fermi level, from both of the system $\text{La}_2\text{CrCoO}_6$ and $\text{La}_2\text{CrNiO}_6$, it was the contribution to Cr-d atom that cover the DOS and which is the reason why we have no band gap and show metallic behavior. In the spin up case for both the compound, below the Fermi level in the valence band, it was the contribution from Cr-d and Co-d/Ni-d atom which contributes to the maxima in DOS. Whereas in the spin down channel in the valence band for both the perovskites, the maximum peaks which appears at ~ -5 eV, it was the Co-d and Ni-d which attributes to the maximum in DOS. From reported optical results, we conclude that both the compounds is optically anisotropic with technical applications.

Conference attended

1. CMDAYS-2016, A National Conference Organized by the Department of Physics, Mizoram University, from 29-31 August 2016
2. CMDAYS-2017, A National Conference Organized by the Department of Physics, Tezpur University, from 29-31 August 2017.
3. 2nd ICC-2017, An International Conference Organized by Govt. Engineering College, Bikaner, Rajasthan, from 24-25 November 2017.

Paper Presentation in Conference

1. Presented a paper entitled “*Study of Electronic and Optical properties of double perovskite Sr_2MgWO_6* ” at CMDAYS-2016, A National Conference Organized by the Department of Physics, Mizoram University from 29-31 August 2016.
2. Presented a paper entitled “*Study of electronic and magnetic properties of Vanadium based double perovskite oxide: Ba_2VNbO_6* ” at CMDAYS-2017, A National Conference Organized by the Department of Physics, Tezpur University, from 29-31 August 2017.
3. Presented a paper entitled “*Electronic and optical properties of double perovskite Ba_2VMoO_6 : FP-LAPW*” at 2nd ICC-2017, An International Conference Organized by the Department of Physics, Govt. Engineering College, Bikaner, from 24-25 November 2017.

CONTENTS

Chapters	Topic	Page
	Title of the thesis	<i>i</i>
	Certificate	<i>ii</i>
	Declaration	<i>iii</i>
	Acknowledgement	<i>iv</i>
	Contents	<i>vi</i>
	List of Figures	<i>ix</i>
	List of Tables	<i>xii</i>
	List of Abbreviations	<i>xiii</i>
	Dedication	<i>xiv</i>
Chapter 1	: Introduction	1
Chapter 2	: Theoretical Formalism and Methodology	15
2.1	: Theory	16
2.2	: Born-Oppenheimer approximation	16
2.3	: DFT General Formulation	17
2.2.1	: Hohenberg and Kohn's Theorem	18
2.2.2	: Kohn Sham Equations	20
2.4	: Local Density Approximation (LDA)	23
2.5	: Generalized Gradient Approximation	25
2.6	: Local Spin density approximation (LSDA)	27
2.7	: The full-potential linearized augmented-plane wave (FP-LAPW) method	28

	2.8	: Modified Becke Johnson Potential (mBJ)	32
	2.9	: Equation of states	35
	2.10	: Optical properties	36
	2.11	: Wein2k code	41
Chapter	3	: Study of Electronic and Optical properties of Double Perovskites A ₂ MgWO ₆ (A = Ba, Sr)	45
	3.1	: Crystal structure	45
	3.2	: Computational details	49
	3.3	: Results of Density of states	49
	3.3.1	: Density of States for Ba ₂ MgWO ₆	49
	3.3.2	: Density of States for Sr ₂ MgWO ₆	52
	3.4	: Energy bands of Ba ₂ MgWO ₆ and Sr ₂ MgWO ₆	55
	3.5	: Results of Optical properties for A ₂ MgWO ₆	57
Chapter	4	: Study of Electronic and Optical properties of Double Perovskites Pb ₂ ScB'O ₆ (B' = Sb, Ta)	62
	4.1	: Crystal structure	62
	4.2	: Results of Density of states	66
	4.2.1	: Density of States for Pb ₂ ScSbO ₆	66
	4.2.2	: Density of States for Pb ₂ ScTaO ₆	71
	4.2.3	: Energy bands in Pb ₂ ScB'O ₆ (B' = Sb, Ta)	76
	4.4	: Results of Optical properties for Pb ₂ ScB'O ₆ (B' = Sb, Ta)	78
Chapter	5	: Study of Electronic and Optical properties of Double Perovskites Ba ₂ VB'O ₆ (B' = Nb and Mo)	84

5.1	: Crystal structure	84
5.2	: Results of Density of states	88
5.2.1	: Density of states for Ba ₂ VNbO ₆	88
5.2.2	: Density of states for Ba ₂ VMoO ₆	91
5.3	: Energy Bands in Ba ₂ VB'O ₆ (B' = Nb, Mo)	94
5.4	: Magnetic moments of Ba ₂ VB'O ₆	98
5.5	: Results of Optical properties for Ba ₂ VB'O ₆	101
Chapter 6	: Study of Electronic and Optical properties of Double Perovskites	
	La ₂ CrB'O ₆ (B' = Co, Ni)	106
6.1	: Crystal structure	106
6.2	: Results of density of states	110
6.2.1	: Density of states for La ₂ CrCoO ₆	110
6.2.2	: Density of states for La ₂ CrNiO ₆	113
6.3	: Energy bands of La ₂ CrB'O ₆	116
6.4	: Magnetic moments of La ₂ CrB'O ₆	118
6.5	: Results of Optical Properties for La ₂ CrB'O ₆	120
Conclusion		125
References	:	128
Bio data	:	138
List of Research Publications		139
Conference attended		141
Reprint of Published Papers		

Chapter 1

Introduction

Chapter 2

Theoretical Formalism and Methodology

Chapter 3

*Study of Electronic and Optical
properties of Double Perovskites
 A_2MgWO_6 (A = Ba, Sr)*

Chapter 4

*Study of Electronic and Optical
properties of Double Perovskites
 $Pb_2ScB'O_6$ ($B' = Sb, Ta$)*

Chapter 5

*Study of Electronic and Optical
properties of Double Perovskites
 $Ba_2VB'O_6$ ($B' = Nb$ and Mo)*

Chapter 6

*Study of Electronic and Optical
properties of Double Perovskites
 $La_2CrB'O_6$ ($B' = Co, Ni$)*

Conclusions

Declaration of the candidate

Mizoram University

19th November 2018

I, Lalhriatpuia Hnamte, hereby declare that the subject matter of this thesis is the record of the works done by me, that the contents of this thesis did not form basis of the award of any previous degree to me or to the best of my knowledge to anybody else, and that the thesis has not been submitted by me to any other University/Institute.

This is being submitted to the Mizoram University for the degree of Doctor of Philosophy in Physics.

(LALHRIATPUIA HNAMTE)

Candidate

(Prof. SUMAN RAI)

Head

(Prof. R.K.THAPA)

Supervisor